Copyright

by

Alexander Borisovich Nepomnyashchii

2011

The Dissertation Committee for Alexander Borisovich Nepomnyashchii certifies that this is the approved version of the following dissertation:

**Electrochemical and Electrogenerated Chemiluminescence Studies of the BODIPY Dyes**

Committee:

_____
Allen J. Bard, Supervisor

_____
Richard M. Crooks

_____
Keith J. Stevenson

_____
C. Buddie Mullins

_____
Brian A. Korgel

# Electrochemical and Electrogenerated Chemiluminescence Studies of the BODIPY Dyes

by

**Alexander Borisovich Nepomnyashchii, B.S.; M.S.**

**Dissertation**

Presented to the Faculty of the Graduate School of

The University of Texas at Austin

in Partial Fulfillment

of the Requirements

for the Degree of

**Doctor of Philosophy**

The University of Texas at Austin

August, 2011

**Dedication**

To my mother

Guzinskaya Liliana Naumovna, my sister Nepomnyashchaya Natalia Borisovna, memories of my father: Nepomnyashchii Boris Isaacovich, grandfather Nepomnyashchii Isaac Samuilovich and grandmothers: Guzinskaya Berta Benzelevna and Bushkova Eha Borukhovna

**Acknowledgements**

I would like to thank my advisor, Dr. Allen J. Bard for his support during all years of my research. I would also like to thank my committee members: Dr. Richard M. Crooks, Dr. Keith J. Stevenson, Dr. C. Buddie Mullins, and Dr. Brian A. Korgel for being members of my committee. My great gratitude goes to members of the Bards lab: Dr. Joaquin Rodriguez-Lopez, Dr. Frank Fan, Angie Nelson, Mei Shen, Dr. Mario Alpuche-Aviles, Dr. Dongping Zhan, Dr. Shanlin Pan, Dr. Carlos Sanchez-Sanchez, Dr. Alessandro Minguzzi, Dr. Matthew Sartin, Dr. Dodzi Zigah, Netz Arroyo and Qian Wang for different helpful advises in research and life throughout my doctoral career. Special thanks go to my great friends from Dr. Crooks lab: Dr. Kwok Fan-Chow and Dr. Javier Guerra for their help during my life in Austin. Big thanks to collaborators in the current projects: Johannes Ahrens and Dr. Sangik Cho and their advisors: Dr. Peter Rossky and Dr. Martin Brö ring. Big thanks also to collaborators in other projects: Dr. Joel Rosenthal, Allen Pistner, Singaravelu Velayudham, Robert Ono, Dani Lyons and their advisors Dr. Steven Lippard, Dr. Shawn Burdette, Dr. Haying Liu, Dr. Christopher Bielawski and Dr. Jonathan Sessler.

**Electrochemical and Electrogenerated Chemiluminescence Studies of the BODIPY Dyes**

Publication No._____

Nepomnyashchii Alexander Borisovich, Ph. D.

The University of Texas at Austin, 2011

Supervisor: Allen J. Bard

Electrochemical and electrogenerated chemiluminescence properties of the BODIPY (boron dipyrromethene) dyes are presented. Some specific features of the BODIPY dyes are obtained and described in the current dissertation. Separation of around 1.0-1.2 V is noticed between two oxidation and reduction waves for one center which is very different from 0.5 V seen for the polycyclic hydrocarbons. Cathodic and anodic stability is shown to depend upon absence or presence of certain degree of substitution. Different ways of electrochemical dimerization are explored and compared with the chemical dimerization. Photophysical and electrochemical properties of monomer, chemically synthesized dimer, trimer and polymer are described and the characteristic features determined.

**Table of Contents**

## Chapter 1: Introduction

### 1.1. Overview

BODIPY, boron dipyrromethene or boraindacene dyes are very important and relatively new conjugated materials which are subject of the extensive research interest (Scheme 1).[1-25]

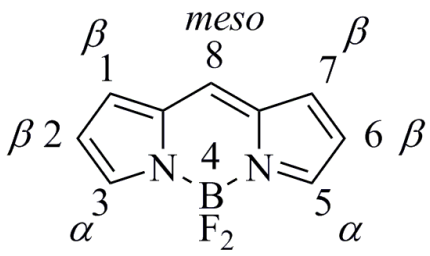


**Scheme 1.**

These B-N compounds show different chemical behavior compared with polycyclic hydrocarbon C-C dyes such as anthracenes and fluorenes.[1] These dyes were discovered in 1960s [26], but large interest in these systems was developed at the beginning of 1990s from Boyer et. el. work who proposed application of these materials as laser dyes. [3,4] These dyes are also widely used for biological labeling studies using fluorescence due to their relatively high solubility in polar solvents and also possibility of simple tuning emission wavelength by adjusting chemical structure.[27] There are hundreds of different fluorescent labels based on BODIPY available at this point for different sensing applications.[6,7,28-30] Research in this area is very active and the first blue emitting compound was recently synthesized in 2010 by Cabrera et. el.[31] Despite a lot of probes available in organic solvents and even mixtures of water and alcohols there are not many

completely water soluble probes developed. Most of the known probes are based on sulfonated dyes.[1] Liu et. el. developed a probe with the long chain of polyethyleneglycols (PEG).[32] Development of aqueous probes is one of the main areas of the research in the field. The other major field for application of these dyes is solar energy conversion.[33-35] The current research is mostly based upon the heterojunction[34] and dye sensitized[33,35] solar cells. There are other proposed applications of these dyes including synthesis of fluorescent nanocars which can mimic biological motions.[9] Application of these systems for biocatalytic Diels-Alder reactions is also shown.[10] Electrochemical and electogenerated chemiluiminescence (ECL) properties can also be very useful to explain structural properties of these BODIPY dyes.[36-40] Electrochemistry is very sensitive to the presence or absence of the substitution and can provide important information about structural properties of certain materials. ECL is also a widely applied technique for biological labeling and there is research done to design multi color probes which can compliment well-known ECL label $Ru(bpy)_3^{2+}$.[41,42] Photophysical, electrochemical and electrogenerated chemiluminescence studies of the multiple BODIPY dyes will be presented in the current dissertation.

## 1.2. Principles of electrochemically induced electron transfer for organic conjugated molecules.

Electron transfer of organic conjugated molecules has been studied for several decades. Electrochemistry is very important to study electron transfer processes due to the possibility to obtain stable ions or radical ions and correspond experimental results with the theoretical predictions based on the molecular orbital calculations.

There are two types of the electrochemical reactions: outer-sphere and inner-sphere.[43] Inner-sphere reactions are usually very complicated due to adsorption phenomena present and corresponding to that influence of the state and nature of the electrode on the electrochemical process. Material, size, electrode roughness and many other parameters causes complications in explanation of the mechanisms of the inner-sphere reactions. Outer-sphere reactions do not depend on the nature of electrode. The electrochemical activity of the compounds is controlled by diffusion or homogeneous kinetics which makes it easier to understand electrochemical behavior and predict electrochemical properties of the studied systems. Solvents such as acetonitrile, dichloromethane and mixture of benzene:acetonitrile allow one to obtain fairly good electrochemical behavior in the range from +2.0 V to -2.0 V. Liquid ammonia, ultra-pure THF, dimethylamine, liquid sulfur dioxide and some other solvents were used for extending the potential range to more negative potentials of around -3.6 V and positive potentials of around +5 V. [44-49] Despite the fact that exact values of potentials reported in the scientific literature are not very precise due to Fe/Fc+ couple used as a reference standard the range of the potentials available can be evaluated with high degree of trust.[50-54]

Electrochemical experiments in clean conditions show appearance of two waves for one center for conjugated polycyclic hydrocarbons. [55]

$$A + e = A^{\bullet -} \quad (1)$$

$$A^{\bullet -} + e = A^{2-} \quad (2)$$

Separation between waves for such systems was determined to be around 0.5-0.7 V depending on the structure of the molecules. Theoretical expectations from molecular orbital calculations based on just gas phase theory will predict separation of around 4-5 V. Deviation of the experimental results from theory is related with the effect of the solvation energy. The difference in electrochemical wave separations between different compounds is related mostly with the change in the gas phase energy due to the increase of the size of the molecules, though the effect of the solvation may also have some importance. There was noticed fact of the decrease in the peak separation for the transition from anthracene to pentacene from around 0.7 V to 0.58 V.[55] Addition of the electrons to different cores is also important especially with the aim of understanding properties of the dimers, trimers, tetramers, pentamers and higher molecular systems such as polymers. The degree of separation for such systems depends upon the degree of sterical interactions between single separate units. Supporting electrolyte and solvent were also shown to have substantial effect on the reactivity of the ferrocene complexes with two or more cores present through ion pairing effect.[56-59] Geiger et. el. showed transition from two simultaneous electron waves to two waves with fairly large separations in case of transtion from DCM to THF using tetrakis(pentafluorophenyl)-borate salts.

Heinze et. el. studied electron transfer processes for the conjugated phenylvinylene oligomers and develop some basic rules based on the obtained experimental data[60-62]:

1) the reduction potentials of the first and second electron transfer are closer with increasing the chain length. The same is true for all consecutive processes;

2) electrons in different units also come in pairs. It is shown experimentally small splittings between first and second electons and third and fourth electron;

3) chemical activity is increasing with increasing the chain length.

Results for the anthracene dimers also show presence of substantial interaction between different units with separation of about 0.2-0.3 V present.[63] There is also a lot of work done describing properties of the molecules with different centers such as for example donor-acceptor molecules though their behavior is very different which makes much harder to make common assumptions.[64-67]

**1.3. Electrogenerated chemiluminescence.**

Electrogenerated chemiluminescence is a chemical phenomenon which is based on obtaining light electrochemically through generation of the radical cations and anions. [68-77] Theory of electrogenerated chemiluminescence is already widely developed with multiple publications in the field. Four main types of the ECL generation are known to this point: annihilation, coreactant, mixed system with fluorescent or nonfluorescent coannihilators. Annihilation ECL is generated by production of positively or negatively charged radical cations and anions which can react with each other in a very limited period of time:

$$A + e = A^{\bullet -} \quad (5)$$

$$A - e = A^{\bullet +} \quad (6)$$

$$A^{\bullet +} + A^{\bullet -} = {}^{1}A^{*} + A \quad (7)$$

$${}^{1}A^{*} = A + hv \quad (8)$$

Schematically annihilation ECL can be presented through molecular orbitals as addition of the electron to the LUMO orbital and ejection of the electron from the HOMO one (Scheme 2).[68]

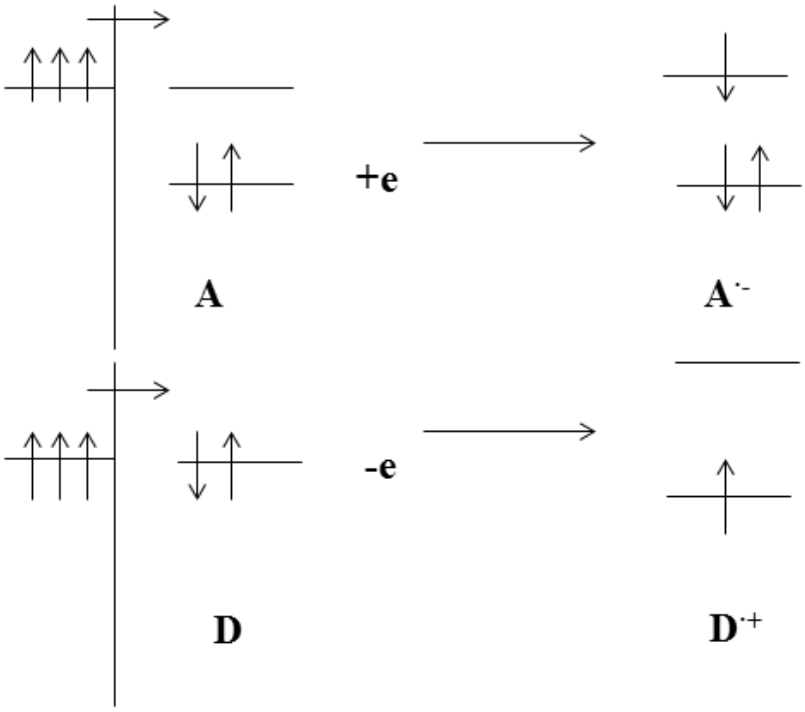


**Scheme 2.** Schematic representation of the ECL process.

Current mechanism is a singlet route ECL generation with sufficient energy to produce needed excited state. The other mechanism is based on the generation of the triplet state. This mechanism was seen for the rubrene, porphyrine and some other systems and proved by magnetic measurments and mixed system experiments.

$$A^{\bullet+} + A^{\bullet-} = {}^3A^* + A \quad (9)$$

$${}^3A^* + {}^3A^* = {}^1A^* + A \quad (10)$$

$${}^1A^* = A + hv \quad (11)$$

Mechanism based on the coreactant ECL is more complicated. In this case active reductant or oxidant is used or generated through irreversible reaction. Real mechanism of the coreactant activity is still under investigation, though significant knowledge about this phenomenon has already been developed. There are many coreactants known as for the reduction as for oxidation : tripropylamine (TPrA), oxalate, benzoyl peroxide, persulfate and so on.[70-80] Application of coreactant for aqueous systems was a breakthrough in electrogenerated chemiluminescence which allows to apply ECL for the biological labeling.[69] All known ECL active compounds have an oxidation or reduction potentials after water oxidation and reduction what exclude usage annihilation ECL from aqueous studies and makes coreactant ECL applicable and useful. Oxalate was a first coreactant used in water by Rubinstein and Bard[69]:

$$A - e = A^{\bullet+} \quad (12)$$

$$A^{\bullet+} + C_2O_4^{2-} = A + C_2O_4^{\bullet-} \quad (13)$$

$$C_2O_4^{\bullet-} = CO_2^{\bullet-} + CO_2 \quad (14)$$

$$A^{\bullet+} + CO_2^{\bullet-} = A^* + CO_2 \quad (15)$$

$$A^* = A + hv \quad (16)$$

TPrA is the main commercially used coreactant which was used by Leland et. el. and nowadays applied by Roche Inc. for blood testing and other medical analyses[71,81-83]:

$$A - e = A^{\bullet +} \quad (17)$$

$$TPrA - e = TPrA^{\bullet +} \quad (18)$$

$$TPrA^{\bullet +} = TPrA^{\bullet} + H^{+} \quad (19)$$

$$A^{\bullet +} + TPrA^{\bullet} = A^* + TPrA \quad (20)$$

$$A + TPrA^{\bullet} = A^{\bullet -} + TPrA^{+} \quad (21)$$

$$A^{\bullet +} + A^{\bullet +} = A^* + A \quad (22)$$

$$A^* = A + hv \quad (23)$$

Benzoyl peroxide (BPO) is the reductive coreactant which causes production of very bright ECL signal in case of electrochemical reduction of the fluorophore. This coreactant which was used by Chandross et. el. and can be considered first coreactant ECL material applied.[78] It is widely used for explanation of the fact that excimer, exciplex or aggregates are responsible for longer wavelength emission. Excimer or exciplex formation by annihilation electrogenerated chemiluminescence was monitored in multiple publications through the appearance of the broad wave.[84-91] Instability on oxidation causes formation of the long wavelength emission which can disappear in case of the production of the excited state by BPO. Mechanism of benzoyl peroxide activity can be presented as:

$$A + e = A^{\bullet -} \quad (24)$$

$$A^{\bullet -} + BPO = BPO^{\bullet -} + A \quad (25)$$

$$BPO + e = BPO^{\bullet -} \quad (26)$$

$$BPO^{\bullet -} = C_6H_5COO^{\bullet} + C_6H_5COO^{-} \quad (27)$$

$$A^{\bullet -} + C_6H_5COO^{\bullet} = A^* + C_6H_5COO^{-} \quad (28)$$

$$A^* = A + hv \quad (29)$$

Two mechanisms are proposed for this system: one of them is direct reduction of the benzoyl peroxide with production of the radical anions as shown in equation 26 and the other one is related with the homogeneous catalytic oxidation of the benzoyl peroxide by the radical anion of the fluorophore with constant recycling of the initial compound as shown in equation 25. Complications of the differentiating between mechanisms is related with the reduction of the benzoyl peroxide prior to the reduction of the ECL emitting compound.

The other reductive coreactant persulfate can be used as for the non-aqueous organic as for the aqueous systems. Sodium or potassium persulfate can be used for aqueous studies as tetrabutylammonium persulfate can be used for experiments in organic solvents. Mechanism of the persulfate activity can be presented as:

$$A + e = A^{\bullet -} \quad (30)$$

$$A^{\bullet -} + S_2O_8^{2-} = A + SO_4^{2-} + SO_4^{\bullet -} \quad (31)$$

$$A^{\bullet -} + SO_4^{\bullet -} = A^* + SO_4^{2-} \quad (32)$$

$$A + SO_4^{\bullet -} = A^{\bullet +} + SO_4^{2-} \quad (33)$$

$$A^{\bullet +} + A^{\bullet -} = A^* + A \quad (34)$$

Homogeneous catalytic reaction as a mechnanism of persulfate activity was proved by the appearance of the dimer peak in case of the reduction of the

diphenylbenzo(k)fluoranthene, which is a good proof for the production of the radical cation.[92] Direct reduction of persulfate with formation of the sulfate radical anions still can not be completely ruled out.

Mixed system ECL can be obtained by using both fluorescent compound or nonfluorescent or weakly fluorescent one.[93-96] Conditions for this case must be formation of the stable radical cation or anion which is energetically sufficient to provide electrogenerated chemiluminescence signal. These stable known cations are formed through oxidation of N,N,N',N'-tetramethyl-p-phenylenediamine (TMPD, Wurster blue) and 10-methylphenothiazine (10-MP) combined with reduction of the fluorescent dye. Mechanism of the electrogenerated chemiluminescence can be presented in this case as:

$$A + e = A^{\bullet -} \quad (35)$$

$$TMPD - e = TMPD^{\bullet +} \quad (36)$$

$$A^{\bullet -} + TMPD^{\bullet +} = A^* + TMPD \quad (37)$$

$$A^* = A + hv \quad (38)$$

Similar mechanism was proposed for 10-MP[94-96]:

$$A + e = A^{\bullet -} \quad (39)$$

$$10\text{-}MP - e = 10\text{-}MP^{\bullet +} \quad (40)$$

$$10\text{-}MP^{\bullet +} + A^{\bullet -} = A^* + 10\text{-}MP \quad (41)$$

$$A^* = A + hv \quad (42)$$

As a conclusion it is possible to say that electrogenerated chemiluminescence has moved from only laboratory technique to a huge business with practical and useful applications.

There is still work to be done to find ECL label complementary to $Ru(bpy)_3^{2+}$ and also develop ECL studies for the effects seen in fluorescence as Förster/Fluorescence Resonance Electron Transfer (FRET) and solvent dependence fluorescence measurments based on PET (Photoinduced Electron Transfer). Studies of aggregates or other supramolecular systems can also add up information about electrogenerated chemiluminescence properties.[97-99]

## Chapter 2: Experimental

### 2.1. Experimental procedures

UV-Vis and fluorescence measurements were performed mostly in DCM and acetonitrile. Fluorescence and absorbance images are shown in Figures 1 and 2. Quantum yield was calculated and compared with the literature results using fluorescein as a standard.

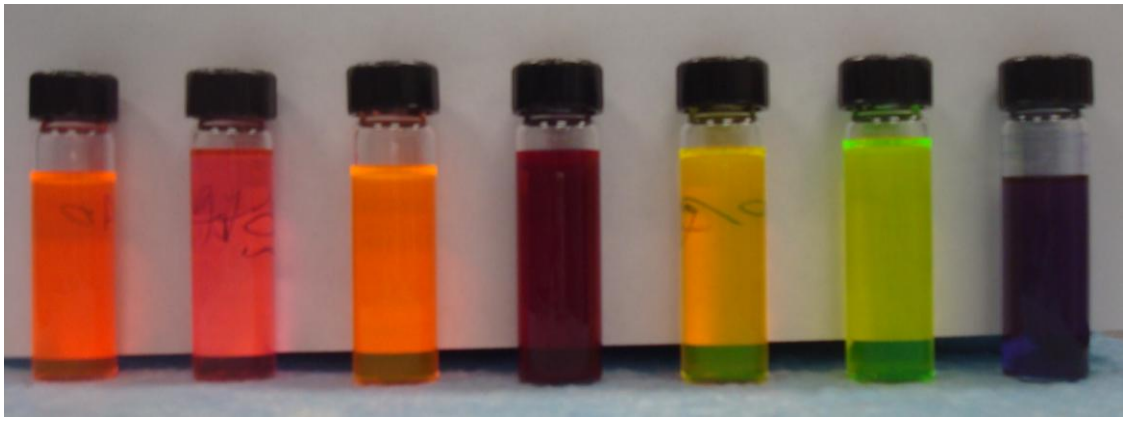

**Figure 1.** UV-Vis images of series of BODIPY dyes

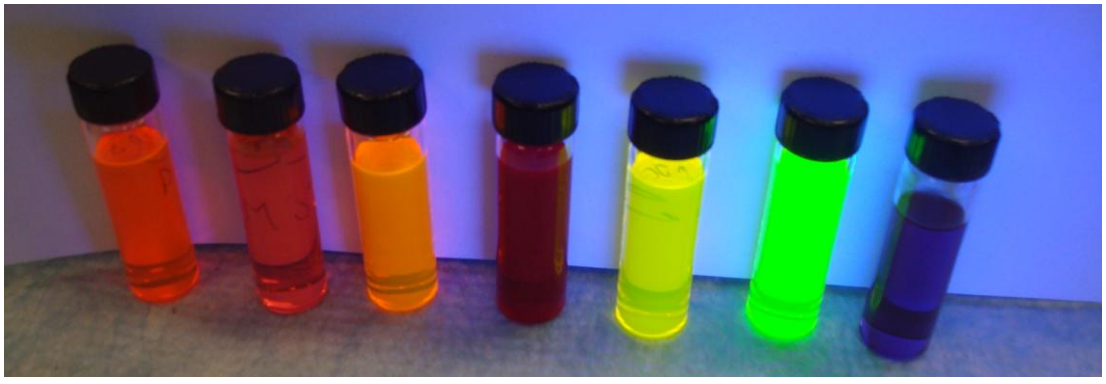

**Figure 2.** Fluorescence images of series of BODIPY dyes obtained in the presence of light.

Absorbance measurements were done using a DU 640 spectrophotometer (Beckman, Fullerton, CA); 1 cm quartz cuvette was used in all measurements. Fluorescence measurements were carried out with a double-beam QuantaMaster Spectrofluorimeter (Photon Technology International, Birmingham, NJ). A 70 W Xe lamp was used as the light source and the slit width was 0.5 mm. Fluorescence concentration measurements were done using a UV lamp as an excitation source and Princeton Instruments Spec-10 CCD Camera (Trenton, NJ) with an Acton SpectraPr-150 monochromator (Acton, MA) as a detector. The CCD wavelengths were calibrated with a Hg/AR pen-ray lamp from Oriel (Stratford, CT). Electrochemical experiments were done under anhydrous oxygen-free conditions. Solutions were prepared in a helium atmosphere drybox (Vacuum Atmospheres Corp., Hawthorne, CA) or in an argon atmosphere drybox (UniLab 2000, M. Braun Inc. USA, Stratham, NH). After preparation, the solution was sealed with a Teflon cap. A 0.0314 $cm^2$ Pt straight working electrode was used for the cyclic voltammetry experiments and a J-type Pt electrode with the same area was used for the ECL experiments with the CCD (Figures 3,4). The geometric electrode area was determined by the chronoamperometry with a 2 mM solution of ferrocene in MeCN assuming a diffusion coefficient, D, of $1.2 \times 10^{-5}$ $cm^2/s$.

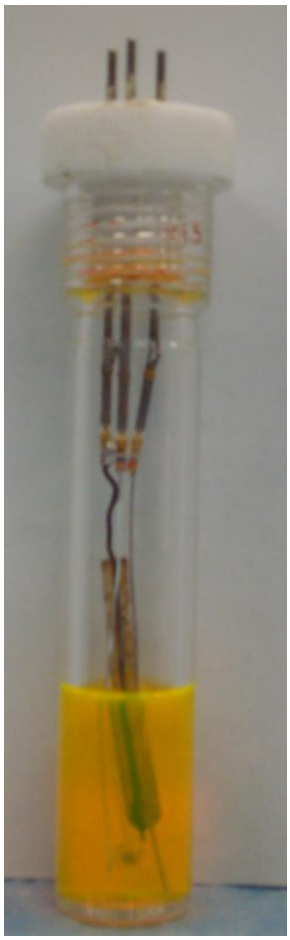

**Figure 3.** Electrochemical and Electrogenerated Chemiluiminescence cell image.

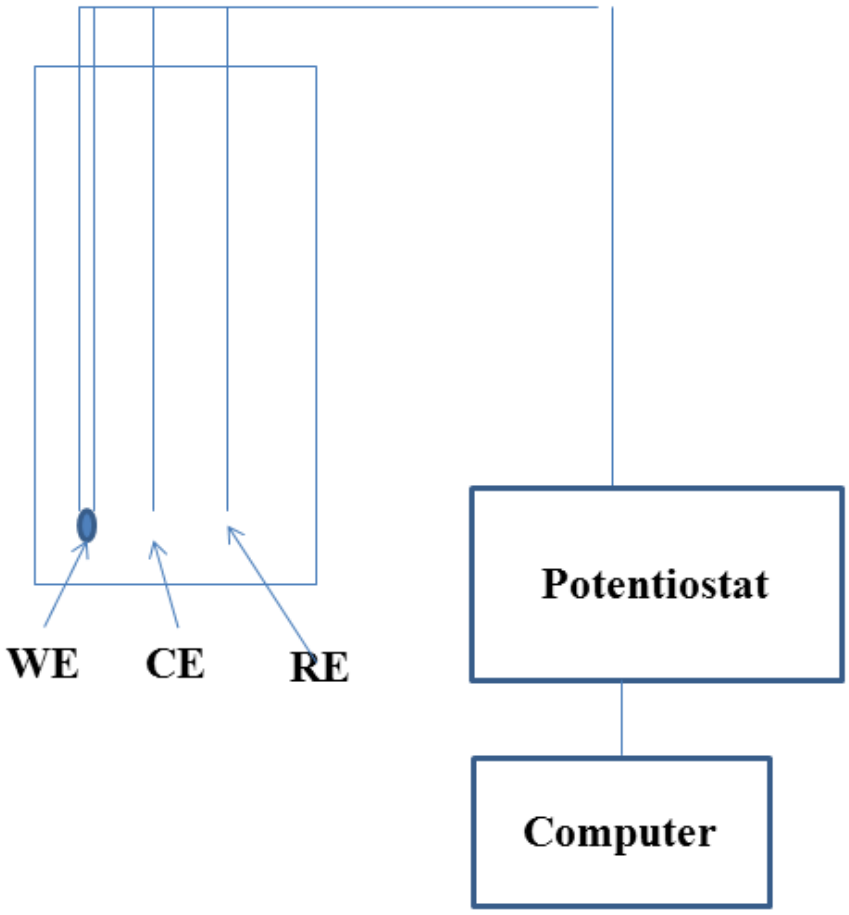


**Figure 4.** Electrochemical cell setup, where WE, CE and RE are working, counter and reference electrode.

The D-values of the dyes were determined by the scan rate dependences from the Randles-Ševčik equation and chronoamperometric pulsing for 1 s and using Cottrell equation. The working electrode was polished after each experiment with 0.3 μm alumina (Buehler, Ltd., Lake Bluff, IL), sonicated in ethanol and in water for 5 min and dried in the oven at 120°C. An Ag wire was used as a quasi-reference electrode QRE) and Pt wire as a counter electrode. Three metal rods was drilled inside the glass and sealed by using epoxy. The potential of the QRE was calibrated using ferrocene as a standard which has $E^{o\,\prime}$ of 0.342 V vs SCE.[100] Cyclic voltammetry and chronoamperometry measurements were carried out with CHI 660 and CHI 660D electrochemical workstations (CH Instruments, Austin, TX). ECL spectra were obtained by using either the CHI 660 or an Eco Chemie Autolab PGSTAT30 potentiostat (Utrecht, the Netherlands). ECL spectra for the annihilation were recorded by potential pulsing with a pulse width of 0.1 s for potentials 80 mV beyond the peak potentials for different amount of time. ECL measurements for the dimers and trimers were done from around 80 mV after the first peak. The spectra were collected by a Princeton Instruments Spec-10 CCD Camera with an Acton SpectraPr-150 monochromator (Figure 5). ECL intensity-time curves were obtained by recording the total emission with a photomultiplier tube (PMT, Hamamatsu R4220, Japan). A Kepco (New York) high voltage power supply operated at standard voltage of -750 V was applied to the PMT (Figure 6).

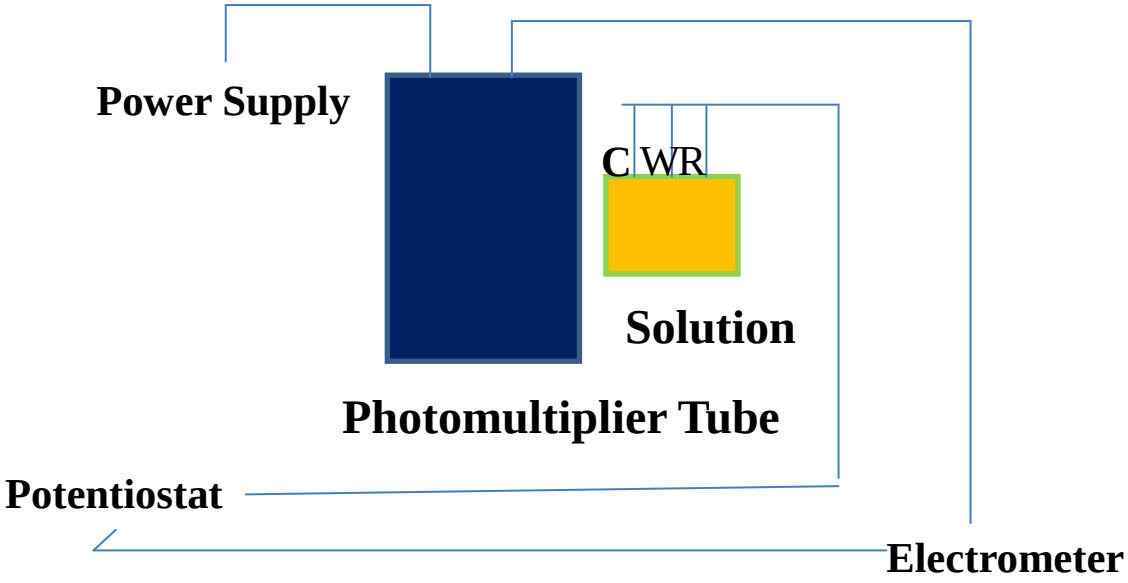


**Figure 5.** Electrogenerated chemiluminescence transient setup.

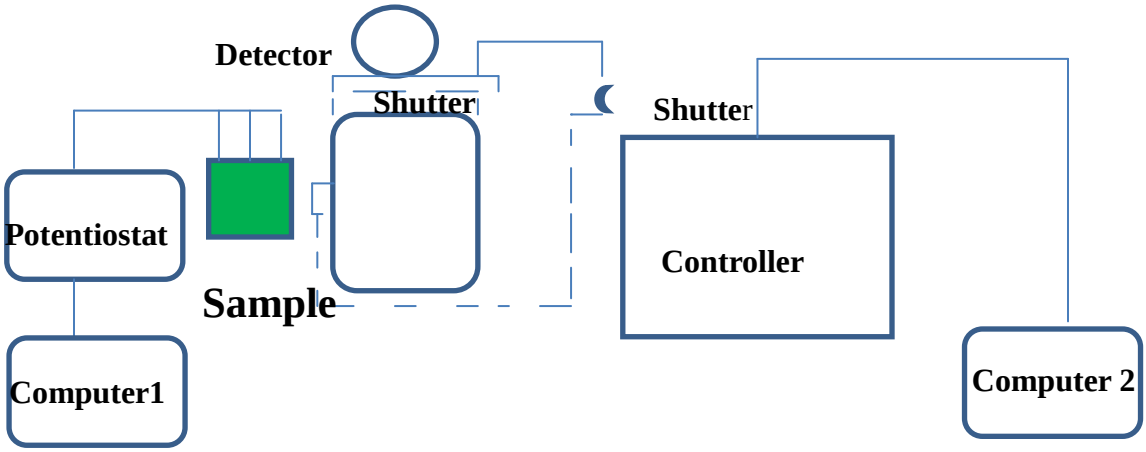


**Figure 6.** Electrogenerated chemiluminescence spectra generation setup, where liquid nitrogen generated detector containing CCD (charge coupled device) was used.[101]

An electrometer (Model 6517, Keithley Instruments Inc., Cleveland, OH) was used to collect the ECL signal from the PMT. Digital simulations were done using Digisim

software (Bioanalytical Systems, West Lafayette, IN).[102-105] Experiments at 77 K were carried out using Spex Fluorolog 1 (Horiba Jobin Yvon, Tokyo, Japan) with Labview software, a 450W sodium lamp and 0.1 mm slit width with a cryostat (5T-100, Janis, Wilmington, MA) using liquid nitrogen and pumping during the experiment to avoid condensation.

## Chapter 3: Results and discussions

### 3.1. Preview

Photophysical and electrochemical studies of the BODIPY dyes are summarized in Tables 1 and 2 and structures with the names are presented in Schemes 3 and 4.

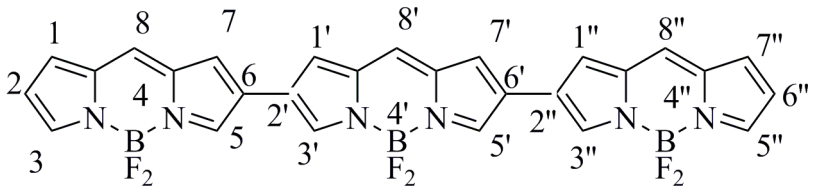

**Scheme 3.** Schematic representation of the BODIPY skeleton.

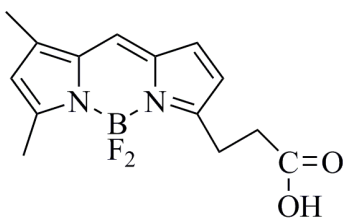

**1**, BODIPY®FL

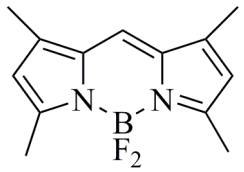

**2**, BODIPY®505/515

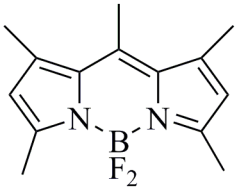

**3**, PM 546

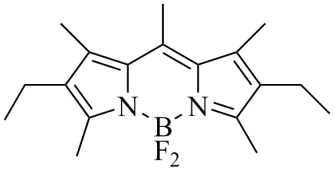

**4**, PM 567

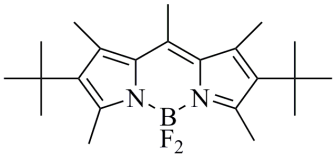

**5**, PM 597

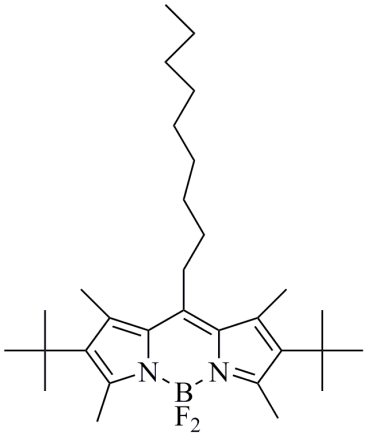

**6**, PM 597-8C9

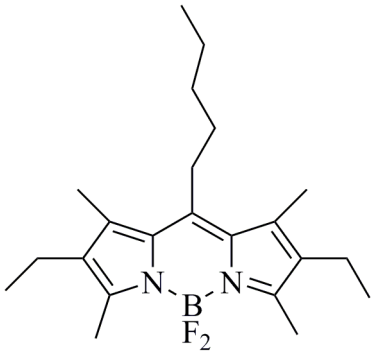

**7**, PM 567A

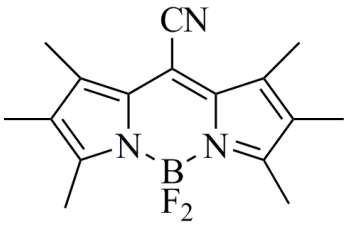

**8**, PM 650

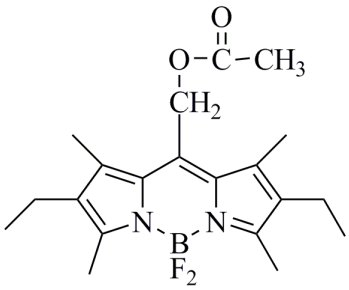

**9,** PM 605

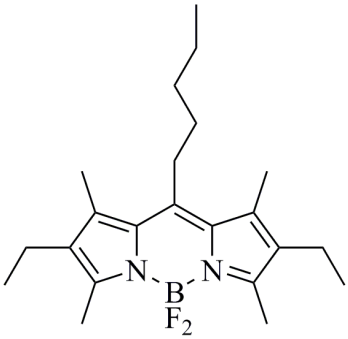

**10,** $B^8$-n-pentyl

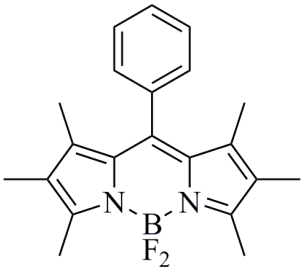

**11**, $B^8$-phenyl

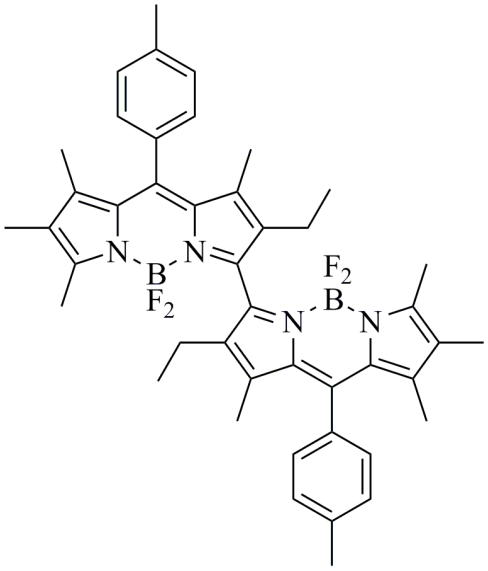

**12**, angular dimer

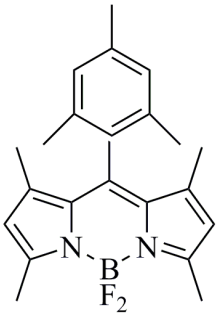

**13**

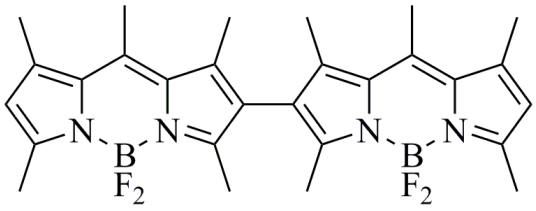

**14**

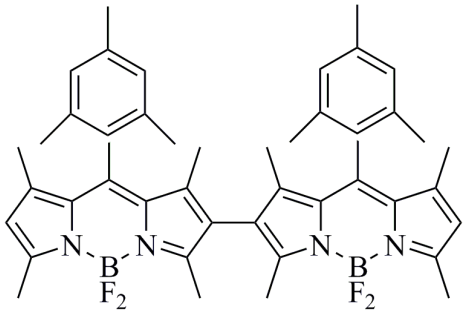

**15**

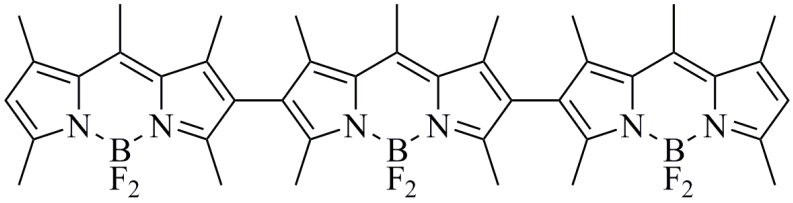

**16**

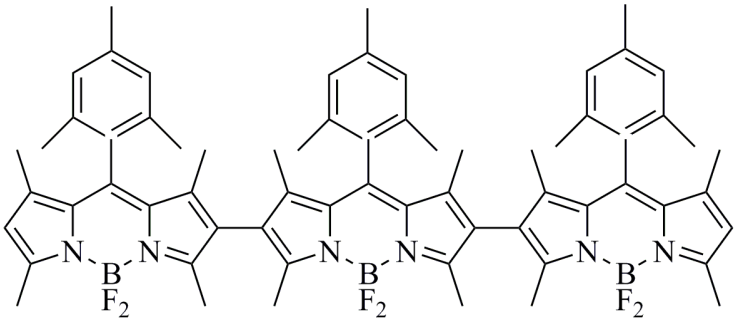

**17**

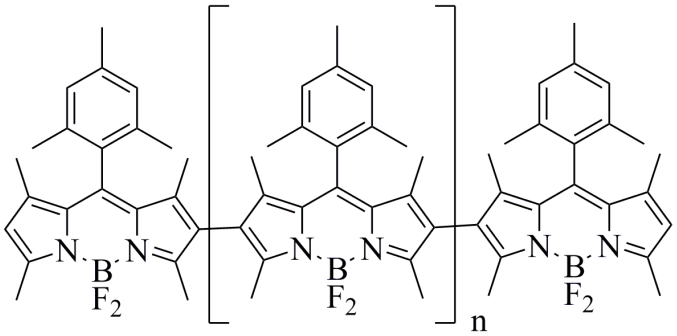

**18**

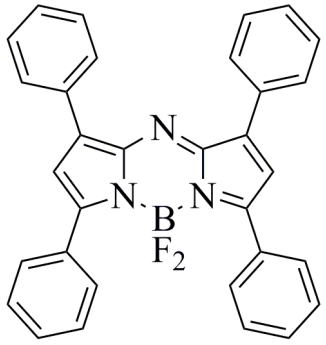

**19**

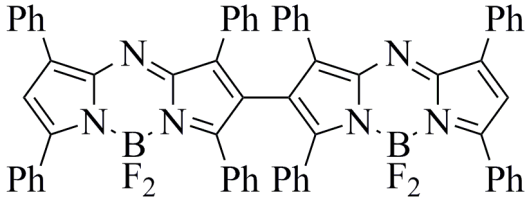

**20**

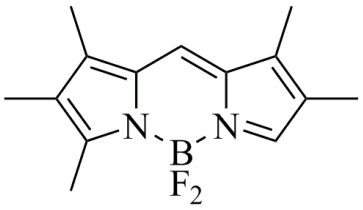

**21**, 1(x3,8)

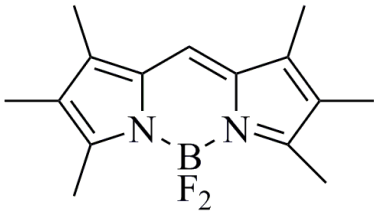

**22**, 2(x8)

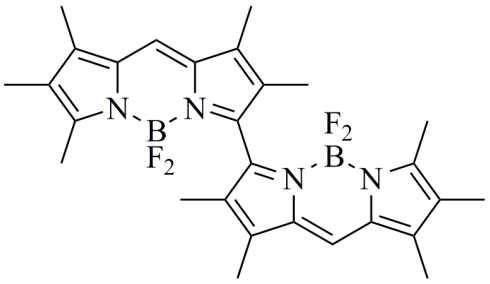

**23**, 3,3'-dimer

**Scheme 4.** Chemical structures of the used dyes: **1** (4,4-difluoro-5,7-dimethyl-4-bora-3a,4a-diaza-s-indacene-3-propionic acid); **2** (4,4-difluoro-1,3,5,7-tetramethyl-4-bora-3a,4a-diaza-s-indacene); **3** (4,4-difluoro-1,3,5,7,8-pentamethyl-4-bora-3a,4a-diaza-s-indacene); **4** (4,4-difluoro-1,3,5,7,8-pentamethyl-2,6-diethyl-4-bora-3a,4a-diaza-s-indacene); **5** (4,4-difluoro-1,3,5,7,8-pentamethyl-2,6-t-butyl-4-bora-3a,4a-diaza-s-indacene); **6** (4,4-difluoro-1,3,5,7-tetramethyl-2,6-t-butyl-8-nonyl-4-bora-3a,4a-diaza-s-indacene); **7** (4,4-difluoro-1,3,5,7-tetramethylmethyl-2,6-diethyl-8-pentyl-4-bora-3a,4a-diaza-s-indacene); **8** (4,4-difluoro-1,2,3,5,6,7-hexamethyl-8-cyano-4-bora-3a,4a-diaza-s-indacene); **9** (4,4-difluoro-1,3,5,7-tetramethyl-2,6-diethyl-8-acetoxymethyl-4-bora-3a,4a-diaza-s-indacene); **10** (4,4-difluoro-1,3,5,7-tetramethyl-2,6-diethyl-8-n-pentyl-3a,4a-diaza-s-indacene; **11** (4,4-difluoro-1,2,3,5,6,7-hexamethyl-8-phenyl-4-bora-3a,4a-diaza-s-indacene); **12** (4,4-difluoro-1,4,5,6-tetramethyl-2-ethyl-8-phenyl-4-bora-3a,4a-diaza-s-indacene)-3-5’-methyl-(4’,4’-difluoro-1’,4’,5’,6’-tetramethyl-2’-ethyl-8’-phenyl-4’-bora-3a',4a'-diaza-s-indacene); **13** (4,4-difluoro-1,3,5,7-tetramethyl-8-mesityl-4-bora-3a,4a-diaza-s-indacene); **14** (4,4-difluoro-1,3,5,7,8-pentametyl-4-bora-3a,4a-diaza-s-indacene)-6-2’-methyl-(4’,4’-difluoro-1’,3’,5’,7’,8’-pentamethyl-4’-bora-3a’,4a’-diaza-s-indacene);

**15** (4,4-difluoro-1,3,5,7-tetramethyl-8-mesityl-4-bora-3a,4a-diaza-s-indacene)-6,2'-methyl-(4',4'-difluoro-1'3',5',7'-tetramethyl-8'-mesityl-4'-bora-3a',4a'-diaza-s-indacene)**; 16** (4,4-difluoro-1,3,5,7,8-pentamethyl-4-bora-3a,4a-diaza-s-indacene)-6,2'-methyl-(4',4'-difluoro-1',3',5',7',8'-pentamethyl-4'-bora-3a',4a'-diaza-s-indacene)-6',2''-methyl-(4'',4''-difluoro-1'',3'',5'',7'',8''-pentametyl-4''-bora-3a'',4a''-diaza-s-indacene); **17** (4,4-difluoro-1,3,5,7-tetramethyl-8-methyl-4-bora-3a'',4a''-diaza-s-indacene)-6,2'-methyl-(4,4-difluoro-1',3',5',7'-tetramethyl-8'-methyl-4'-bora-3'a,4'a-diaza-s-indacene)-6',2''-(4",4"-difluoro-1'',3'',5'',7''-tetramethyl-8"-methyl-4"-bora-3"a,4"a-diaza-s-indacene); **18 polymer**; **19** (4,4-difluoro-1,3,5,7-tetramethyl-8-aza-4-bora-3a,4a-diaza-s-indacene); **20** (4,4-difluoro-1,3,5,7-tetramethyl-8-aza-4-bora-3a,4a-s-indacene)-6,2'-methyl-(4'4'-difluoro-1',3',5',7'-tetramethyl-8'-aza-4'-bora-3'a,4'a-s-indacene); **21** (4,4-difluoro-1,2,5,6,7-pentamethyl-4-bora-3a,4a-s-indacene); **22** (1,2,3,5,6,7-hexamethyl-4-bora-3a,4a-s-indacene-4-bora-3a,4a-s-indacene); **23** (1,2,5,6,7-pentamethyl-4-bora-3a,4a-s-indacene)-3,5'-methyl-(1',2',3',6',7'-pentamethyl-4'-bora-3'a,4'a-indacene).

**Table 1. Photophysical Properties of the Studied BODIPY Compounds.**

| *Dye* | $\lambda_{max}(abs)$ *(nm)* | $\lambda_{max}(fluor)$ *(nm)* | $\varepsilon(10^4\ M^{-1}\ cm^{-1})$ | $\Phi_{fluor}$ | $E_s$ *(eV)* |
|---|---|---|---|---|---|
| **1** | 352,506 | 515 | 0.74,8.2 | 0.99 | 2.41 |
| **2** | 352,505 | 515 | 0.71,7.9 | 0.98 | 2.41 |
| **3** | 360,496 | 512 | 0.70,7.9 | 0.99 | 2.42 |
| **4** | 371,521 | 538 | 0.68,7.5 | 0.99 | 2.31 |
| **5** | 379,527 | 566 | 0.60,6.8 | 0.75 | 2.19 |
| **6** | 386,524 | 588 | 0.60,5.2 | 0.50 | 2.11 |
| **7** | 368,520 | 532 | 0.79,8.4 | 0.99 | 2.33 |
| **8** | 432,596 | 623 | 0.79,4.6 | 0.50 | 1.99 |
| **9** | 385,549 | 572 | 0.68,6.8 | 0.92 | 2.17 |
| **10** | 372,518 | 532 | 0.74,8.80 | 0.8 | 2.33 |
| **11** | 389,466, 556 | 643 | 1.66, 6.44, 7.36 | 0.7 | 1.93 |
| **12** | 376,523 | 541 | 0.70,8.60 | 1.0 | 2.29 |
| **13** | 359,501 | 513 | 0.74,8.7 | 0.97 | 2.43 |

Table 1 is continued.

| | | | | | |
|---|---|---|---|---|---|
| **14** | 368, 526 | 563 | 1.5, 15.0 | 0.66 | 2.20 |
| **15** | 368, 535 | 573 | 1.6, 15.7 | 0.66 | 2.17 |
| **16** | 370,550 | 587 | 2.3,22.5 | 0.60 | 2.13 |
| **17** | 372,562 | 596 | 2.35, 23.0 | 0.60 | 2.09 |
| **18** | 378,590 | 614 | 11.0, 155.0 | 0.35 | 2.02 |
| **19** | 468, 647 | 682 | 0.60, 8.5 | 0.30 | 1.82 |
| **20** | 488, 696 | 720 | 1.2, 16.0 | < 0.01 | 1.72 |
| **21** | 383,524 | 537 | 0.9, 8.8 | 1.0 | 2.30 |
| **22** | 380, 529 | 541 | 1.0, 8.9 | 1.0 | 2.29 |
| **23** | 387, 489, 562 | 650 | 1.66, 6.44, 7.36 | 0.7 | 1.91 |

Scheme 1 shows list of the compounds used in the current investigations. Large series of compounds were studied and properties of all the studied compounds are described in different chapters of dissertation.

**Table 2.** Electrochemical and Electrogenerated Chemiluminescence Properties of BODIPY Compounds.

| *Dye* | $E_{1/2}$ *(V vs. SCE)* | | $\lambda_{max}$ | $\Phi_{ECL}$ | $\Delta H_s$ | *D x* $10^6$ |
|---|---|---|---|---|---|---|
| | $A/A^-$ | $A/A^+$ | *(ECL) (nm)* | | *(eV)* | $(cm^2/s)$ |
| **1** | -1.27 | 1.16 | 532 | 0.0006 | 2.23 | 7.0 |
| **2** | -1.22 | 1.11 | 534 | 0.002 | 2.23 | 7.0 |
| **3** | -1.22 | 1.12 | 540 | 0.006 | 2.24 | 7.0 |
| **4** | -1.37 | 0.95 | 551 | 0.21 | 2.22 | 6.6 |
| **5** | -1.34 | 0.98 | 572 | 0.15 | 2.22 | 6.2 |
| **6** | -1.31 | 0.99 | 600 | 0.05 | 2.20 | 6.0 |
| **7** | -1.33 | 1.02 | 566, 706 | 0.19 | 2.25 | 6.1 |
| **8** | -0.82 | 1.14 | 630 | 0.01 | 1.98 | 6.9 |
| **9** | -1.2, -1.42 | 0.98 | 614 | 0.002 | 2.24 | 6.1 |
| **10** | -1.21 | 1.30 | 540, 669 | 0.18 | 2.30 | 6.1 |
| **11** | -1.40 | 1.01 | 560 | 0.17 | 2.22 | 6.3 |
| **12** | -1.34, -1.59 | 0.97, 1.47 | 666 | 0.1 | 2.17, 2.85 | 5.0 |

Table 2 is continued.

| | | | | | | |
|---|---|---|---|---|---|---|
| **13** | -1.19 | 1.14 | 538 | 0.007 | 2.24 | 7.0 |
| **14** | -1.17, -1.29 | 1.09, 1.31 | 587 | 0.008 | 2.18 | 5.2 |
| **15** | -1.15, -1.27 | 1.10, 1.37 | 596 | 0.008 | 2.16 | 5.2 |
| **16** | -1.15, -1.24, -1.43 | 1.04, 1.17, 1.42 | 607 | 0.011 | 2.09 | 4.8 |
| **17** | -1.13, -1.23, -1.43 | 1.11, 1.24, 1.50 | 608 | 0.016 | 2.08 | 4.8 |
| **18** | many | many | 620 | <0.001 | 1.90 | 1.4 |
| **19** | -0.44 | 1.14 | 695 | <0.001 | 1.40 | 7.0 |
| **20** | -0.37, -0.5 | 1.10, 1.24 | - | - | - | 5.2 |
| **21** | -1.29 | 1.09, 1.54 | 560, 656 | 0.005 | 2.28 | 6.8 |
| **22** | -1.27 | 1.08 | 565 | 0.008 | 2.25 | 6.6 |
| **23** | -1.20, -1.57 | 0.97, 1.47 | 679 | 0.004 | 2.07 | 5.2 |

### 3.2. Dependence of Electrochemical and ECL properties on the Structure of BODIPY Dyes. Unusually Large Separation Between Sequential Electron Transfers.

#### 3.2.1. Photophysical studies.

Photophysical studies of the selected BODIPY dyes were carried out for all dyes presented in Scheme 5 and shown in Figure 7.

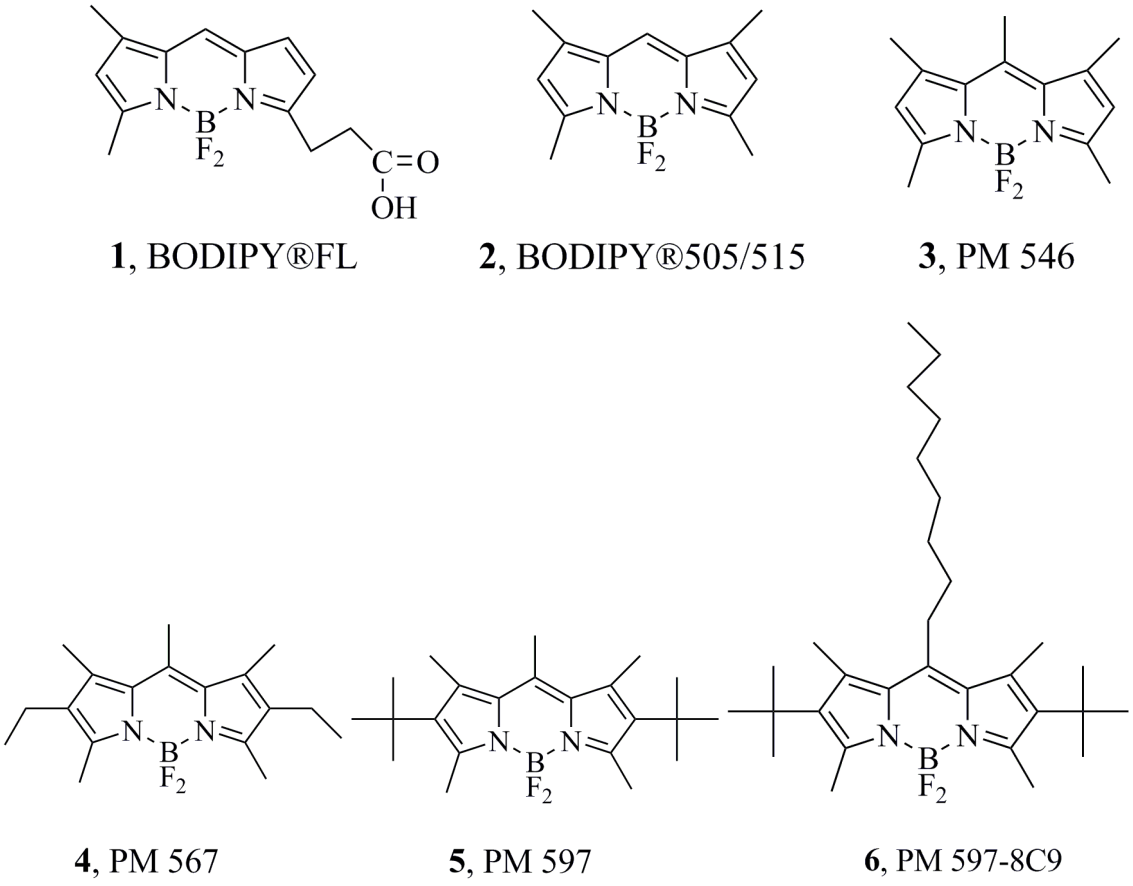

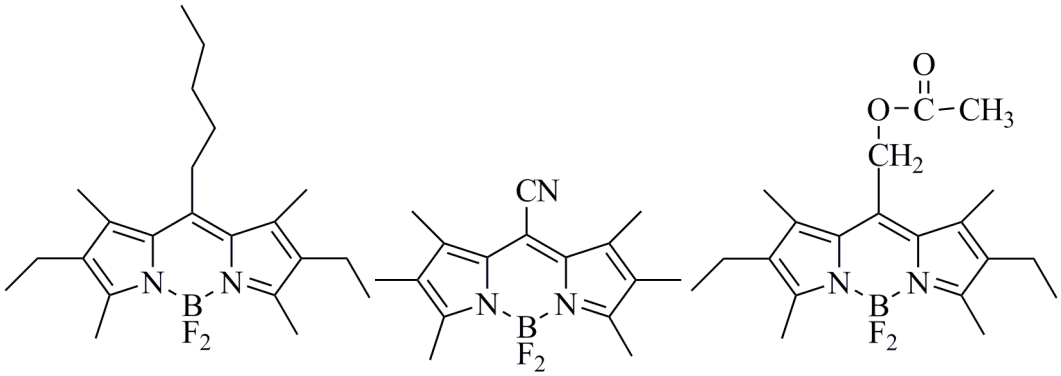


**7**, PM 567A **8**, PM 650 **9,** PM 605

**Scheme 5.** Chemical structures of the used dyes used in the current chapter.

All of the compounds showed high fluorescence quantum yields, $\Phi_{fluor}$; these were highest for the green and yellow fluorescent dyes and lower for the red fluorescent alkyl substituted dye molecules and in the presence of the cyano group.

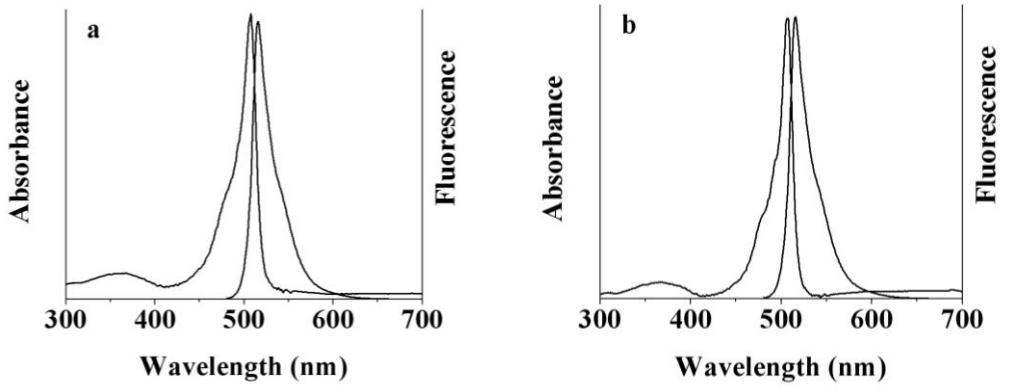

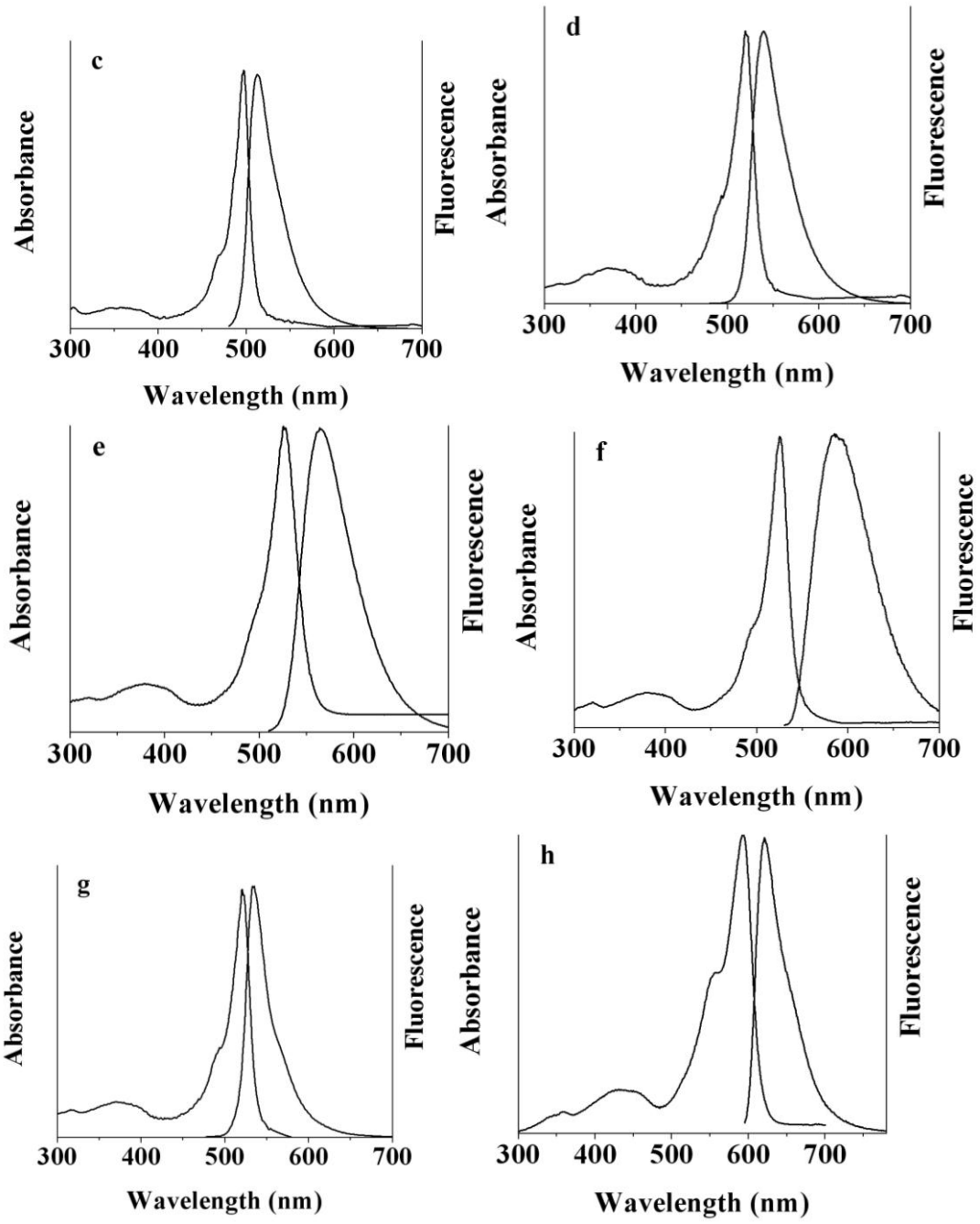
c
Absorbance
Fluorescence
300
400
500
600
700
Wavelength (nm)
d
Absorbance
Fluorescence
300
400
500
600
700
Wavelength (nm)
e
Absorbance
Fluorescence
300
400
500
600
700
Wavelength (nm)
f
Absorbance
Fluorescence
300
400
500
600
700
Wavelength (nm)
g
Absorbance
Fluorescence
300
400
500
600
700
Wavelength (nm)
h
Absorbance
Fluorescence
300
400
500
600
700
Wavelength (nm)

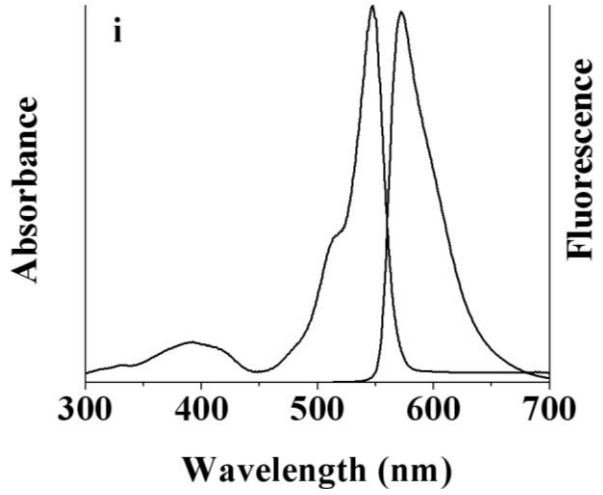


**Figure 7.** Absorption and fluorescence spectra of 2 μM BODIPY dyes in DCM: (a) **1**; (b) **2**; (c) **3**; (d) **4**; (e) **5**; (f) **6**; (g) **7**; (h) **8**; (i) **9**.

Dyes without substitution in positions 2 and 6 (**1, 2** and **3**) show green PL (Figure 7a-c). Addition of alkyl substitution to these positions causes a bathochromic shift of the absorbance and fluorescence spectra. Methylation of positions 2 and 6 caused a red shift of the fluorescence from green to yellow (**4** and **7**) due to the stabilization of the excited state through a positive inductive effect (Figure 7d,g). Addition of the bulkier t-butyl substituents to positions 2 and 6 caused an even larger spectral red shift (**5** and **6**) and also a larger Stokes shift compared with methylated dyes as a result of the geometric restrictions (Figure 7e,f). Dyes **5** and **6** also showed broader emission, which can be taken as evidence of a larger degree of steric interactions in the system. Contrary to this, alkylation of the meso position does not have a substantial effect on the spectra. There is a small blue-shift with addition of a donating group, although this effect depends on the molecular structure. The spectroscopic properties of the meso-cyanide dye **8** are special due to the high red shift as compared with non-substituted compounds by simply

changing substitution in one position (Figure 7g). The cyano group is an electron acceptor and can provide stabilization of the LUMO state, causing a decrease in the energy band gap. This shift was only seen for addition of the cyano group to the meso-position, since its presence in positions 2 and 6 result in an emission wavelength that is very close to the corresponding alkyl derivatives. The effect of the cyano group on the fluorescence is opposite to the effect of donor methyl groups. Dye **9** has an acetoxymethyl group in its structure in the meso-position. This dye showed relatively high fluorescent activity with a maximum at 575 nm and an intermediate Stokes shift of 32 nm (Figure 7h).

### 3.2.2. Electrochemical properties

Cyclic voltammograms of the dyes are shown, for initial scans towards negative and positive potentials (Figures 8-13).

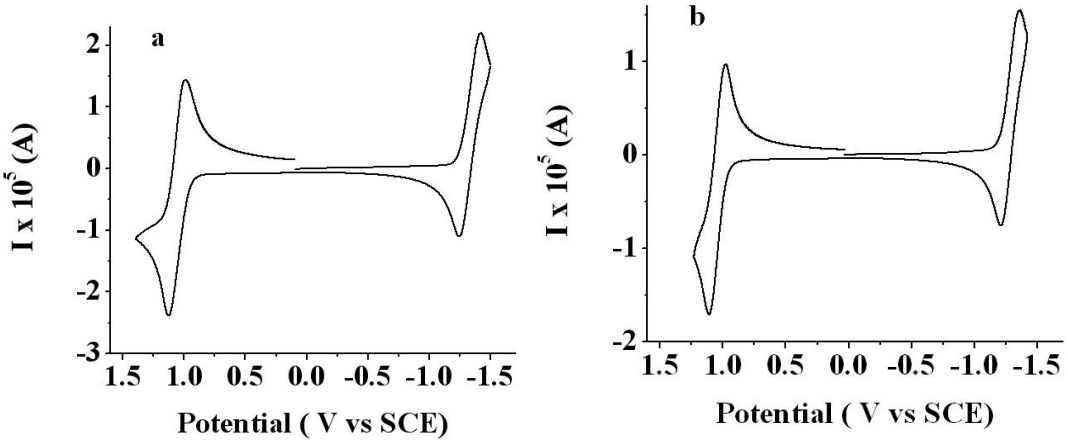

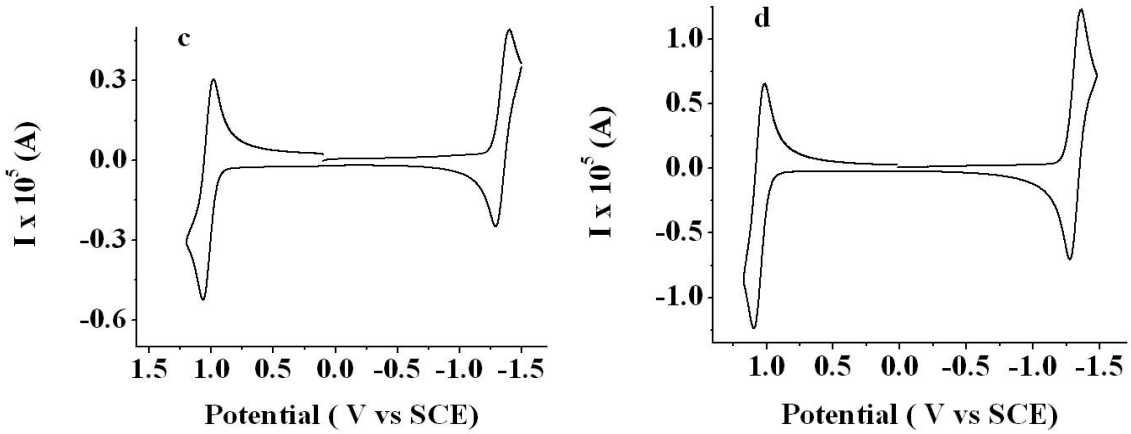


**Figure 8.** Cyclic voltammograms of the completely substituted BODIPY dyes (**4-7**) at a scan rate of 0.1 V/s in DCM at Pt working electrode (area = 0.0314 $cm^2$); supporting electrolyte: 0.1 M $TBAPF_6$; (a) 3 mM **4**; (b) 2.2 mM **5**; (c) 0.6 mM **6**; (d) 1.5 mM **7.**

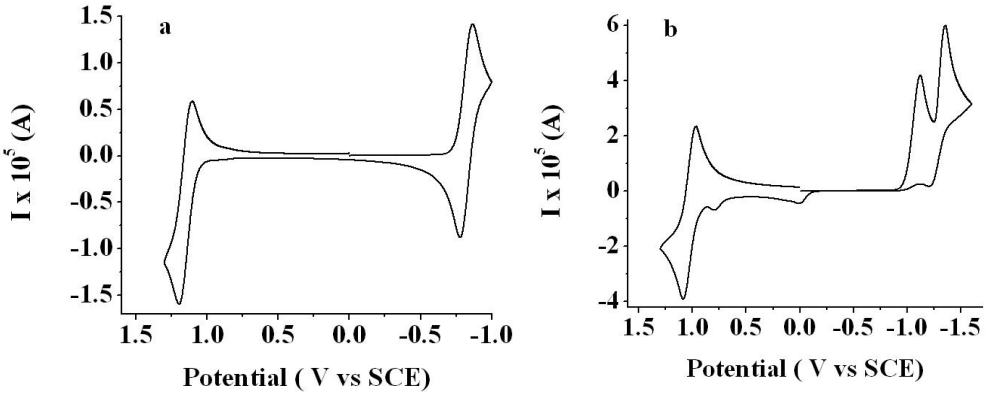


**Figure 9.** Cyclic voltammograms of BODIPY dyes **8** and **9** at a scan rate of 0.1 V/s in DCM at Pt working electrode (area = 0.0314 $cm^2$); supporting electrolyte: 0.1 M $TBAPF_6$; (a) 2.5 mM **8**; (b) 7 mM **9**.

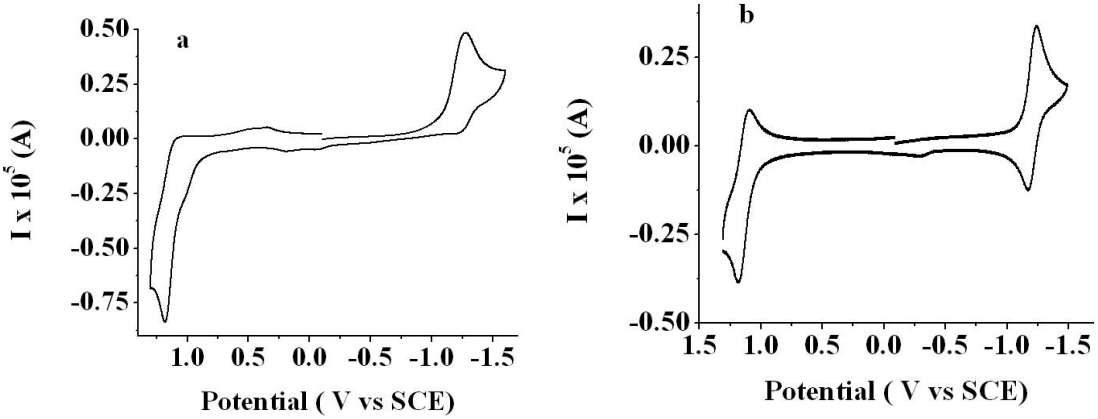

**Figure 10.** Cyclic voltammograms of 2,6,8-unsubstituted BODIPY dyes at a scan rate of 0.1 V/s in DCM at Pt working electrode (area = 0.0314 $cm^2$); supporting electrolyte: 0.1 M $TBAPF_6$: (a) 0.7 mM **1**; (b) 0.4 mM **2**.

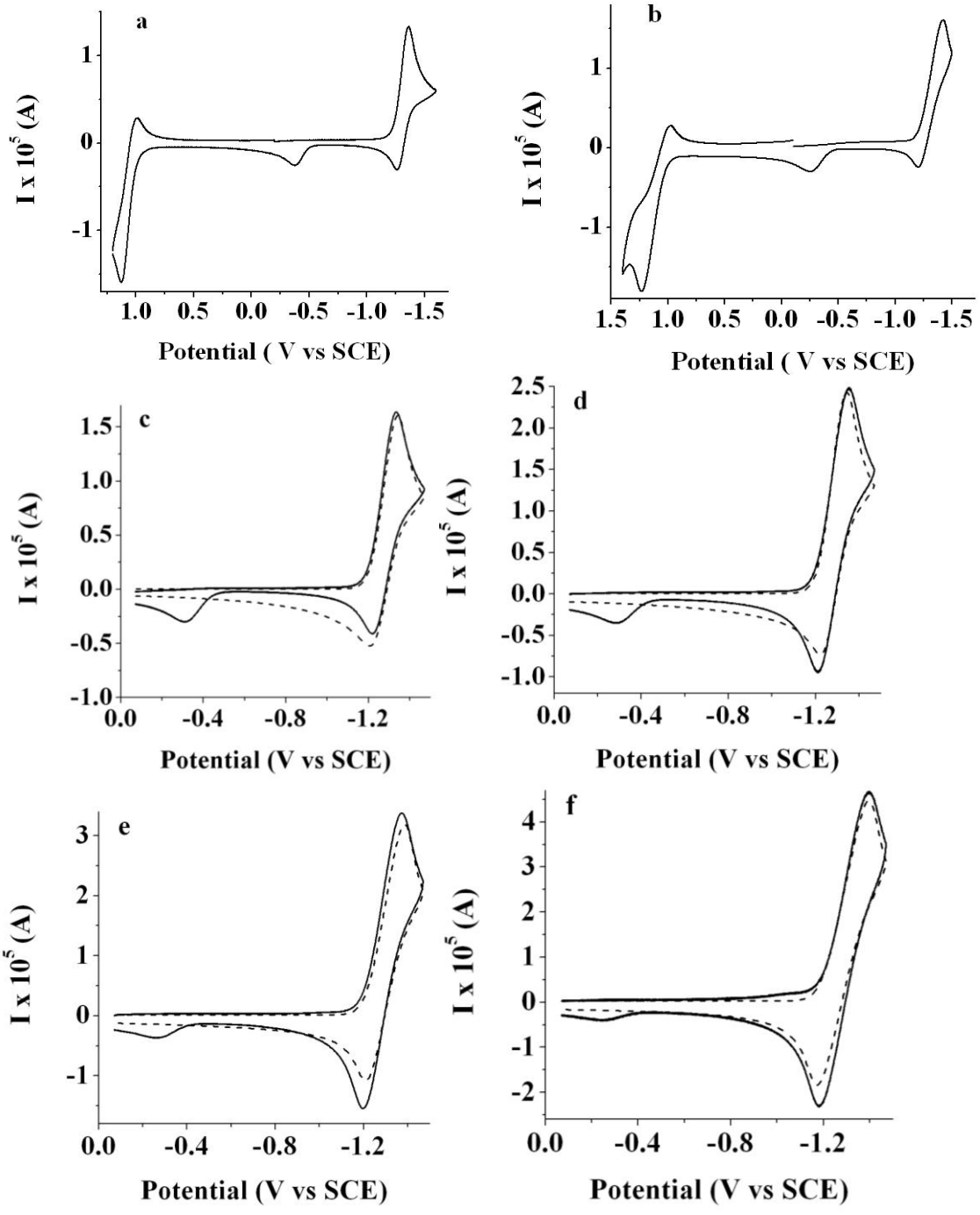

**Figure 11.** (a) and (b) Cyclic voltammograms for (a) 1.9 mM and (b) 2.3 mM of **2**; (c)-(f) Experimental (solid line) and simulated parameters (dashed line) for reduction of 2.4 mM of **2**; (c) 0.1 V/s; (d) 0.25 V/s; (e) 0.5 V/s; (f) 1 V/s; Experimental data: solvent: DCM; supporting electrolyte: 0.1 M $TBAPF_6$; electrode area: 0.0314 $cm^2$. Simulated data: diffusion coefficient 7.0 x $10^{-6}$ $cm^2/s$; uncompensated resistance 2000 Ω, capacitance 3 x $10^{-7}$ F and kinetics constant of 2 $s^{-1}$ were used in simulations.

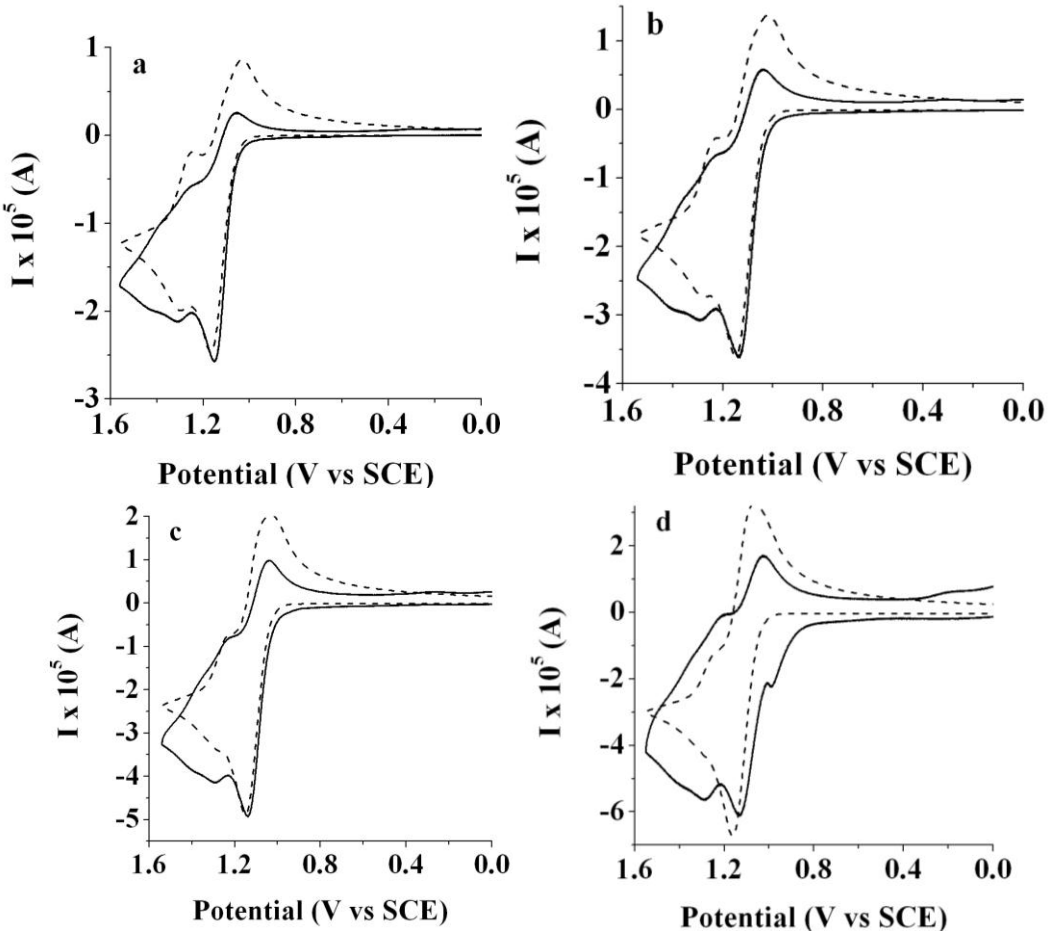

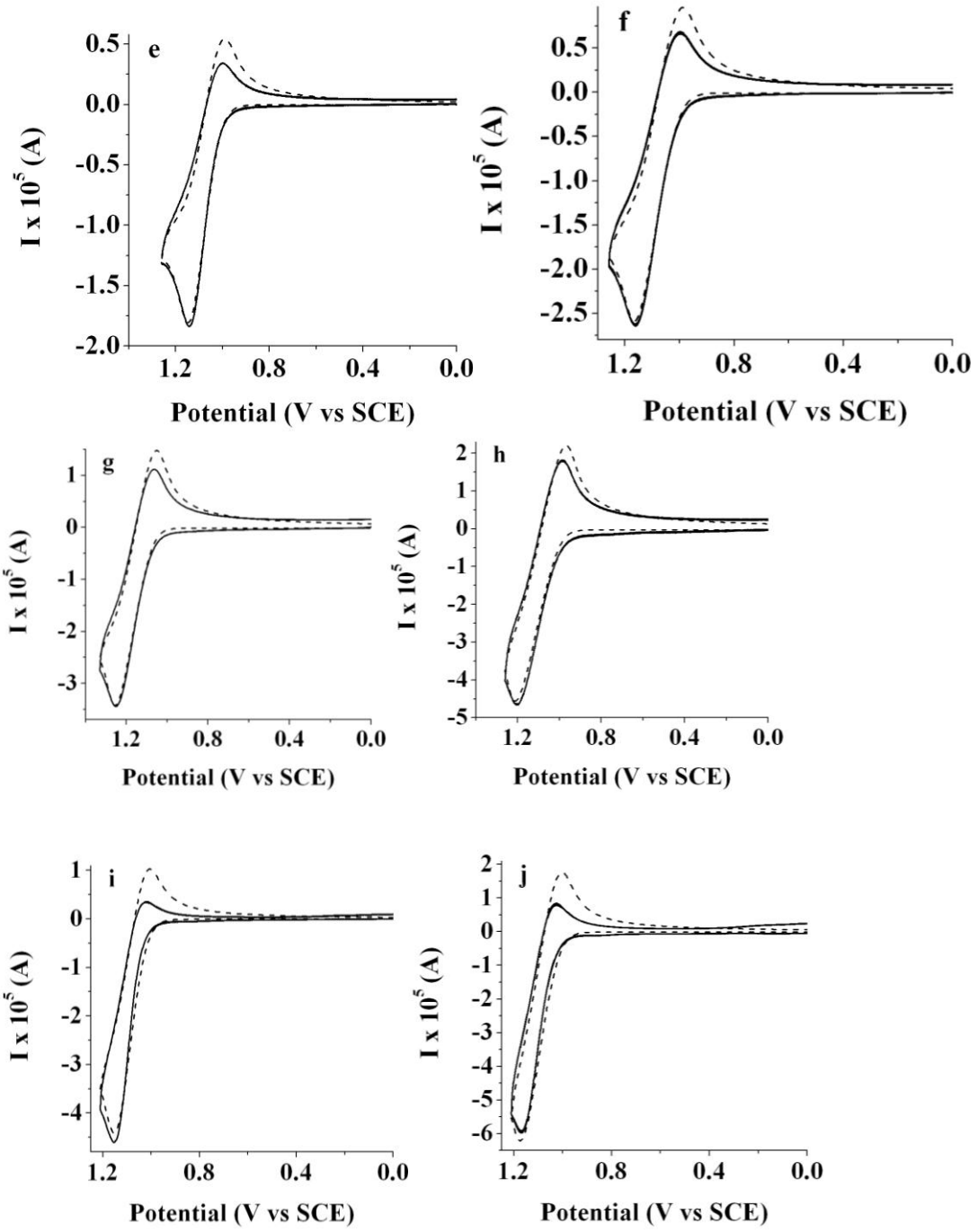
e
f
g
h
i
j
I x 10^5 (A)
Potential (V vs SCE)

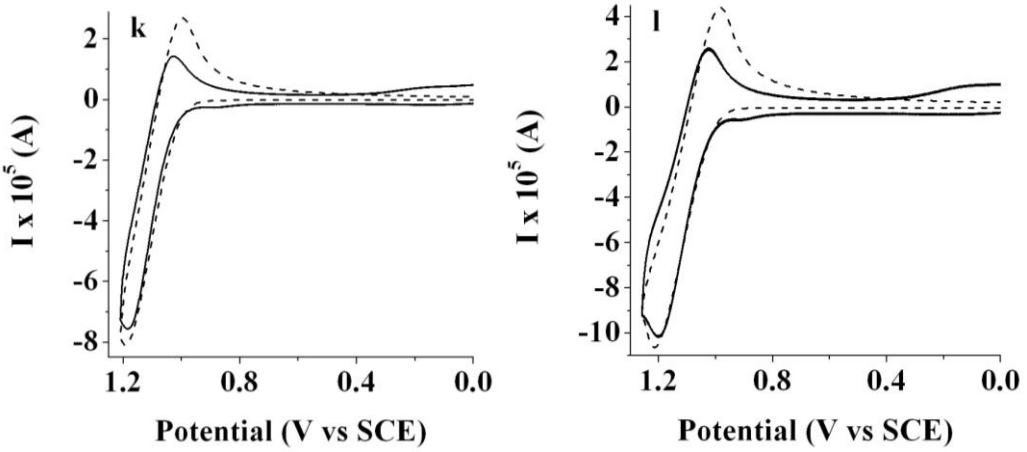


**Figure 12.** (a-h) Experimental (solid line) and simulated (dashed line) data for 2.4 mM **2**: (a) and (e) 0.1 V/s; (b) and (f) 0.25 V/s; (c) and (g) 0.5 V/s; (d) and (h) 1 V/s; Experimental (solid line) and simulated (dashed line) data for 5.2 mM **2**: (i) 0.1 V/s; (j) 0.25 V/s; (k) 0.5 V/s; (l) 1 V/s. Experimental data: solvent: DCM; supporting electrolyte: 0.1 M $TBAPF_6$; electrode area: 0.0314 $cm^2$. Simulated data: diffusion coefficient for the monomer is 7.0 x $10^{-6}$ $cm^2/s$ and dimer 5.2 x $10^{-6}$ $cm^2/s$; uncompensated resistance 2000 Ω (a-h) and 1000 Ω (i-l), capacitance 3 x $10^{-7}$ F, dimerization constant of 400 $M^{-1}$ $s^{-1}$ and $10^{10}$ $s^{-1}$ deprotonation constant were used in simulations.

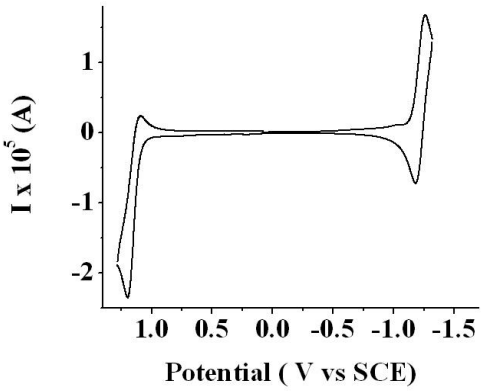


**Figure 13.** Cyclic voltammogram of 2.2 mM 2,6-unsubstituted BODIPY dye **3** at a scan rate of 0.1 V/s in DCM at Pt working electrode (area = 0.0314 $cm^2$); supporting electrolyte: 0.1 M $TBAPF_6$.

Electrochemical studies of the totally substituted dyes **4, 5, 6** and **7** show reversible reduction and oxidation waves in both positive and negative directions with peaks near

-1.4 V and 1.3 V that depend slightly on the substituent present (Figure 8). The cyclic voltammograms are for initial scans in the negative direction. Experiments with initial scans to the positive direction do not show the appearance of any additional peaks. There is a slightly smaller separation between the oxidation and reduction peaks for dyes **5** and **6** containing the t-butyl groups (Figure 8b,c). Thus both radical anion and cation are quite stable because of the substituents, which block dimerization and attack by nucleophilic and electrophilic species. Cyclic voltammograms of dye **8** show a reversible reduction with $E_{1/2}$ = -0.82 V and reversible oxidation with $E_{1/2}$ =1.14 V (Figure 9a). The addition of the acceptor cyano group in the 8 position makes this species much easier to reduce by about 0.4 to 0.5 V. This corresponds fairly well with the photophysical properties and longer emission wavelength for **8**. Dye **9**, with an acetoxymethyl-substituent in the 8 position, shows high stability on oxidation, but instability on reduction because of electron transfer to the substituent (Figure 9b). This produces an additional 1e reduction wave with a peak at -1.2 V, which is earlier than the next BODIPY wave with a peak at -1.42 V. There is also an additional small oxidation peak at 0.1 V when the potential was first scanned in the negative direction that is not present on an initial positive scan. This is therefore from products of the reduction. The additional waves could correspond to ester decomposition products that are sometimes seen for aromatic esters.[106] However, simple alkyl esters are usually not oxidized easily.

Both oxidation and reduction for dye **1,** which is unsubstituted in positions 1, 2, 6 and 8 are electrochemically irreversible (Figure 10a). No electrochemical waves were observed that were attributable to the reduction of propionic acid in the studied range. Dye **2** with

positions 2, 6 and 8 missing shows similar behavior to **1,** with slightly higher reversibility on the oxidation because of the presence of the substitution in position 1 (Figure 10b). There is also a noticeably higher degree of irreversibility on reduction with higher concentrations of the dye with formation of a surface wave at around 0 V (Figure 11a,b). Reduction behavior can be simulated by assuming an EC mechanism with the kinetic constant of 2 $s^{-1}$ (Figure 11c-f). There is no evidence of coupling processes on reduction, such as concentration dependent CV behavior. However on oxidation, the appearance of a second wave while scanning to further positive potentials and concentration dependence can be seen as evidence for a coupling reaction (Figure 12). A dimerization mechanism with the coupling constant of 400 $M^{-1}$ $s^{-1}$ is proposed as the reaction mechanism and fitted to digital simulations:

$$R\text{-}H_2 \rightarrow R\text{-}H_2^{\bullet+} + e \qquad E_{1/2}{}^1 = 1.11\ V \qquad (43)$$

$$R\text{-}H_2^{\bullet+} + R\text{-}H_2^{\bullet+} \rightarrow H_2R\text{-}RH_2^{2+} \qquad k_{dim} = 400\ M^{-1}\ s^{-1} \qquad (44)$$

$$H_2R\text{-}RH_2^{2+} \rightarrow HR\text{-}RH + 2H^+ \ \text{(fast)} \qquad k > 10^4\ s^{-1} \qquad (45)$$

$$HR\text{-}RH \rightarrow HR\text{-}RH^{\bullet+} + e \qquad E_{1/2}{}^2 = 1.03\ V \qquad (46)$$

$$HR\text{-}RH^{\bullet+} \rightarrow HR\text{-}RH^{2+} + e \qquad E_{1/2}{}^d = 1.27\ V \qquad (47)$$

Concentration dependence can be seen as a proof that oxidative coupling is responsible for the appearance of the second electrochemical wave and not just consecutive reaction with solvent.[107-109] Deprotonation constant of more $10^4$ $s^{-1}$ also fits simulation fairly well and the number shown in the equation corresponds with the fast process. The electrode must be continuously polished during electrochemical investigations because of the

formation of a blocking film after several consecutive cycles. This may be seen as a further sign of the coupling processes. Dye **3** shows nernstian reduction, but oxidation behavior similar to **1** and **2,** due to the presence of the methyl group in the position 8 and absence of substitution in positions 2 and 6 (Figure 13). This confirms that missing substitution in positions 2 and 6 affects the oxidation but not the reduction.

### 3.2.3. Potential difference between sequential oxidation and reduction waves

Oxidation and reduction scans of the dyes to more negative and more positive potentials can provide information about the energies needed to form the dianions and dications of these compounds (Figure 14).

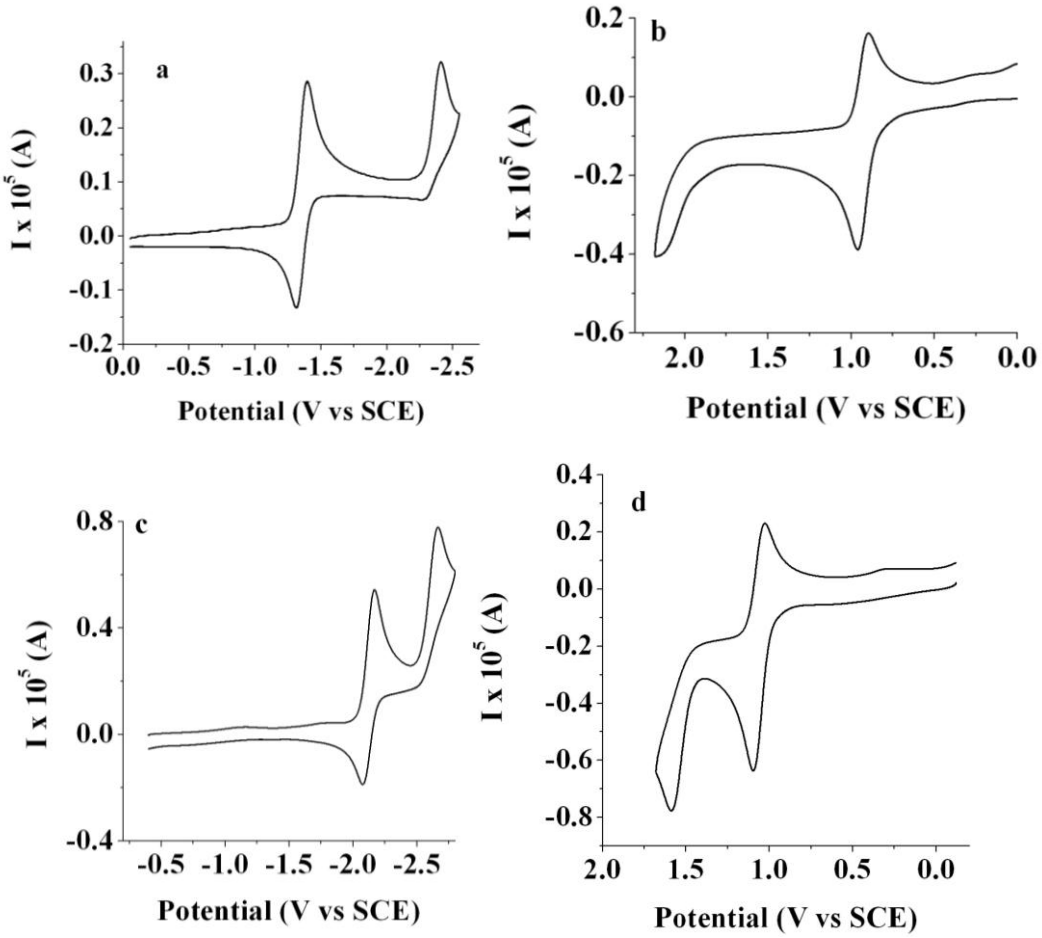


**Figure 14.** Cyclic voltammograms of (a,b) BODIPY dye **4** and (c,d) 9,10-diphenylanthracene at a scan rate of 0.1 V/s at Pt working electrode (area = 0.0314 $cm^2$); supporting electrolyte: 0.1 M $TBAPF_6$; solvent THF: (a) 0.5 mM **4**; (c) 1.0 mM 9,10-diphenylanthracene; solvent: acetonitrile: (b) 0.6 mM **4**; (d) 1.0 mM 9,10-diphenylanthracene.

Reduction of the dyes at more negative potentials generally produced a second peak attributed to the addition of a second electron. Most reduction experiments were carried out in THF because it has a wider potential range for reduction than MeCN and DCM and a higher stability of anions. All oxidations were studied in MeCN, which showed a relatively high stability of the radical cations over a wide potential window. The separation between the first and second reduction waves ($\Delta E_c$) was 1.0 to1.25 V, while that for the oxidation waves ($\Delta E_a$) was 1.2 to 1.3 V for the alkyl substituted dyes (Figure 14a,b). The second reduction and oxidation waves are irreversible, as is frequently seen with dications and dianions. The general instability of the dianions usually involves a following homogeneous reaction that causes a shift of the waves to less extreme potentials (i.e. to more positive potentials for oxidation and more negative potentials for reduction). Reversible behavior to the dianion and clean electrochemistry at very negative potentials can be seen in liquid ammonia, but this can only increase $\Delta E_c$. Experiments with many other BODIPY have demonstrated that an unusually large potential separation between two sequential reduction and oxidation waves is a characteristic feature of these dyes, as opposed to what is seen in general for aromatic compounds. For example the widely-investigated polycyclic hydrocarbon 9,10-diphenylanthracene (DPA) (Scheme 6) shows two oxidation and two reduction waves with the separation of 0.5 V (Figure 14c,d)[50]; this behavior is similar to the $\Delta E_c$ and $\Delta E_a$ seen for many polycyclic hydrocarbons. Electronic structure calculations were carried out to investigate the cause of this unusually large splitting between waves in the BODIPY dyes (Scheme 7, Table 3).

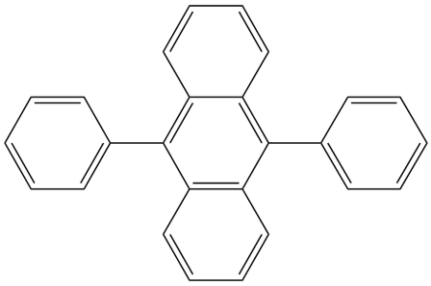

**Scheme 6.** Chemical structure of 9,10-diphenylanthracene.

Calculations of the thermodynamic properties of the completely substituted compounds **4** and **7** are compared with those for DPA. These represent sterically hindered systems with relatively high electrochemical stability on both oxidation and reduction. The parameters used in the calculations are presented in the dissertation of Sangik Cho[110]. The scheme used in the calculations is presented[111]:

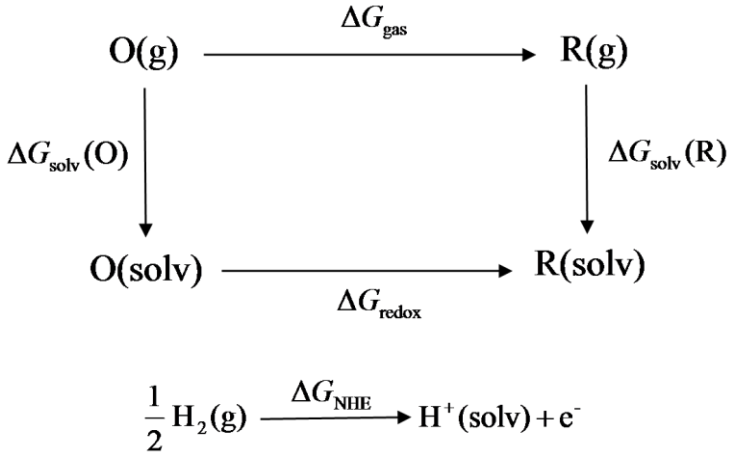


**Scheme 7.** Thermodynamic cycle connecting the oxidized (O) and the reduced state (R) in a solvent.

**Table 3.** Experimental and calculated reduction and oxidation potentials of BODIPY core, dyes **4** and **7** and 9,10-diphenylanthracene in tetrahydrofuran (reductions) and MeCN (oxidations).

| Compound | Half reaction | Electrode Potential | | Calculated Energy Terms, eV | |
|---|---|---|---|---|---|
| | | Exp. E °[a] | Calc. E °[b] | $\Delta\varepsilon_{elec.}$ [c] | $\Delta\Delta G_{solv}$ [d] |
| **4** | ox2 → ox1 | ~2.3 | 2.31 | -11.08 | 4.59 |
| | ox1 → neu | 0.94 | 0.89 | -6.52 | 1.44 |
| | neu → re1 | -1.37 | -1.67 | -0.83 | -1.70 |
| | re1 → re2 | ~-2.46 | -3.04 | 3.68 | -4.83 |
| **7** | ox2 → ox1 | ~2.3 | 2.40 | -10.99 | 4.40 |
| | ox1 → neu | 0.94 | 0.93 | -6.47 | 1.35 |
| | neu → re1 | -1.33 | -1.65 | -0.87 | -1.66 |
| | re1 → re2 | ~-2.42 | -3.06 | 3.49 | -4.62 |
| DPA | ox2 → ox1 | ~1.7 | 1.71 | -10.17 | 4.27 |
| | ox1 → neu | 1.2 | 0.89 | -6.38 | 1.30 |
| | neu → re1 | -2.1 | -2.10 | -0.34 | -1.75 |
| | re1 → re2 | -2.6 | -2.87 | 3.26 | -4.58 |

[a] Reference to SCE obtained from 0.342 V vs SCE for ferrocene couple.

[b] Reference to SCE obtained from 0.241 V vs NHE assuming aqueous system.

[c] The difference in electronic energies of reduced and oxidized species from DFT.

[d] The difference in $\Delta G_{solv}$ of reduced and oxidized species.

The calculated electrode potentials for both the reduction steps -2/-1 and -1/0 and oxidation steps +2/+1 and +1/0 agree quite well. The average difference between the first and the second electrode potentials for the BODIPY compounds is (experimental) 1.5 eV (oxidative wave) and 1.0 eV (reductive wave) and (calculated) 1.4 eV for both oxidative

and reductive waves. For 9,10-diphenylanthracene, the experimental values are 0.5 eV on both oxidative and reductive waves, compared to calculated values of 0.8 eV. Based on the calculations, one can compare the electronic (gas phase) and the solvation effects. For the BODIPY compounds the average difference of the solvation effects (the difference in $\Delta\Delta G_{solv}$ for all splittings) is 3.1 eV as compared to 2.9 eV for the splitting in DPA, so the solvation contribution is close to the same in both compounds, as would be expected from the similar size of the two molecules: 48 atoms for **4** and 44 for DPA. However the difference in $\Delta\varepsilon_{elec}$ (or $\Delta G_{gas}$), 4.5 eV for BODIPY vs. 3.6 eV for DPA is more significant. Thus the difference in electrochemical response is mainly accounted for by differences in the electronic properties, $\Delta\varepsilon_{elec}$, that are clear in the gas phase. The other features seen in calculations are a positive charge on the boron atom and a negative charge on the nitrogens, and the relatively large electron density on the central meso atom, that corresponds well with previous results. This then rationalizes why the absence of substitution in position 2 and 6 affects the stability of the radical cation and position 8 influences the stability of the anion radical.

### 3.2.4. Electrogenerated chemiluminescence

Dye **4** shows very stable orange ECL emission by radical ion annihilation with a maximum at 535 nm (Figure 15a).

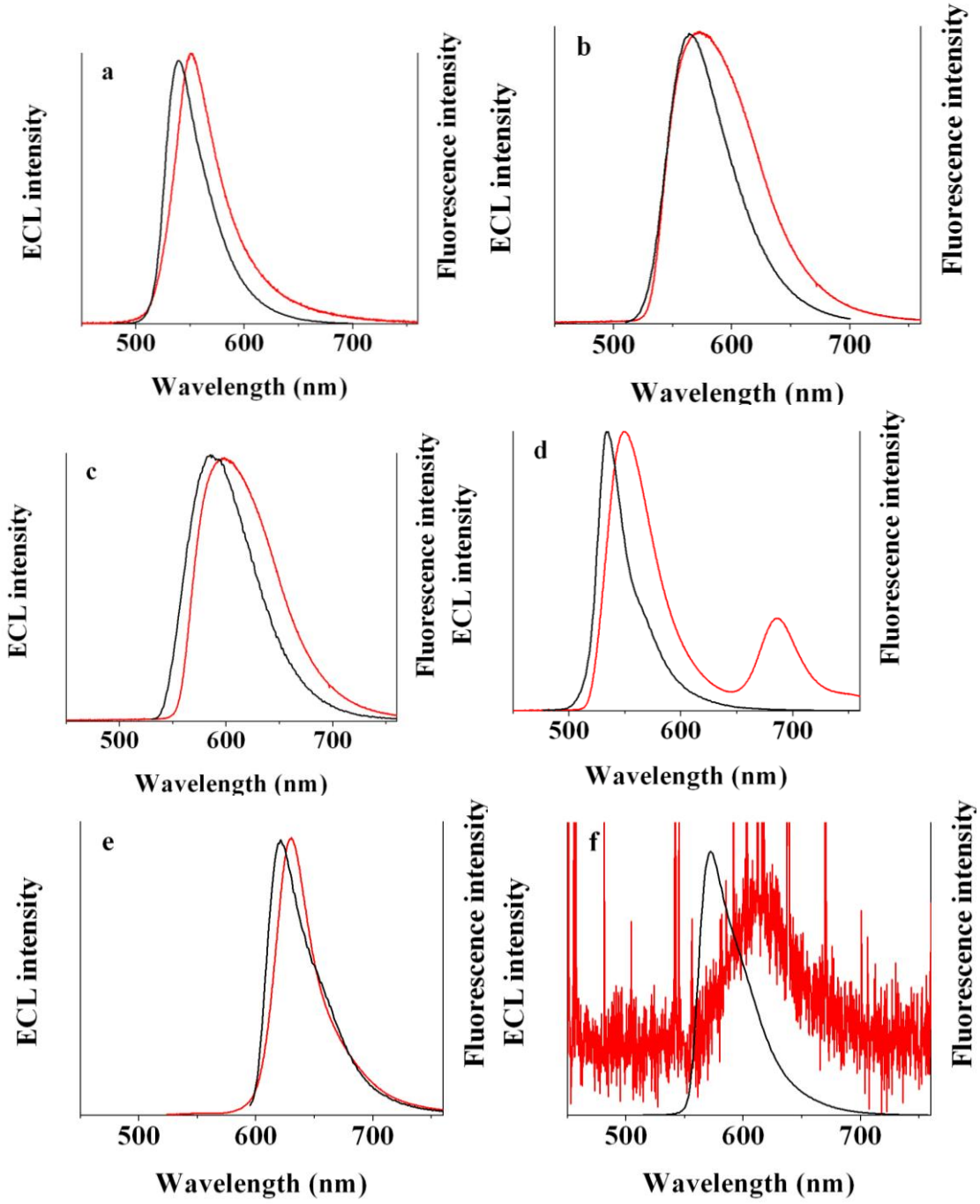
a
ECL intensity
Fluorescence intensity
500
600
700
Wavelength (nm)
b
ECL intensity
Fluorescence intensity
500
600
700
Wavelength (nm)
c
ECL intensity
Fluorescence intensity
500
600
700
Wavelength (nm)
d
ECL intensity
Fluorescence intensity
500
600
700
Wavelength (nm)
e
ECL intensity
Fluorescence intensity
500
600
700
Wavelength (nm)
f
ECL intensity
Fluorescence intensity
500
600
700
Wavelength (nm)

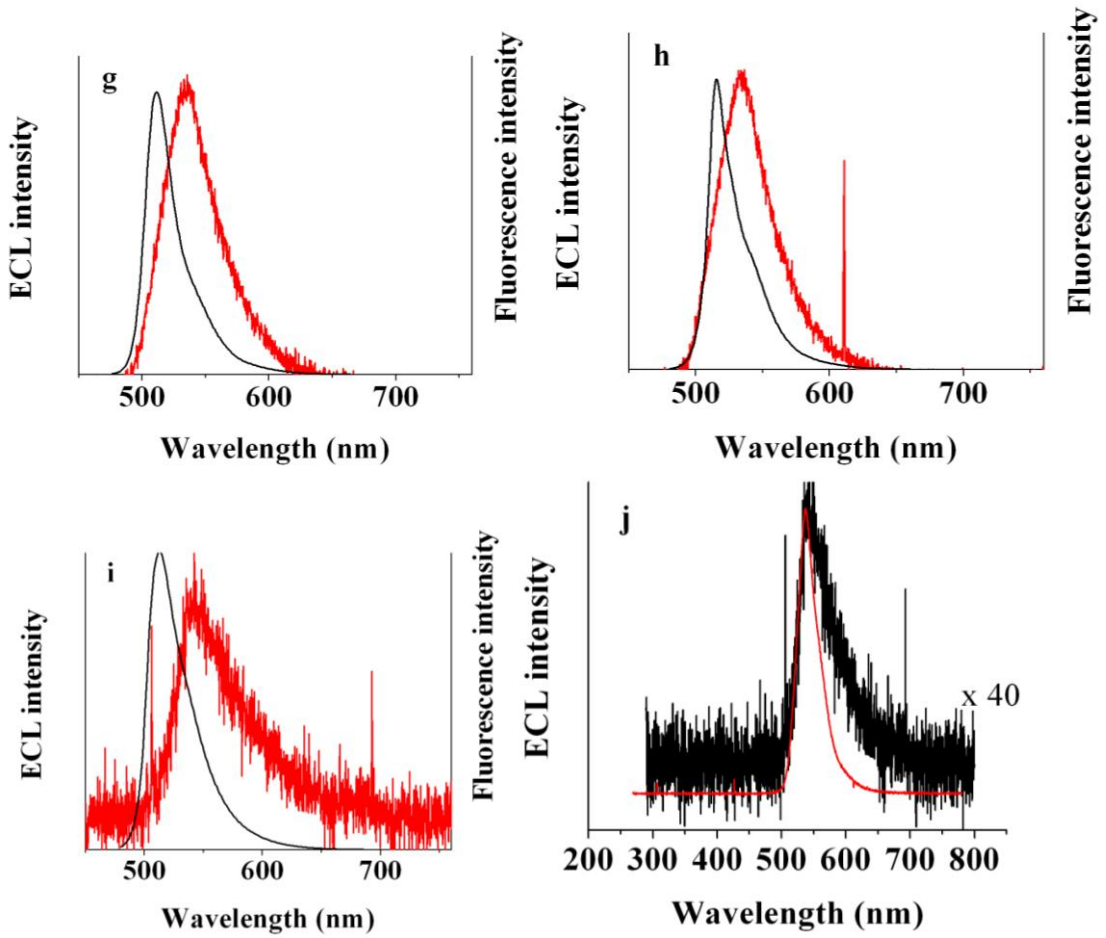


**Figure 15.** (a) ECL (red line) and fluorescence (black line) spectra for the BODIPY dyes of certain concentration: (a) 2.2 mM **4** (b) 2.2 mM **5**; (c) 2.2 mM **6**; (d) 2.3 mM **7**; (e) 2.2 mM **8**; (f) 2.2 mM **9** (g) 2 mM **1**; (h) 2.3 mM **2**; (i) 2.3 mM **3**; (a), (b), (c), (d), (e), (i) annihilation generated ECL; (g), (h), (i) in the presence of 10 mM BPO; (f) in the presence of 0.1 M TPrA; (j) comparison spectra of the annihilation ECL (black line) and in the presence of 10 mM BPO (red line); time of stepping: 1 minute and frequency of 10 Hz were used for all experiments; annihilation ECL was done from 80 mV of the peaks; coreactant ECL was done from 80 mV of the reduction and oxidation peaks; solvent: DCM in all cases except (f) where acetonitrile was used.

The peak position of the ECL spectrum is slightly red shifted as compared with the fluorescence spectrum due to an inner filter effect. Quantum efficiency calculations for ECL were carried out for multiple potential step annihilation experiments and obtained values were compared with results under similar for $Ru(bpy)_3^{2+}$. The uncertainty of results is at least ±20 % depending on the structure of the compound due to the possibility of fouling of the electrode from following chemical reactions (Figure 15b,c). Dyes **5** and **6** show broader ECL behavior under the same conditions comparable with the broader PL emission. No longer wavelength emission, attributable to aggregate or reaction product formation is seen for **6,** because of the presence of the blocking *tert*-butyl groups (Figure 15c). A longer wavelength band is seen with **7** however (Figure 15d). The intensity of ECL is lower for **6** compared with **5**, but sufficient to be able to record spectra with the CCD camera. Dye **8** shows a red shifted ECL compared with the alkyl substituted dyes as seen also with the PL results (Figure 15e). The relatively low ECL intensity for dye **8** compared with the methyl or ethyl substituted dyes can be explained by the presence of the acceptor cyano group that increases the nonradiative decay of the excited states. Annihilation experiments of dye **9** with reduction and oxidation at 80 mV past the peaks only produced low light intensities, insufficient to obtain spectra. Thus TPrA was used as a coreactant to obtain ECL spectra (Figure 15f). This low intensity of the spectrum can be caused by the unstable reduction product. Dyes **1** and **2** did not generate spectra, but the use of a reductive coreactant such as benzoyl peroxide (BPO) produced ECL emission of sufficient intensity to generate spectra (Figure 15g,h).

Attempts to use the oxidative coreactant TPrA were unsuccessful probably because oxidation in the presence of the BODIPY causes oxidative coupling with film formation. Compound **1** is used as a lipid probe in the fluorescence studies, but its ECL applicability in this case is complicated by the lack of substituents leading to instability of the radical ions, which is not a factor in PL studies. Dye **3** can generate light by an annihilation reaction although the efficiency is much lower compared with coreactant ECL as a result of the coupling process on oxidation (Figure 15i,j). No ECL products for the dimerization were observed because of the high stability of the radical anion and also fast film formation on oxidation.

The enthalpy of annihilation can be estimated from thermodynamics parameters: $\Delta G_{ann} = \Delta H_s - T\Delta S$, where entropic term is approximately equal to 0.1 eV. The process goes through the singlet state if the electrochemical energy is larger than the excited state energy needed to produce singlet state ($E_s$) (Tables 1 and 2). The results for the energy of annihilation and energy needed for ECL are fairly close for all used in all studies compounds. Similar phenomenon was seen for the compounds investigated in the next chapters and will not be discussed their.

### 3.3. Electrochemistry and Electrogenerated Chemiluminescence of n-Pentyl and Phenyl BODIPY Species. Formation of Aggregates from the Radical Ion Annihilation Reaction.

#### 3.3.1. Photophysical studies.

Absorption spectra of **10** show the presence of the usual BODIPY S0-S1 transition in the visible wavelength range and the S0-S2 transition in the UV (Scheme 8, Figure 16).

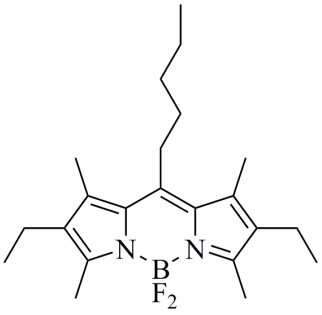

**10,** $B^8$-n-pentyl

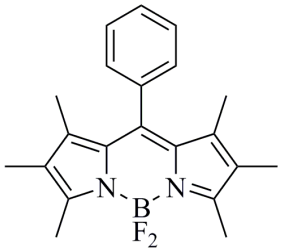

**11**, $B^8$-phenyl

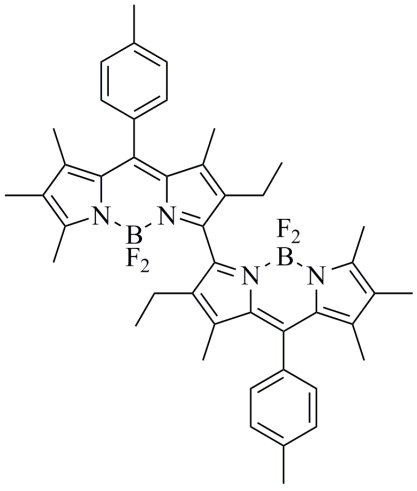

**12**, angular dimer

**Scheme 8.** Structures of the compounds used in the current chapter.

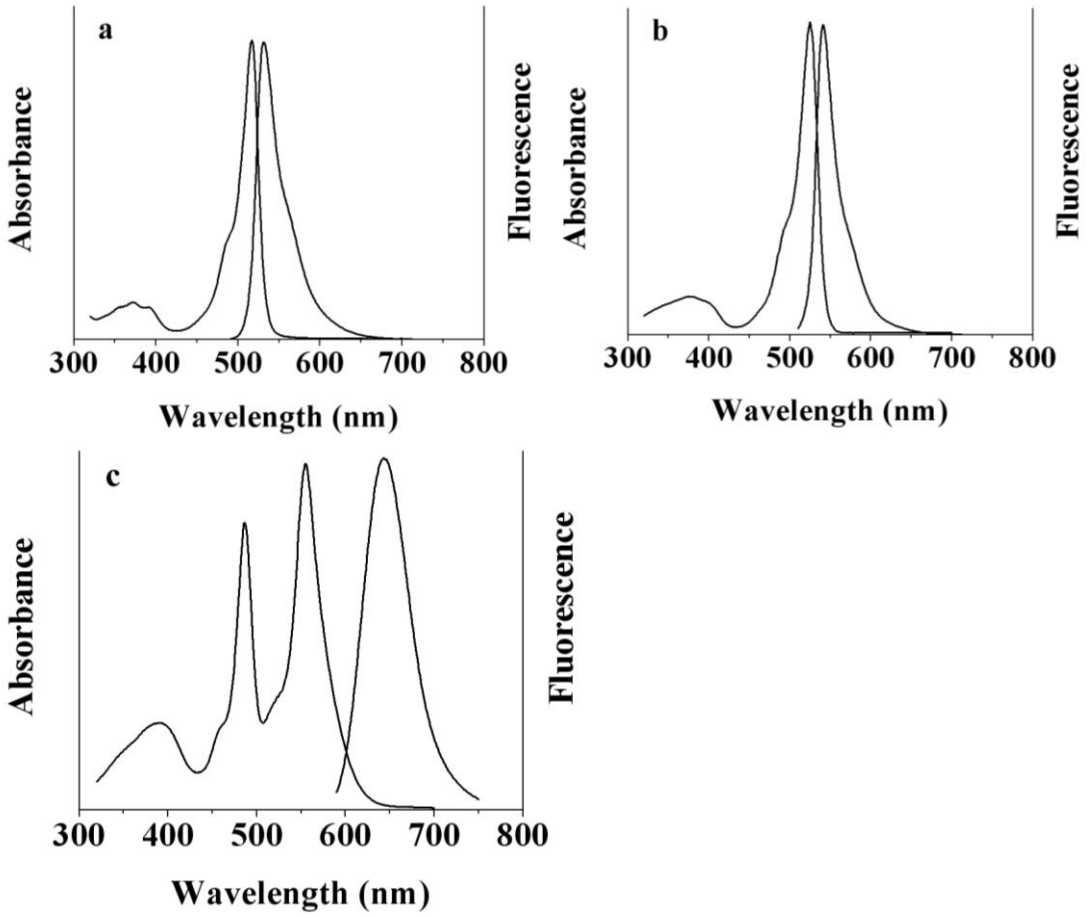


**Figure 16.** Absorption and fluorescence spectra of 2 μM BODIPY dyes: (a) **10** ($B^8$-n-pentyl) in acetonitrile; (b) **11** ($B^8$-phenyl) in DCM; (c) Dimer **12** in DCM.

Only one PL emission peak is observed over a concentration range of 10 μM to 5 mM (Figure 17).

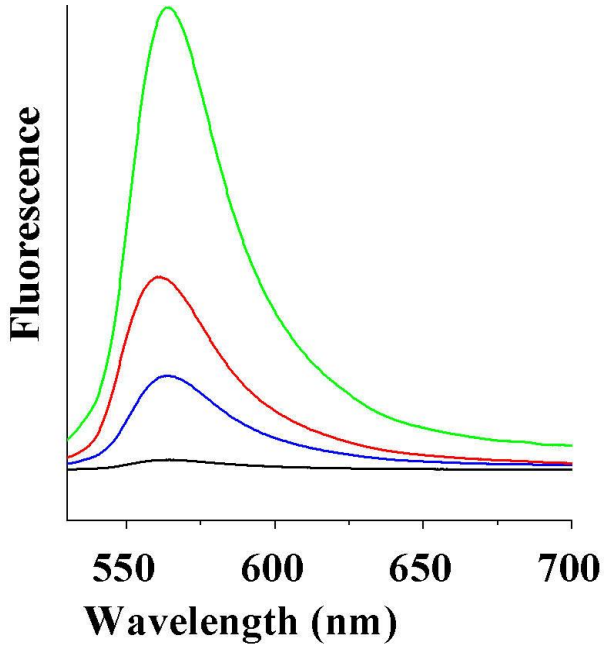


**Figure 17.** Fluorescence spectra for different concentrations of **10** ($B^8$-n-pentyl) in acetonitrile: (a) 0.01 mM (black line); 0.2 mM (blue line); 1 mM (red line); 5 mM (green line).

The quantum yield is 0.7 to 1 in MeCN, as is typical of many BODIPY dyes, with a relatively small Stokes shift. Addition of alkyl groups into the meso position causes no substantial changes in the spectroscopic properties, so the fluorescence maxima of $B^8$-n-pentyl **10** and the $B^8$-amide are about the same.[37] Absorption spectra of $B^8$-n-pentyl show the presence of the usual BODIPY S0-S1 transition in the visible wavelength range and the S0-S2 transition in the UV. Only one PL emission peak is observed over a concentration range of 10 μM to 5 mM (Figure 17). The quantum yield is 0.7 to 1 in MeCN, as is typical of many BODIPY dyes, with a relatively small Stokes shift. Addition of alkyl groups into the meso position causes no substantial changes in the spectroscopic properties, so the fluorescence maxima of **10** and the $B^8$-amide are about the same.

No evidence of dimerization or aggregation, e.g. changes with concentration, was found by the fluorescence measurements. **11** in DCM showed the usual BODIPY absorption (Figure 16b), and the dimer showed excitonic splitting of the S0-S1 523 nm transition in the monomer to one at lower and the other at higher energy (Figure 16c).[112] The fluorescence emission of the dimer **12** shows a peak red shifted as compared with the monomer. Fluorescence studies showed no differences over a wide range of concentrations, suggesting the absence of the intermolecular interactions. **11** and **12** showed the same location of the fluorescence emission in MeCN, DCM, ethanol and acetone with a dependence of the fluorescence quantum yield on solvent.

### 3.3.2. Electrochemical Studies

**10** showed chemically reversible electrochemistry on both oxidation and reduction (Figure 18).

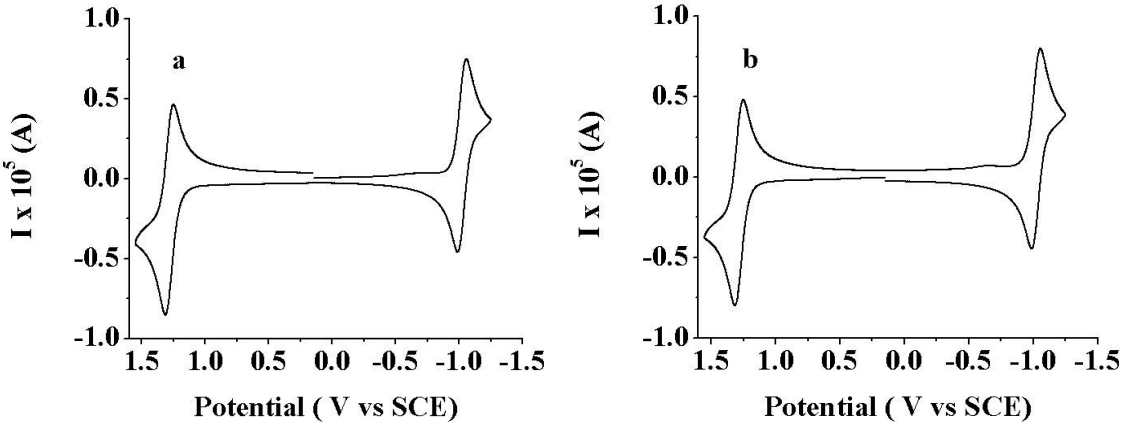


**Figure 18.** Cyclic voltammogram of 1.5 mM **10** ($B^8$-n-pentyl) at a scan rate of 0.1 V/s in acetonitrile at platinum working electrode (area = 0.0314 $cm^2$); supporting electrolyte: 0.1 M $TBAPF_6$: (a) forward scan to the negative direction; (b) forward scan to the positive direction.

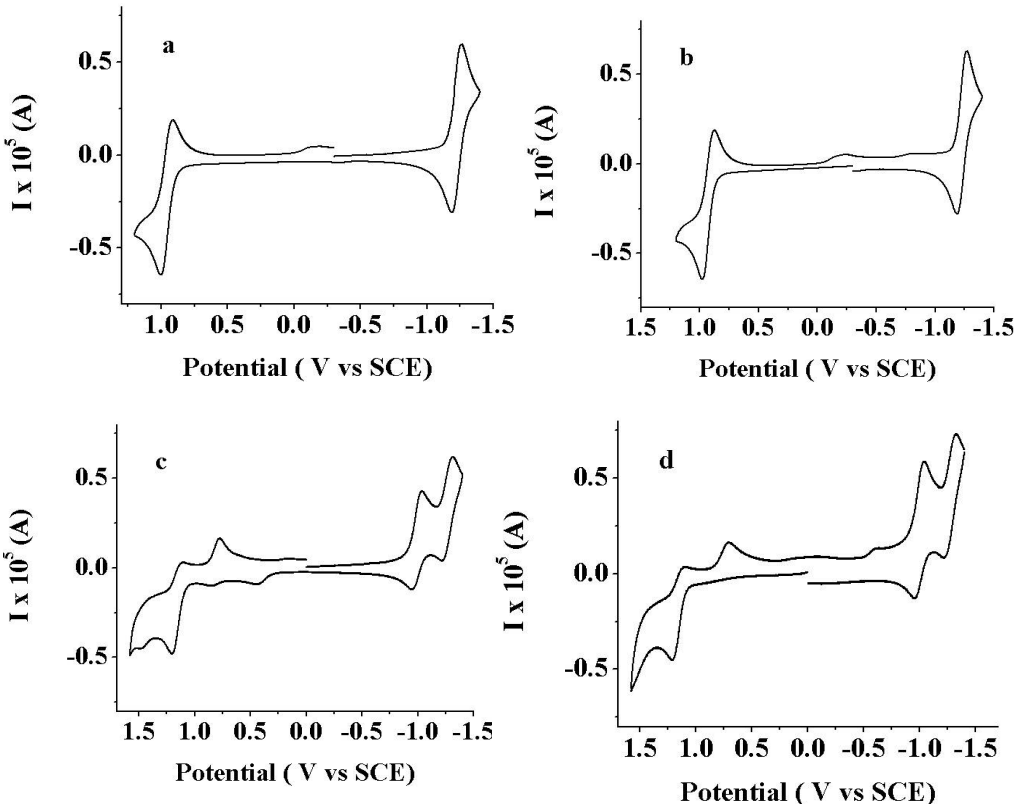


**Figure 19.** Cyclic voltammogram of 1.0 mM **11** ($B^8$-phenyl) (a) and (b) and 1.4 mM dimer (c) and (d) at a scan rate of 0.1 v/s in acetonitrile at platinum working electrode (area = 0.0314 $cm^2$); supporting electrolyte: 0.1 M $TBAPF_6$; (a) and (c) forward scan to the positive direction; (b) and (d) forward scan to the negative direction.

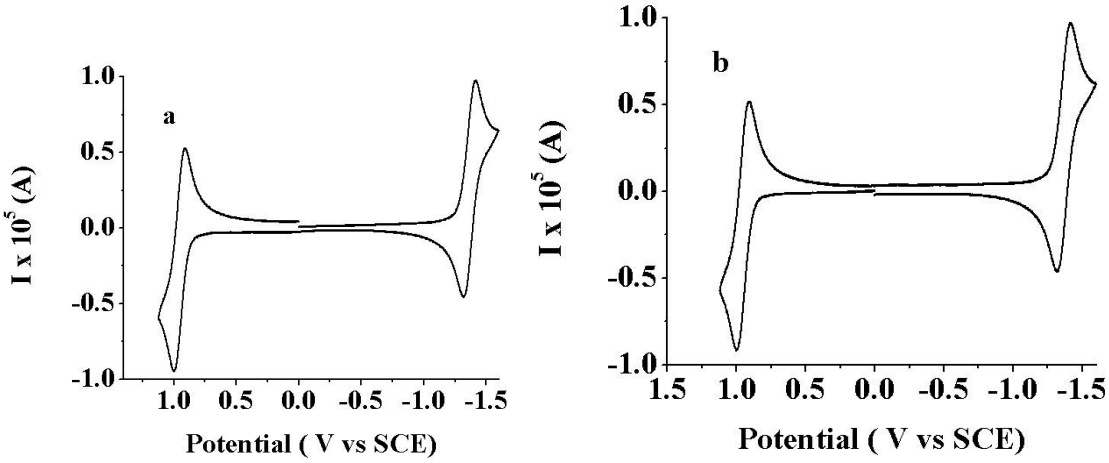


**Figure 20.** Cyclic voltammogram of 1.5 mM **11** ($B^8$-phenyl) at a scan rate of 0.1 v/s in DCM at platinum working electrode (area = 0.0314 $cm^2$); supporting electrolyte: 0.1 M $TBAPF_6$; (a) forward scan to the negative direction; (b) forward scan to the positive direction.

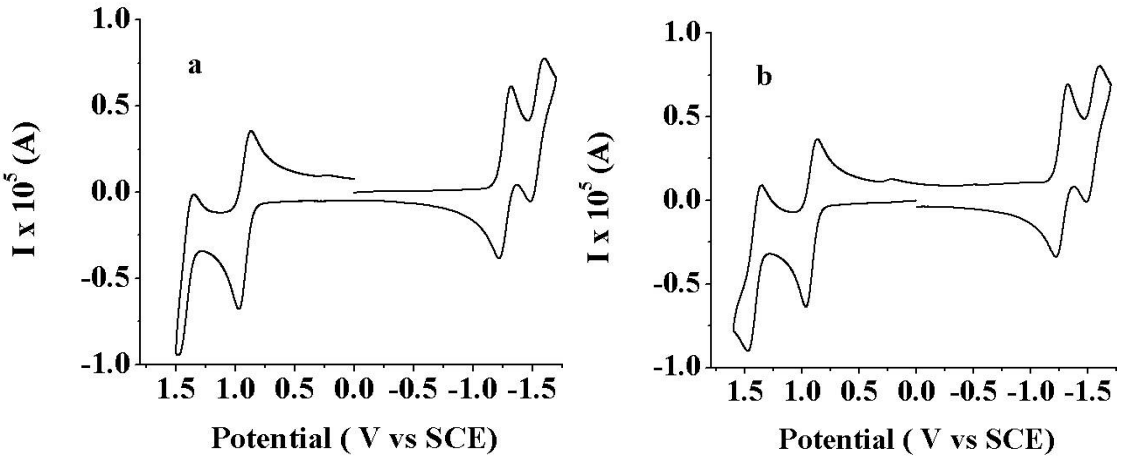


**Figure 21.** Cyclic voltammogram of 1.4 mM dimer **12** at a scan rate of 0.1 v/s in DCM at platinum working electrode (area = 0.0314 $cm^2$); supporting electrolyte: 0.1 M $TBAPF_6$; (a) forward scan to the negative direction; (b) forward scan to the positive direction.

Electrochemical studies of **11 i**n MeCN showed similar behavior to the **10**, with some small reduction waves on a reverse scan following the oxidation; the dimer, however, show a higher instability of the reduced and oxidized species, probably because of a reaction with trace impurities, probably water, in the MeCN (Figure 19). By changing the solvent from MeCN to DCM more reversible and cleaner electrochemistry on both oxidation and reduction was seen, especially for the dimer. The electrochemistry of $B^8$-phenyl showed behavior similar to the $B^8$-n-pentyl dye with one electron reduction and oxidation waves and very similar half wave potential difference between oxidation and reduction processes (Figure 20). The dimer possesses contrasting electrochemical behavior when compared with typical BODIPY monomers, showing two reversible reduction and oxidations waves, with a splitting between peaks of about 0.24 V for the

reduction and 0.5 V for the oxidation (Figure 21). The much smaller splitting between these waves in the dimer suggests consecutive addition or removal of electrons from the two BODIPY centers. The diffusion coefficients determined for **10** and **11** are fairly close and larger than for the larger aromatic dimer. Thus this work confirms that BODIPY dyes completely substituted with alkyl or aryl groups show reversible electrochemistry, where the difference in the redox potentials is related to the substituent in the 8-position and the number of the subunits. The nernstian behavior and high stability of substituted BODIPY compounds make them especially appropriate for the electrochemical study of intermolecular interactions.

### 3.3.3. Electrogenerated Chemiluminescence

The excited states for all of these compounds can be generated by electron transfer between the oxidized and reduced forms by electrochemical pulsing or scanning between the appropriate potentials.

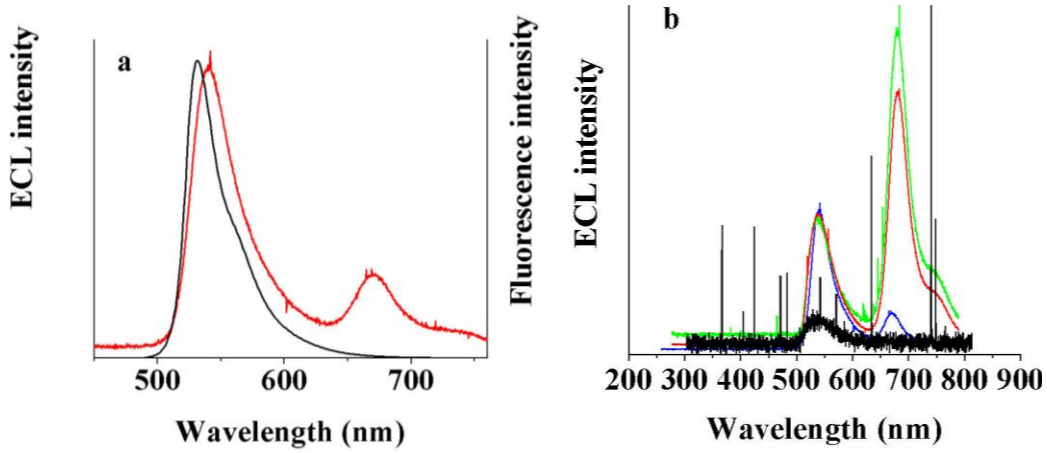

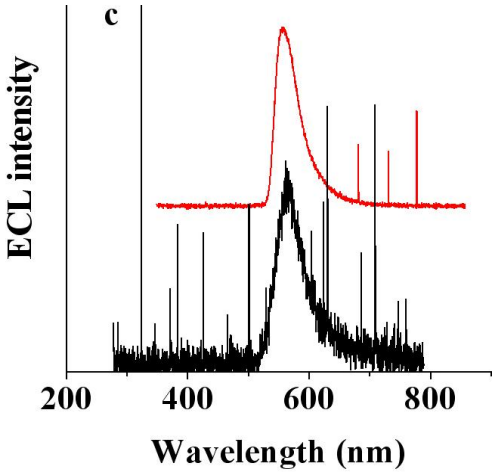


**Figure 22.** (a) ECL (red) and fluorescence (black) spectra for **10** ($B^8$-n-pentyl) dye in acetonitrile; Concentration of the **10** ($B^8$-n-pentyl) for ECL measurements is 0.2 mM and for the fluorescence one is 2 μM; (b) ECL spectra for different concentrations of the **10** ($B^8$-n-pentyl): 0.01 mM (black line), 0.2 mM (blue line); 1 mM (red line); 5 mM (green line); (c) ECL spectra for 1 mM of **10** ($B^8$-n-pentyl) in the presence of 50 mM TPrA (black line) and 50 mM BPO (red line). ECL spectra were generating by pulsing from -1.29 V to 1.38 V for the annihilation process and from 0 to -1.29 V in the presence of BPO and from 0 to 1.38 V for the TPrA case. Platinum working electrode with area of 0.0314 $cm^2$ and 0.1 M $TBAPF_6$ was used for all measurements. Frequency of pulsing of 10 Hz was used for all experiments. Time of stepping: 1 minute.

ECL spectra for **10** show presence of two peaks: one with the wavelength maximum close to that seen in fluorescence and one at a longer wavelength (Figure 22), just like the ECL behavior seen with the $B^8$amide. The only difference is the size of the shift of the long wavelength peaks, 190 nm for the $B^8$ amide vs. 129 nm for **10**. In both cases, there is a small shoulder also seen at an even longer wavelength. However when the excited state is generated with a coreactant, either TPrA at oxidative potentials or BPO at reductive potentials, only a single ECL peak is observed that is very close to the fluorescent spectrum (Figure 22c). A slightly longer wavelength for the ECL first peak compared with the fluorescent peak obtained at much lower concentrations can be attributed to an

inner filter effect as seen for PL experiments at high concentrations, e.g. where an apparent shift of the wavelength for the fluorescence is seen. Thus, the excited state associated with the long-wavelength ECL peak (at ~ 670 nm) is favorably formed in the annihilation process. This effect of the lack of a second peak or broad long wavelength emission in the presence of a coreactant has been seen in other studies. Studies with both coreactants also exclude the possibility that a slight instability of either radical anion or cation produces a product that emits at longer wavelength.

The ECL spectra of the **11** and **12** show a single peak with a wavelength close to that in the fluorescence spectra for both compounds (Figure 23a,b). The ECL spectra for the **11** and **12** was generated in both DCM and MeCN and show the same ECL maximum with a higher intensity with DCM compared to MeCN, probably because of stability issues and also higher fluorescence quantum efficiency for the DCM.[113]

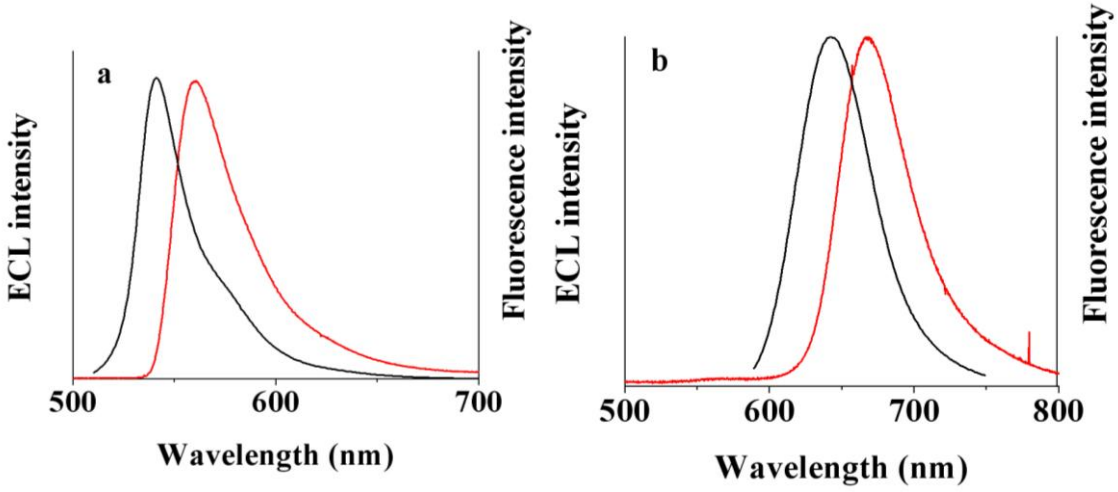


**Figure 23.** (a) ECL (red line) for 1 mM and fluorescence spectra for 2 μM of the **11** ( $B^8$-phenyl) in DCM. ECL spectra were generated by pulsing potential at a frequency of 10 Hz from 1.09 V to -1.48 V. (b) the same studies for the dimer **12** except the potential was stepped from 1.05 V to -1.42 V; Platinum electrode area = 0.0314 $cm^2$;

0.1 M $TBAPF_6$ was used as a supporting electrolyte for all measurements. Time of stepping: 1 minute.

A comparison of the ECL spectra of **10** and **12** at two different concentrations clearly shows that the relative size of the long wavelength band, absent for the **12**, is strongly concentration dependent.

**Discussion**

An ongoing question that arises in many ECL studies where the annihilation reaction results in the occurrence of a second peak at longer wavelengths that is not seen in PL is the cause of such a peak. For example, in the annihilation ECL for **10**, the peak could arise from an excimer or other noncovalent aggregation of molecules, film formation, or dimerization or the production of other chemical species from reactions of the radical ions that emit at longer wavelengths. The current study provides evidence that aggregate formation may be responsible for the longer wavelength ECL and not other effects. Film formation can be excluded, because BODIPY films generally do not show high fluorescence efficiency in the absence of the bulky substituents. The **10** films show low fluorescence emission, but we were not able to generate stable ECL spectra. The formation of products from the reactions of the radical ions is also unlikely in this case, since the CV behavior shows good stability of both the radical anion and cation. Formation of covalent dimer is unlikely for the same reason, even though the spectrum is close to that seen with the $B^8$-phenyl dimer. The **10** dye is completely substituted with simple alkyl chains, so there is no likely site for formation of a covalent dimer, even on

radical ion annihilation. While formation of an excimer on radical annihilation in ECL, as has been proposed in other studies, is a possibility, since the intensity of the long wavelength emission is essentially absent when the ECL is generated with coreactants (either TPrA or BPO), the shape of the emission peak is too sharp compared to that seen for typical excimers. Generally excimer emission is characterized by a very broad emission, since there is no stable ground state of the emitting species. The best explanation is that an aggregate of **10** forms on radical annihilation.

Thus the process proposed is:

$B^8$-n-pentyl + e $\rightarrow$ $B^8$-n-pentyl$^{\bullet-}$ (48)

$B^8$-n-pentyl – e $\rightarrow$ $B^8$-n-pentyl $^{\bullet+}$ (49)

$B^8$-n-pentyl$^{\bullet-}$ + $B^8$-n-pentyl$^{\bullet+}$ $\rightarrow$ ($B^8$-n-pentyl$^+$ $B^8$-n-pentyl$^-$ )$^*$ (excited aggregate formation) (50)

$B^8$-n-pentyl$^{\bullet-}$ + $B^8$-n-pentyl$^{\bullet+}$ $\rightarrow$ $^1B^8$-n-pentyl$^*$ + $B^8$-n-pentyl (51)

($B^8$-n-pentyl$^+$ $B^8$-n-pentyl$^-$)$^*$ $\rightarrow$ ($B^8$-n-pentyl$^+$ $B^8$-n-pentyl$^-$) + hν (52)

A degree of aggregation of two is shown in the proposed mechanism, but a higher degree of aggregation is also possible. The main feature of an aggregate with a long wavelength emission close to the covalent dimer with a perpendicular orientation is seen in this case.[113]

Perhaps the presence of the n-pentyl chain assists in the formation of the aggregates, since an analogous process is not seen with the phenyl substituent. The possibility for the formation of the excimers or aggregates for the BODIPY compounds with a long chain

present has already been shown in case of the lipid systems where long wavelength red fluorescence at 630 nm corresponded with a main fluorescence peak at 515 nm is observed.[114,115] The formation of aggregates with a long wavelength emission close to that seen for the covalent dimer has also been reported in a frozen matrix at low temperatures for a BODIPY dye. However we did not observe any difference in a DCM matrix of fluorescence at 77 K and at room temperature for **10** (Figure 24). The ECL technique can provide some insight into intermolecular interactions that describe some degree of bonding that are not obtained by CV, but clear identification of the products remains challenging.

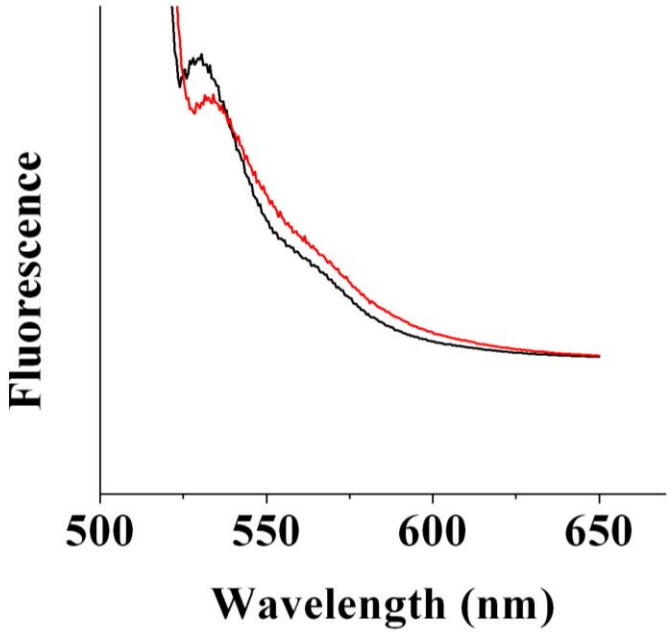


**Figure 24.** Fluorescence spectra of **10** ($B^8$-n-pentyl) at room temperature (red line) and 77 K (black line) in DCM.

### 3.4. Photophysical, electrochemical and electrogenerated chemiluminescence of the BODIPY dyes. Multiple sequential electron transfer in BODIPY monomers, dimers, trimers and polymer.

#### 3.4.1. Photophysical studies

The photophysical characterization of all the compounds was done in a solution of $CH_2Cl_2$ (Scheme 9, Figure 25).

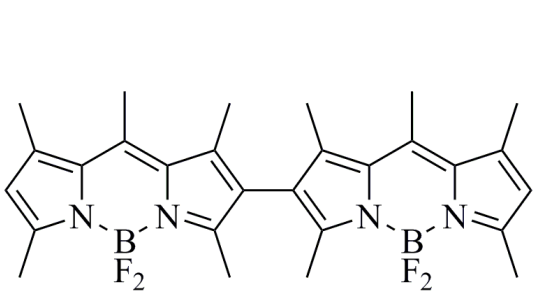

**14**

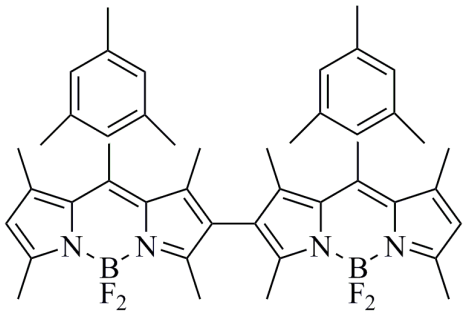

**15**

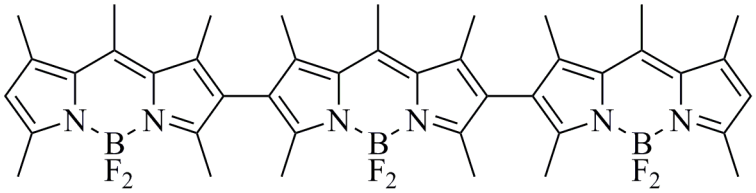

**16**

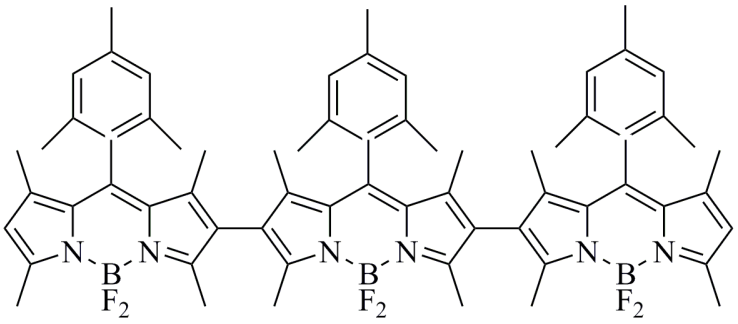

**17**

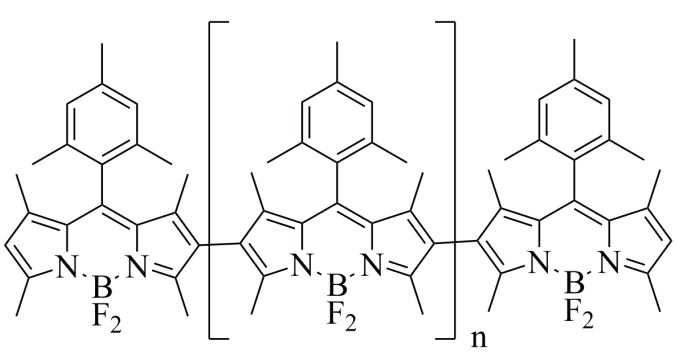

**18**

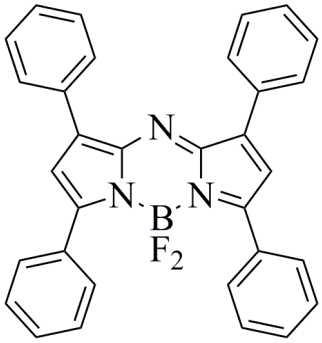

**19**

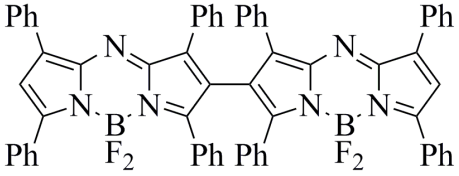

**20**

**Scheme 9.** Structural representation of the BODIPY monomers, dimers and trimers used in this chapter.

$B^8$-substituted mesityl monomer **13** show behavior similar with **2** with slightly shifted to longer wavelength absorption and fluorescence maximum (Figure 25a).

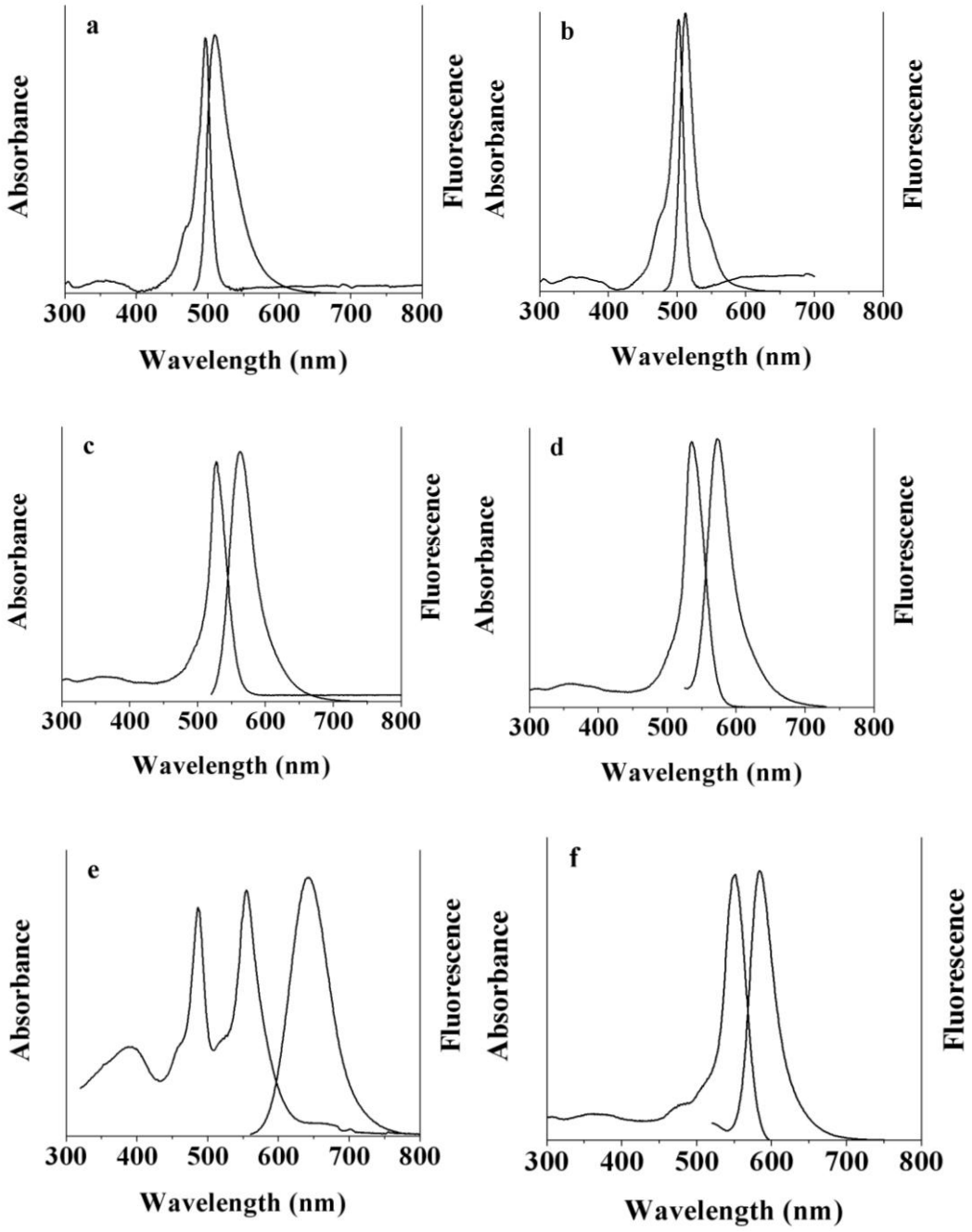

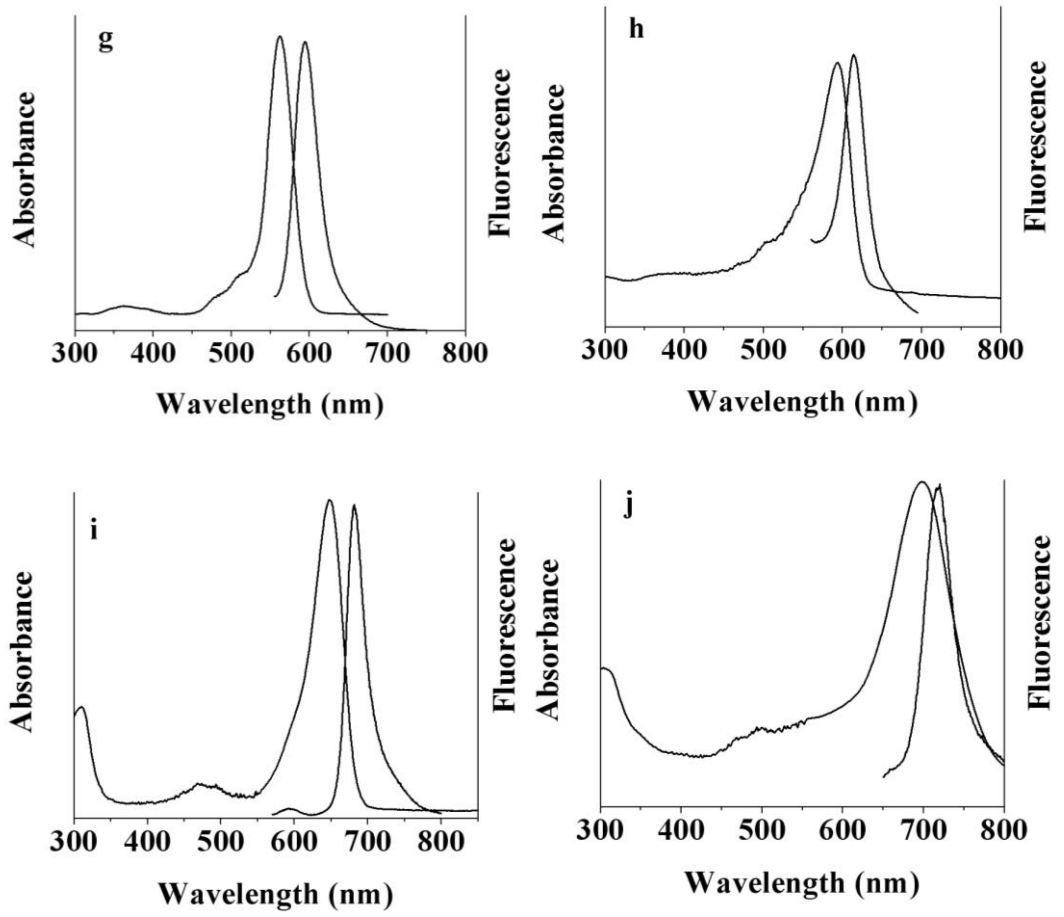


**Figure 25.** Absorbance and fluorescence spectra of 2 μM BODIPY dyes: (a) **13**; (b) and (c) **dimer 14** and **15**; (d) and (e) **trimer 16** and **17**; (f) **polymer 18**; (g) **aza-BODIPY monomer 19**; (h) **aza-BODIPY dimer 20**.

The dimers show characteristic S1-S0 and S2-S0 transitions common for the BODIPY dyes. The mesityl substituted dye also shows slightly red-shifted absorbance and fluorescence compared with the methyl one, similar to monomers (Figure 25b,c). However there is a huge difference in the behavior of linear dimers **14** and **15** compared

with **angular dimer 12**. The linear dimers show a very small degree of exciton splitting in the absorbance compared with **11** with high degree of splitting and visible presence of the two absorption peaks instead of the seen for the S1-S0 transition.

The trimers **16** and **17** show similar behavior to the linear dimers and the absence of the substantial exciton splitting (Figure 25d,e). Comparison of the monomers, dimers and trimers shows a red shift of the wavelength for the absorbance going from monomer to dimer to trimer corresponding to the interactions inside a linear alignment of the same chromophors according to the exciton model of Kasha and also partially due to a higher degree of conjugation. Absorbance maxima are red-shifted around 29 to 34 nm in case of the transition from monomer to dimer and around 24 to 27 nm for the case of transition from dimer to trimer, which shows a smaller change in the absorbance properties with addition of consecutive BODIPY units. Fluorescence results show a similar trend with a large change of around 50 nm in case of transition from monomer to dimer and only around 20 nm for the transition to trimer. These photophysical properties correspond with increase of the Stokes shift from the 12 to 16 nm for monomers compared with 37 to 38 nm for the dimer and 34 to 37 nm for the trimer. This increase of the Stokes shift corresponds with higher non-radiative decay and a smaller value of the fluorescence quantum yield for the dimer and trimer compared with the monomer. The trimers show a similar Stokes shift to the dimers probably due to the diminished influence of the interactions with addition of more and more similar units. There is also a smaller change of the quantum yield in going from dimer to trimer relative to transition from monomer to dimer. The **polymer 18** shows appearance of S1-S0 absorbance transition at 590 nm and

fluorescence maximum at 614 nm, which is slightly larger than the trimer, at 596 nm (Figure 25f). The linear **polymer** shows fluorescence maximum still blue-shifted compared with the **angular dimer**.

The **aza-BODIPY monomer 19** shows red-shifted absorbance and fluorescence compared with the same $C^8$ dye with the characteristic BODIPY dye S2-S0 and S1-S0 transitions (Figure 25g). Fluorescence studies show a substantial fluorescence signal for the monomer, although with less efficiency compared with the $C^8$ dye. The absorption of the **aza-BODIPY dimer 20** is red-shifted about 40 nm compared to the monomer (Figure 25h). There is seen much higher quenching effect for the dimer with the quantum yield of less than 0.01.

### 3.4.2. Electrochemical results

Electrochemical results for the BODIPY monomers with positions 2 and 6 missing are shown in previous chapter. Mesityl substituted dye show electrochemical properties similar to the methyl substituted dye with slight difference in electrochemical potentials for oxidation and reduction (Figure 26).

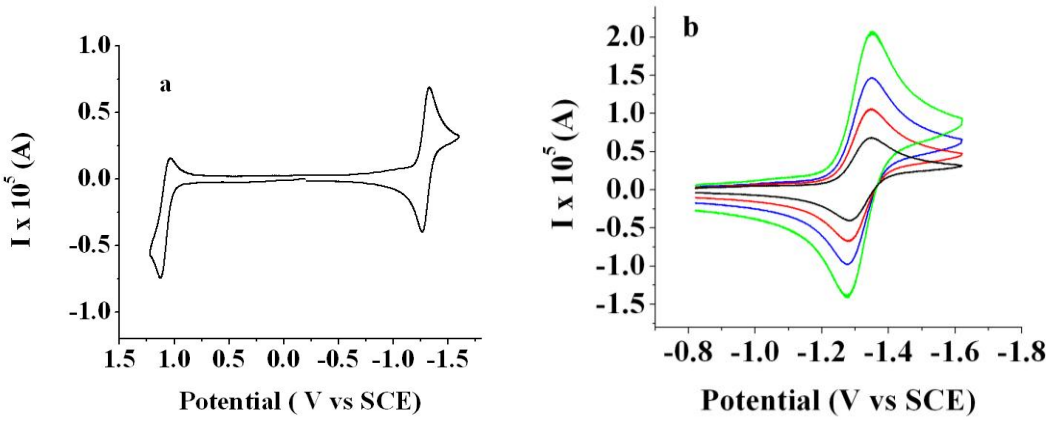

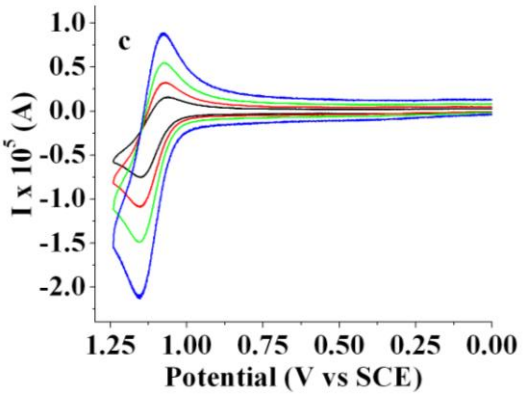


**Figure 26.** Cyclic voltammograms of (a),(d) 1.0 mM **13**; (b) scan rate dependence while scanning in negative and (c) positive direction for **13**; solvent: DCM; supporting electrolyte: $TBAPF_6$; platinum electrode area: 0.0314 $cm^2$.

The linear dimers show presence of the two one-electron waves on both reduction and oxidation (Figure 27).

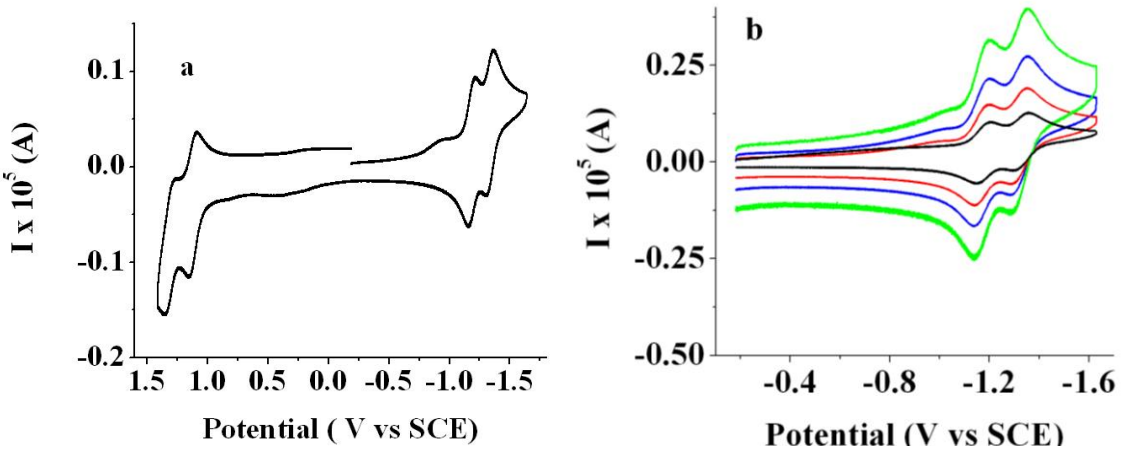

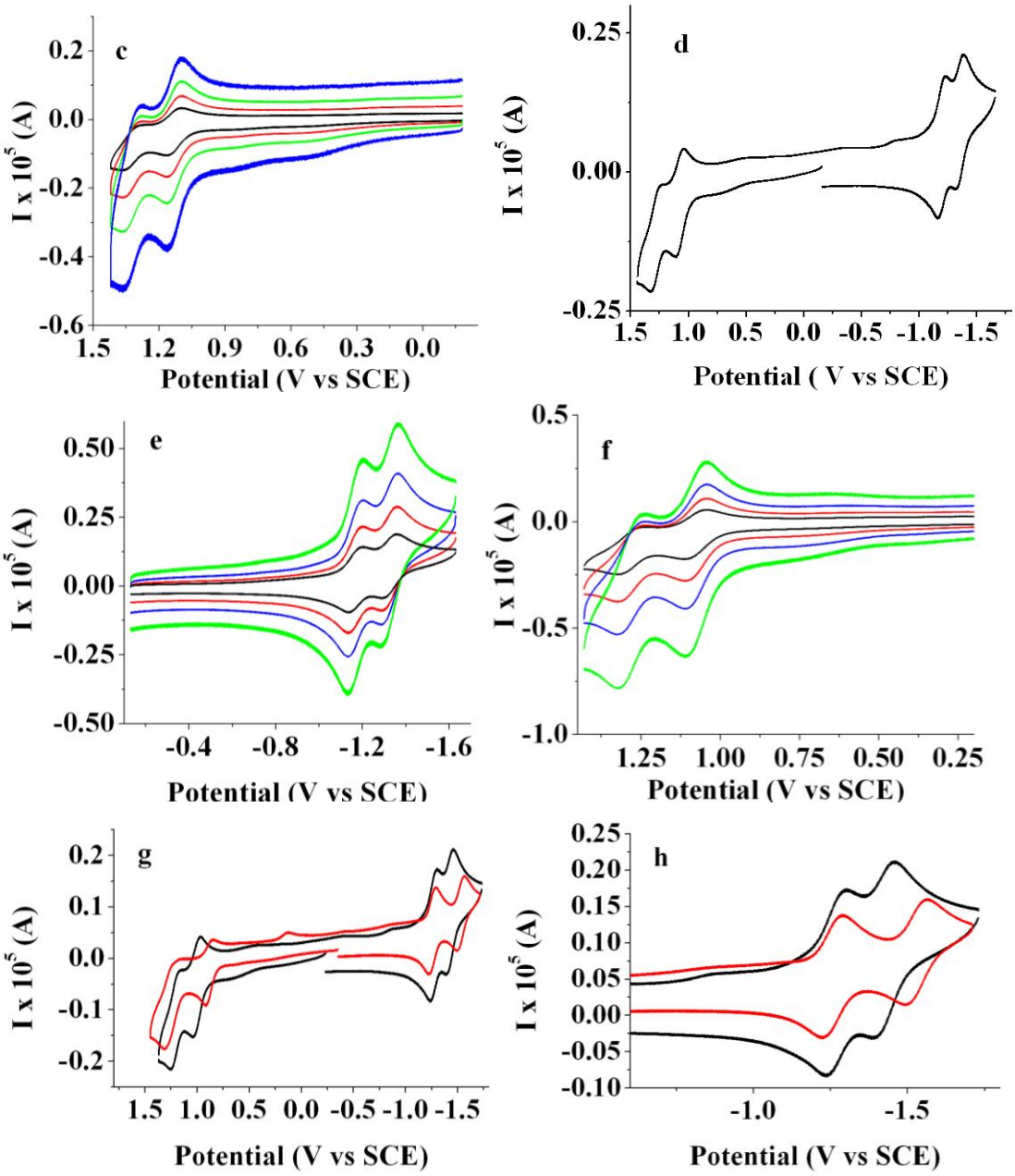
c
I x 10^5 (A)
Potential (V vs SCE)
d
I x 10^5 (A)
Potential ( V vs SCE)
e
I x 10^5 (A)
Potential (V vs SCE)
f
I x 10^5 (A)
Potential (V vs SCE)
g
I x 10^5 (A)
Potential (V vs SCE)
h
I x 10^5 (A)
Potential (V vs SCE)

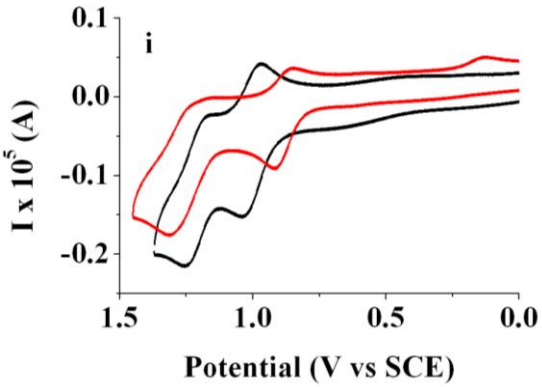


**Figure 27.** Cyclic voltammograms of (a) 0.14 mM **dimer 14** and (d) 0.3 mM **dimer 15**; (b) and (e) scan rate dependence while scanning in negative and (c) and (f) in positive direction; (g)-( i) comparison of the oxidation and reduction potential between 0.2 mM **dimer 14** and 0.15 mM **dimer 12**, where in (g) full scan shown and (h) and (i) parts for the reduction (h) and oxidation (i) highlighted; solvent: DCM; supporting electrolyte: $TBAPF_6$; platinum electrode area: 0.0314 $cm^2$.

The fact that the second waves occur as separate ones at more extreme potentials is consistent with a significant interaction between both BODIPY units. The reduction peak potentials for the dimer **14** are -1.17 V and -1.29 V compared with the oxidation potentials which are 1.09 V and 1.31 V. There is no evidence of substantial dimerization or other chemical processes for both oxidation and reduction products of the dimers, so a simple EE mechanism with two nernstian electrochemical waves was assumed for the simulation (Figures 28, 29).

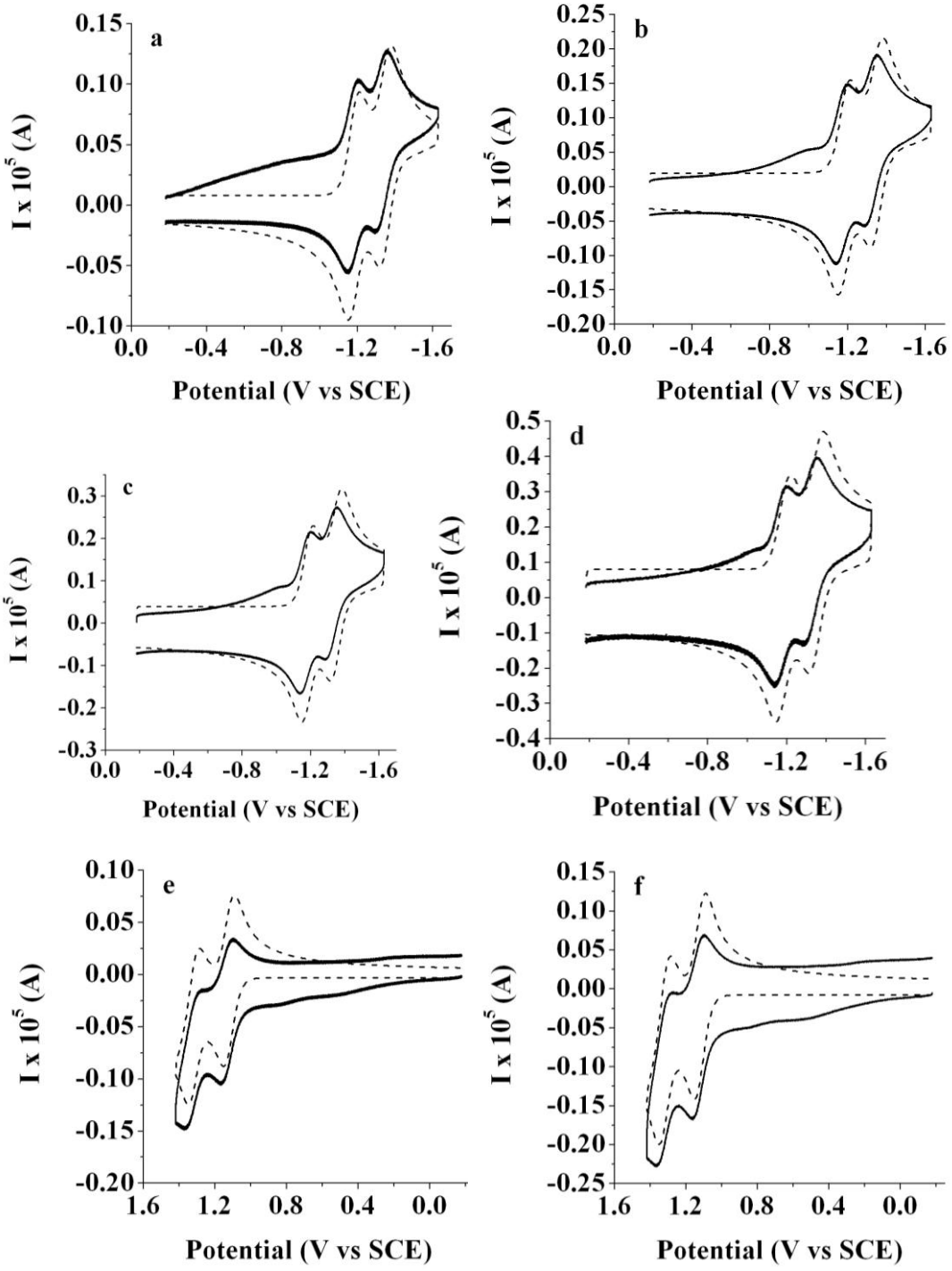
a
b
c
d
e
f
I x 10^5 (A)
Potential (V vs SCE)

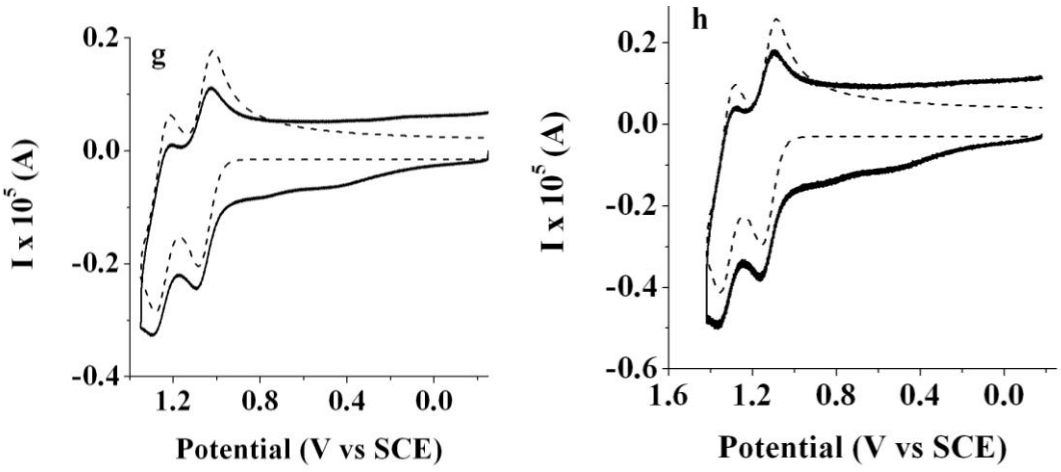


**Figure 28.** Experimental (solid) and simulated (dashed) line cyclic voltammograms of 0.14 mM **dimer 14** during the scan in the negative direction (a)-(d) and positive direction (e)-(h). Scan rate (a) and (e) 0.1 V/s; (b) and (f) 0.25 V/s; (c) and (g) 0.5 V/s; (e) and (h) 1 V/s. Experimental data: solvent: DCM; supporting electrolyte: 0.1 M $TBAPF_6$; platinum electrode area 0.0314 $cm^2$. Simulated data: diffusion coefficient: 5.2 x $10^{-6}$ $cm^2/s$; uncompensated resistance 1800 Ω; capacitance 3 x $10^{-7}$ F.

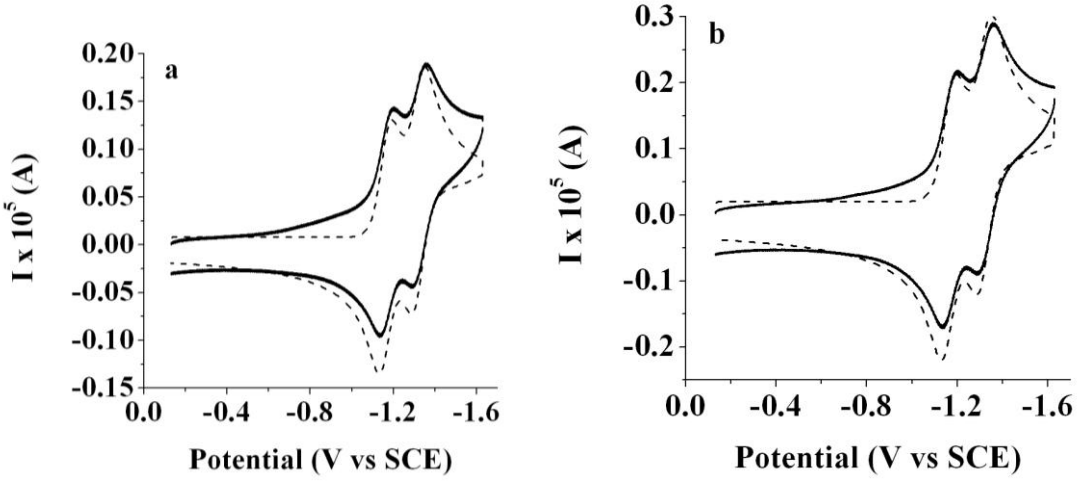

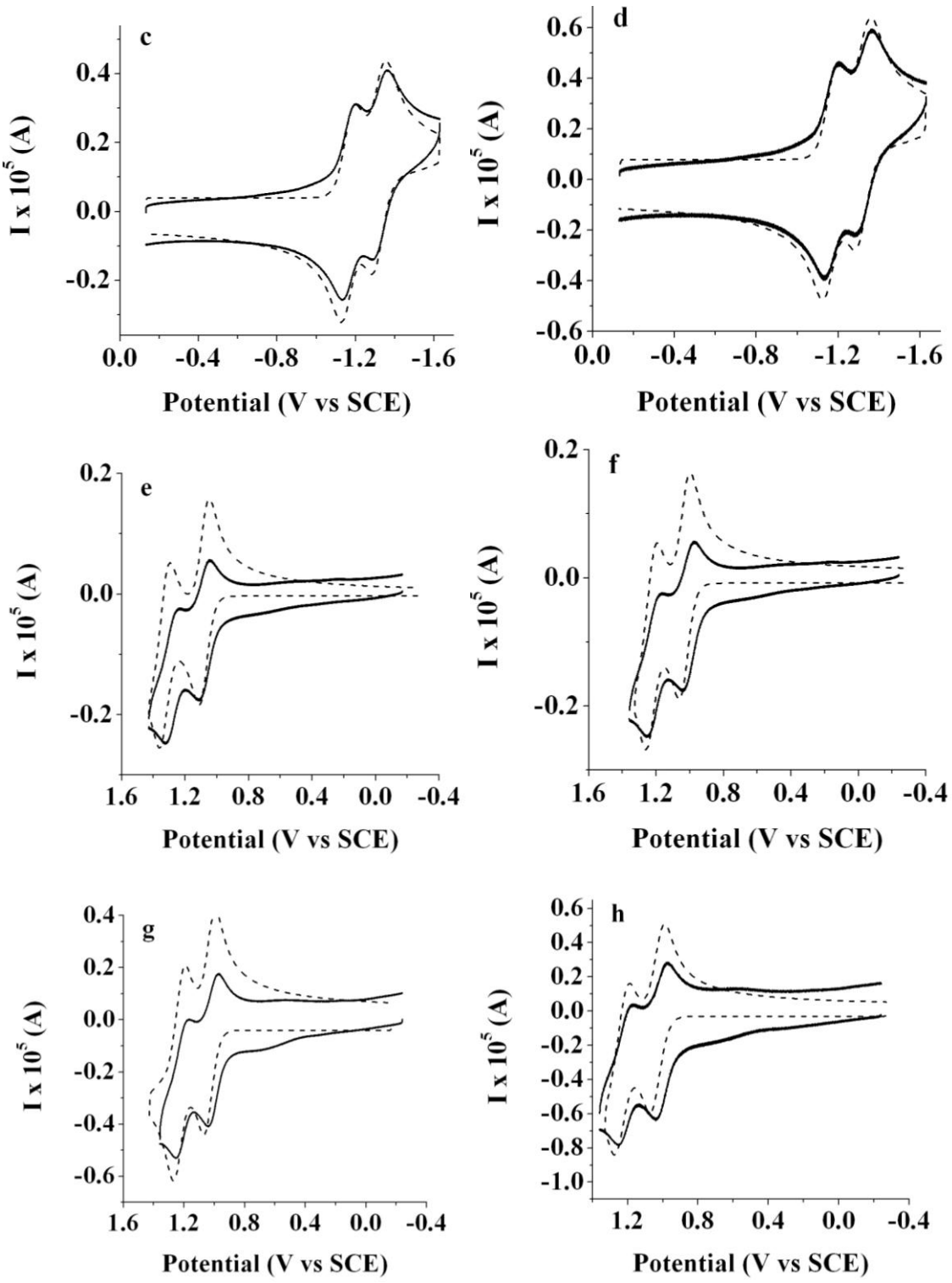


**Figure 29.** Experimental (solid) and simulated (dashed) line cyclic voltammograms of 0.2 mM **dimer 15** during the scan in the negative direction (a)-(d) and positive direction

(e)-(h). Scan rate (a) and (e) 0.1 V/s; (b) and (f) 0.25 V/s; (c) and (g) 0.5 V/s; (e) and (h) 1 V/s. Experimental data: solvent: DCM; supporting electrolyte: 0.1 M $TBAPF_6$; platinum electrode area 0.0314 $cm^2$. Simulated data: diffusion coefficient: 5.2 x $10^{-6}$ $cm^2/s$; uncompensated resistance 1800 Ω; capacitance 8 x $10^{-7}$ F.

Some instability on oxidation on repeated cycling, however, results in some film formation, suggesting possible slow coupling, consistent with the absence of substitution in the positions where chain propagation occurs. Dimer **15** shows similar electrochemical behavior as **14** with about the same oxidation and reduction potentials. The degree of the separation between reduction and oxidation waves for both compounds is also substantially less than that of the **11**, which is electrochemical evidence for a smaller degree of interaction between BODIPY units in case of the dimer formed through position 2/6 compared with position 3 (Figure 27g-i). **11** also show the same phenomenon of larger peak separation on oxidation compared with reduction, which seems to be a characteristic feature of these dyes. As a result the larger degree of separation on oxidation cannot be explained by the fact of some small instability on oxidation as the **11** has all positions substituted. A higher degree of separation between the two oxidation waves compared with the reduction ones can be explained by the fact that most LUMO electron density is localized at the position 8 with the HOMO concentrated at the pyrollic units. Thus it is easier to add a second electron to the center of the molecule compared with removing an electron from the backbone. The greater interaction appears to be due to the withdrawing electrons from the LUMO compared with addition of electrons to HOMO.

Trimer **16** shows three one-electron transitions for both oxidation and reduction (Figure 30).

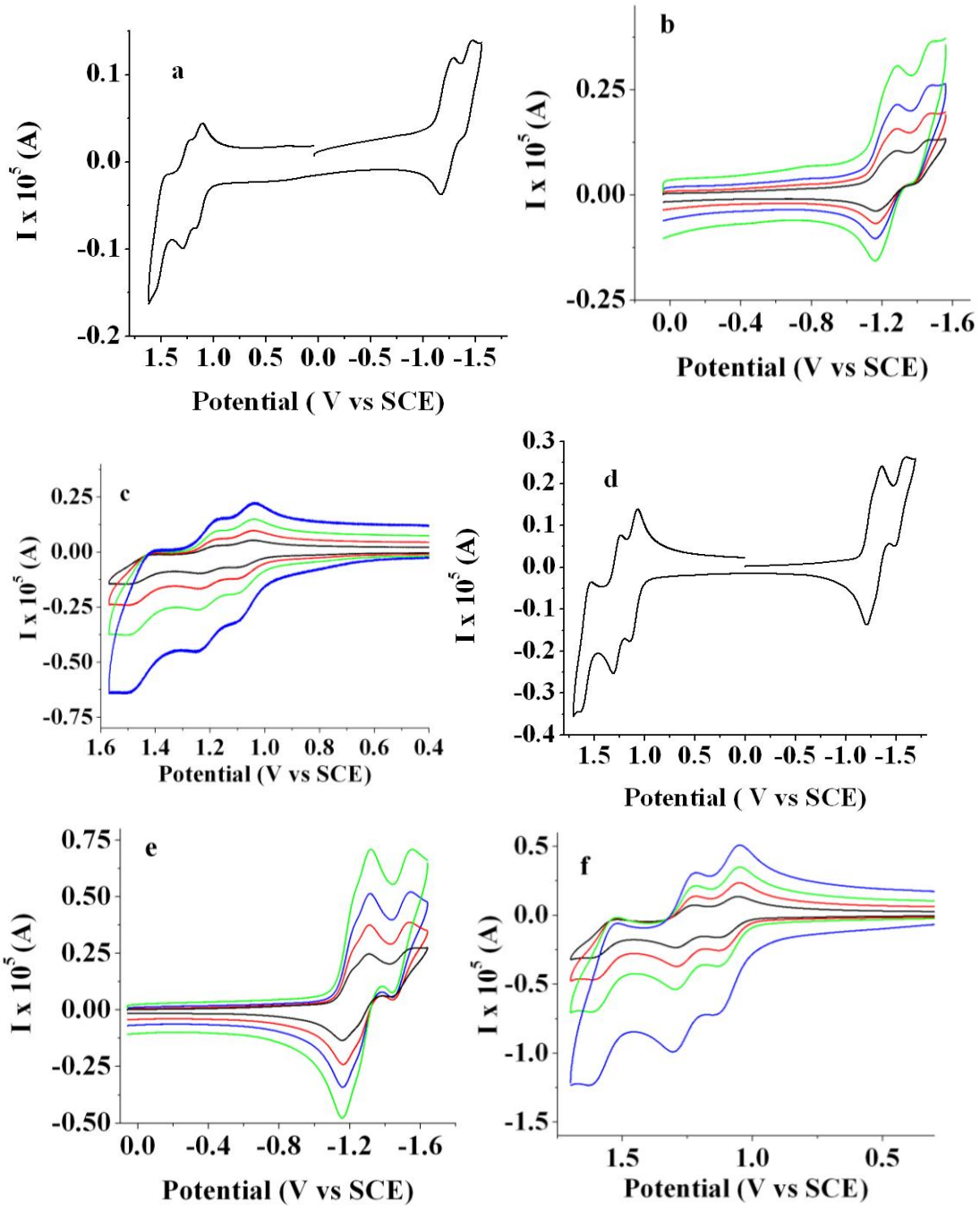


**Figure 30.** Cyclic voltammograms of (a) 0.1 mM **trimer 16** and (d) 0.24 mM **trimer 17**; (b) and (e) scan rate dependence while scanning in negative and (c) and (f) in positive

direction; solvent: DCM; supporting electrolyte: $TBAPF_6$; platinum electrode area: 0.0314 $cm^2$.

The oxidation shows three clear peaks while on reduction the first two peaks are merged to produce a two-electron wave with a shoulder. The reduction half-wave potentials for 0.14 mM of the **16** are at -1.15 V, -1.24 V and -1.43 V and oxidation half-wave potentials are at 1.04 V, 1.17 V and 1.42 V, as obtained from digital simulations assuming an EE mechanism with three nernstian waves (Figures 31, 32).

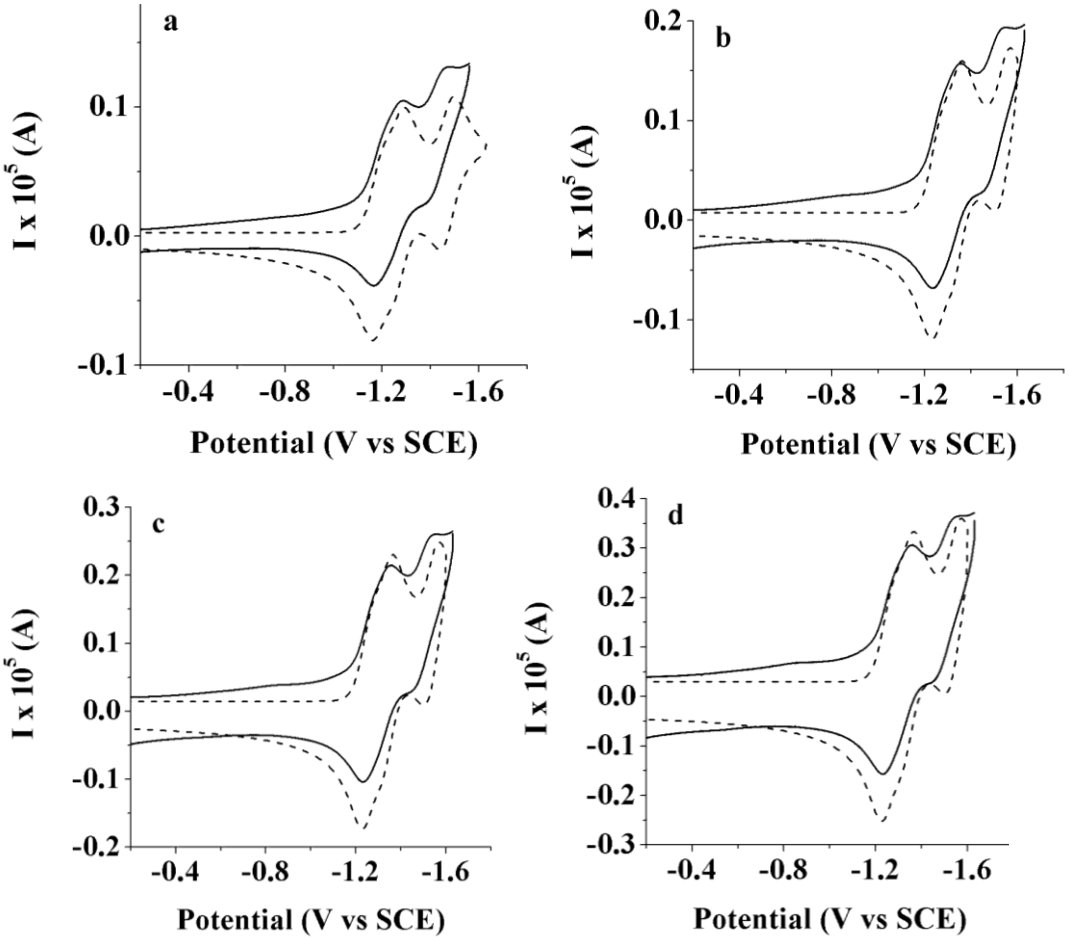

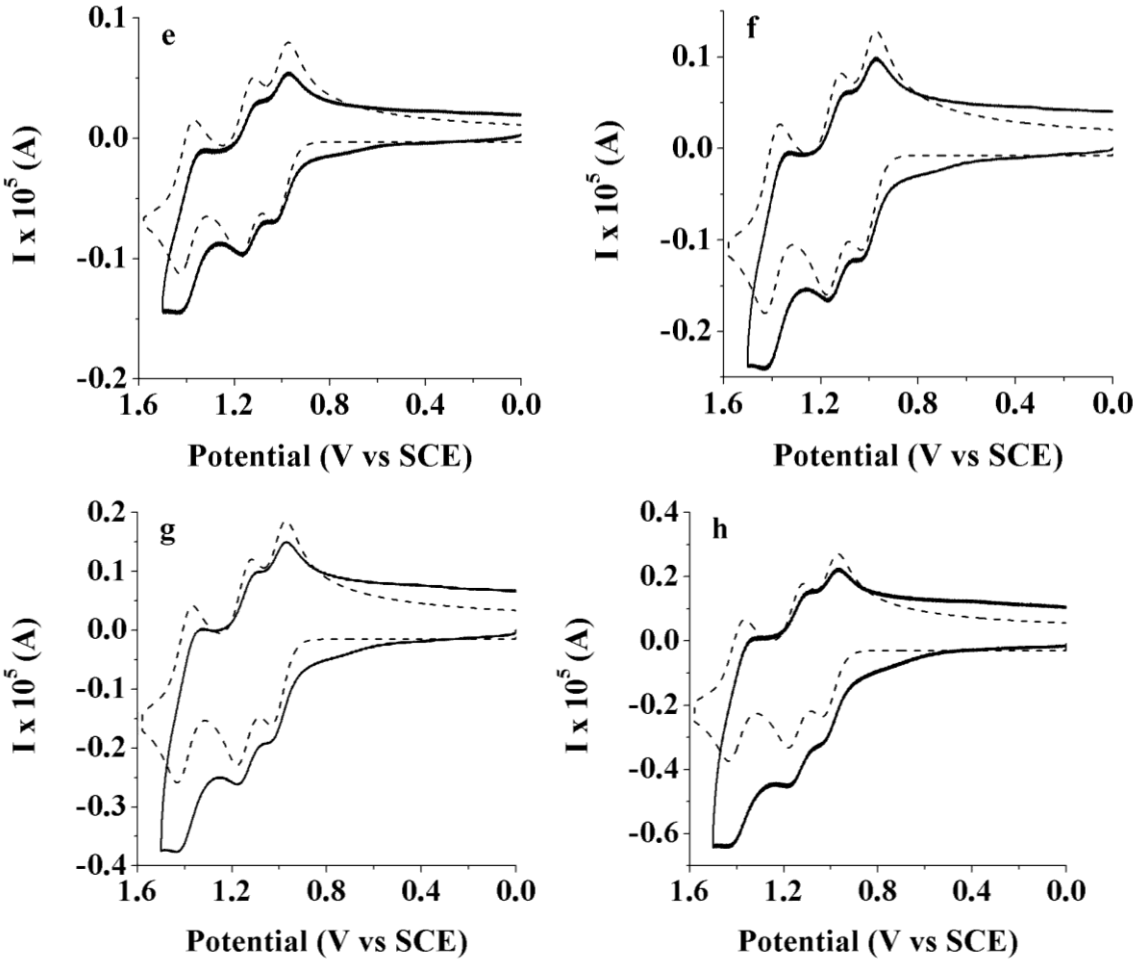


**Figure 31.** Experimental (solid) and simulated (dashed) line cyclic voltammograms of 0.1 mM **trimer 16** during the scan in the negative direction (a)-(d) and positive direction (e)-(h). Scan rate (a) and (e) 0.1 V/s; (b) and (f) 0.25 V/s; (c) and (g) 0.5 V/s; (e) and (h) 1 V/s. Experimental data: solvent: DCM; supporting electrolyte: 0.1 M $TBAPF_6$; platinum electrode area 0.0314 $cm^2$. Simulated data: diffusion coefficient: 4.8 x $10^{-6}$ $cm^2/s$; uncompensated resistance 1800 Ω; capacitance 3 x $10^{-7}$ F.

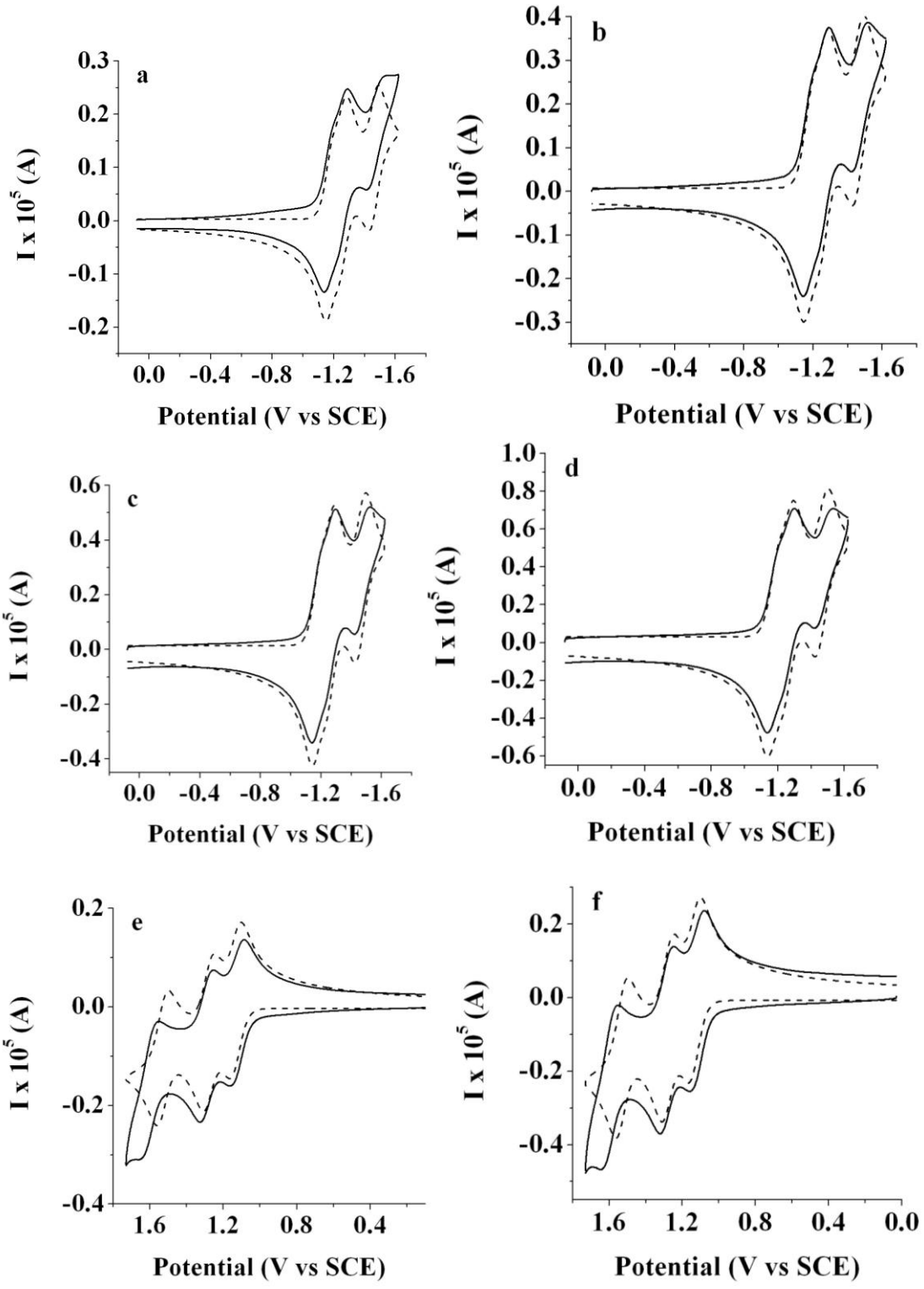
a
b
c
d
e
f
I x 10^5 (A)
Potential (V vs SCE)

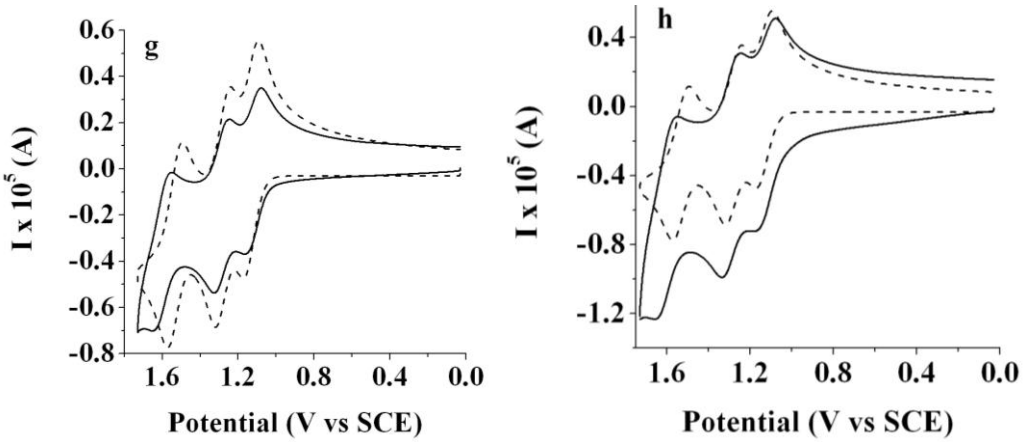


**Figure 32.** Experimental (solid) and simulated (dashed) line cyclic voltammograms of 0.24 mM **trimer 17** during the scan in the negative direction (a)-(d) and positive direction (e)-(h). Scan rate (a) and (e) 0.1 V/s; (b) and (f) 0.25 V/s; (c) and (g) 0.5 V/s; (e) and (h) 1 V/s. Experimental data: solvent: DCM; supporting electrolyte: 0.1 M $TBAPF_6$; platinum electrode area 0.0314 $cm^2$. Simulated data: diffusion coefficient: 4.8 x $10^{-6}$ $cm^2/s$; uncompensated resistance 1800 Ω; capacitance 3 x $10^{-7}$ F.

**17** shows very similar behavior. The trimers show, as the dimers, a smaller separation between the first and second reduction peaks compared with the oxidation. The extent of separation between the two reduction and two oxidation peaks decreases from dimer to trimer. As expected it is harder to withdraw or add a third electron compared with the second one because of the greater electrostatic repulsion. Similar effects have been seen, e.g. for truxene-oligofluorene compounds, and many others.[116] **18** shows the presence of multiple one-electron peaks corresponding to a series of waves, as expected from the results with dimer and trimer (Figure 33).

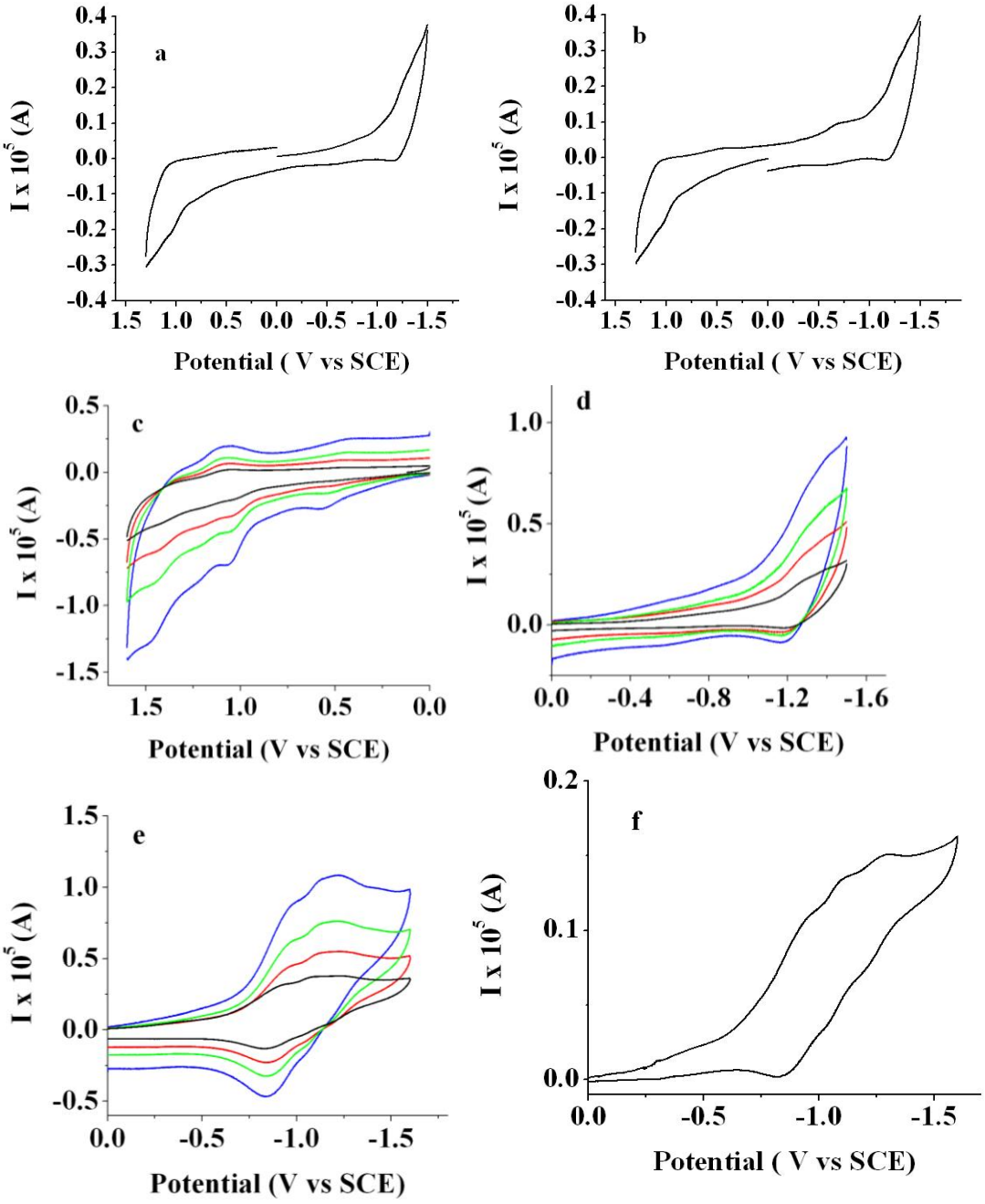
a
b
c
d
e
f
I x 10^5 (A)
Potential ( V vs SCE)
Potential (V vs SCE)

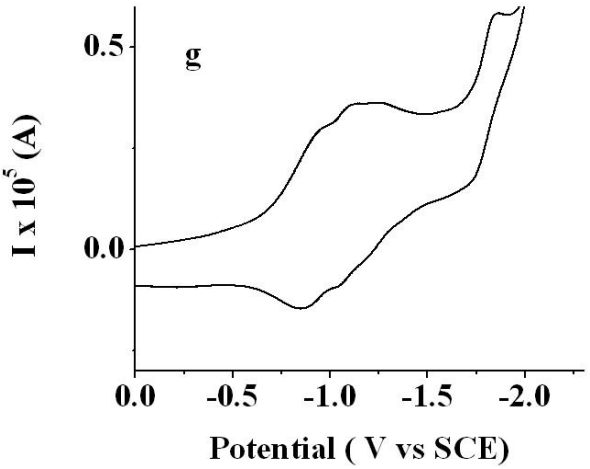


**Figure 33.** Cyclic voltammograms of 0.15 mM **polymer 18** in DCM during scan in (a) negative and (b) positive direction; scan rate dependence during scan in (c) negative and (d) positive direction, where 1 V/s (blue line), 0.5 V/s (green line); 0.25 V/s (red line) and 0.1 V/s (blue line); (e)-(g) cyclic voltammograms **of polymer 18** in THF: (e) scan rate dependence for 0.15 mM **polymer 18**, where 1 V/s (blue line), 0.5 V/s (green line); 0.25 V/s (red line) and 0.1 V/s ( black line); (f) scan rate 0.01 V/s; (g) scan to -2.5 V. Electrode area: 0.0314 $cm^2$; supporting electrolyte: $TBAPF_6$.

This is especially clear for the experiment in THF, where appearance of about 20 consecutive reduction waves is noticed. A diffusion coefficient of $1.4 \times 10^{-6}$ $cm^2/s$ was estimated by using equation (6) from the overall limiting current values.[117]

$$(D_p/D_m) = (M_m/M_p)^{0.55} \quad (53)$$

It is difficult to simulate electrochemical behavior of the **polymer 18** because of the polydispersity of the polymer and also the influence of many peak splittings and rate constants on the electrochemical reduction process. This can also cause a deviation of the number of electron transfers from the number expected from the gel permeation studies, 24, and the expected diffusion current. The oxidation also shows multiple electron transfers, but observation of all multiple transitions is limited by the potential window.

The **aza-BODIPY monomer 19** shows a nernstian reduction wave with a peak potential shifted positive by about 0.8 V compared to the $C^8$-BODIPY (Figure 34a-e).

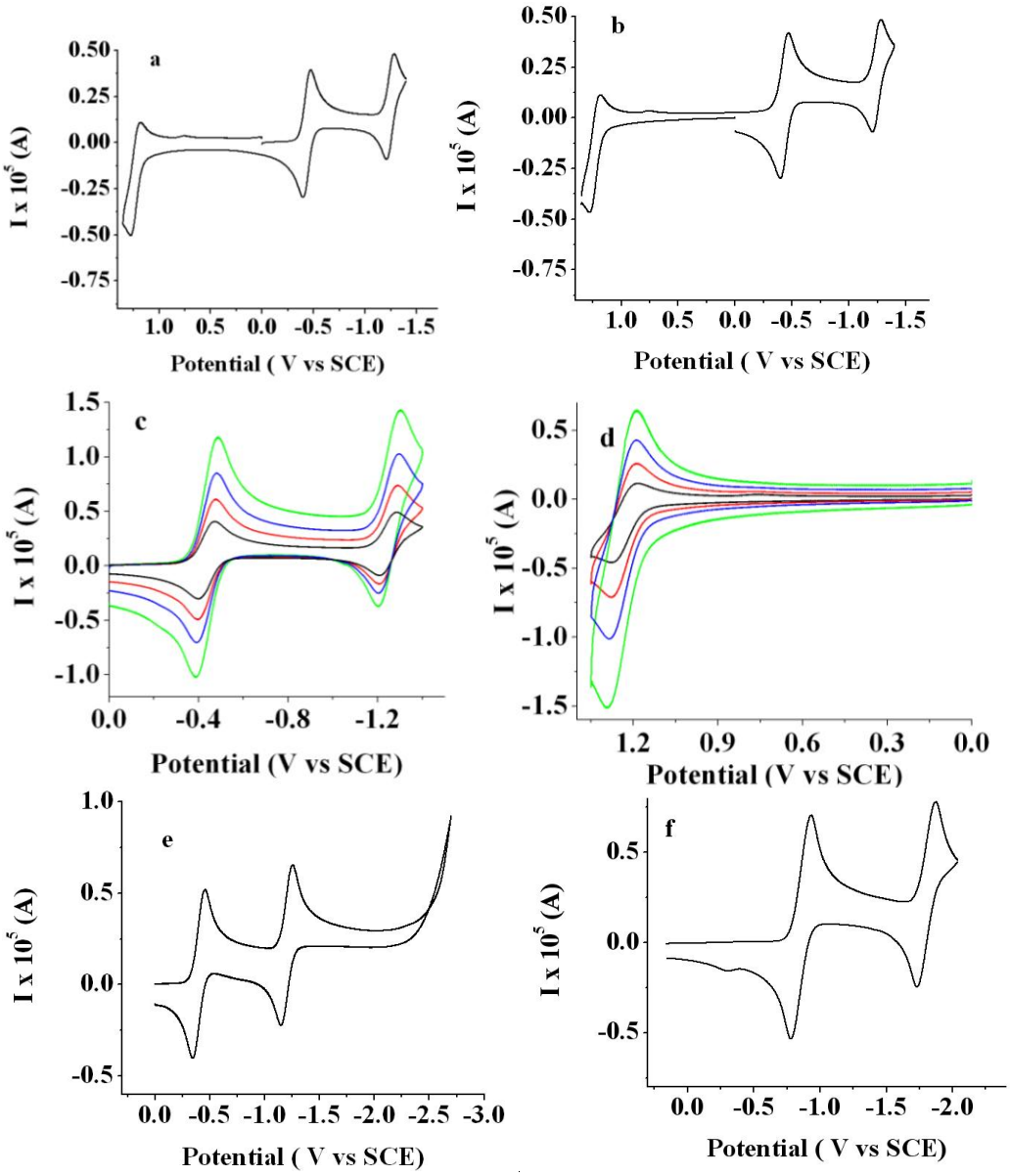


**Figure 34.** Cyclic voltammograms of 0.6 mM **aza-BODIPY monomer 19** at a scan rate of 0.1 V/s in DCM at platinum working electrode (area = 0.0314 $cm^2$); supporting electrolyte: 0.1 M $TBAPF_6$; (a) forward scan to the negative direction; (b) forward scan to the positive direction; scan rate dependence for oxidation (c) and reduction (d); (e) scan for 0.8 mM aza-BODIPY in THF; (f) CV for dye **8** at 0.1 V/s.

It is possible to see a second reversible reduction wave for these species in DCM (Figure 34a-c). The separation between the two reduction waves is around 0.82 V, which is smaller than 1.09 V seen for the $C^8$ system (which shows unusually large separations between the first two electron additions). The separation between consecutive peaks is however still larger than that in 9,10-diphenylanthracene and other polycyclic hydrocarbons (about 0.5 V). A slight decrease in the separation between the two reduction waves is seen with addition of the acceptor group, i.e. 1.09 V for alkyl substituted dye, 0.98 V for the 8-cyano substituted dye **8** compared to that with the acceptor atom nitrogen, i.e. 0.82 V for aza-BODIPY (Figure 34a-c,e,f). Reduction of the **19** in THF at more negative potentials shows the absence of any electrochemical processes up to -3.0 V (Figure 34e). As with the $C^8$-BODIPY, oxidation of the aza-compound also shows some dimer formation. Simulations including formation of the dimer on oxidation were carried out and show a rate of dimerization about the same as with the analogous $C^8$-BODIPY (Figure 35).

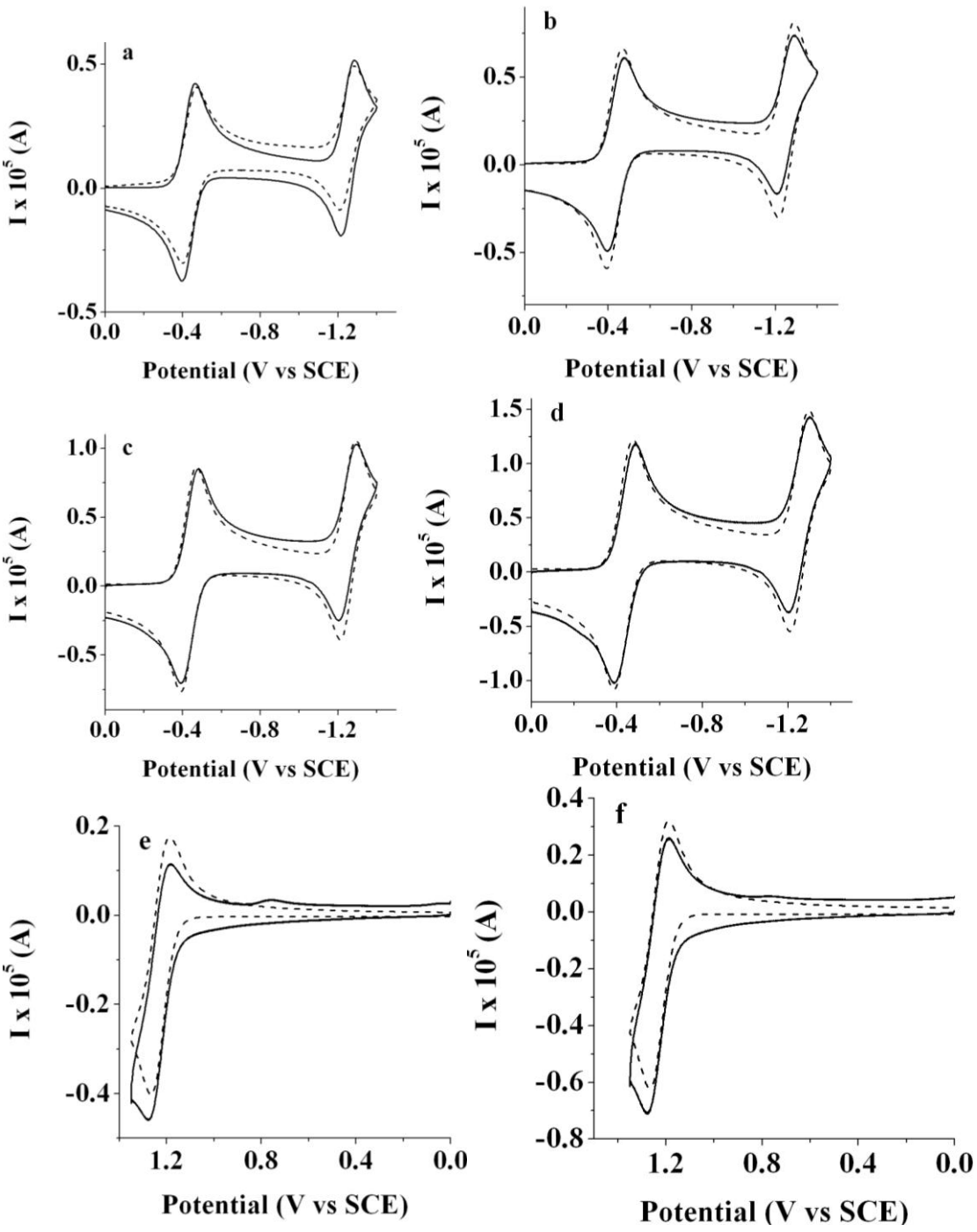
a
b
c
d
e
f
I x 10^5 (A)
Potential (V vs SCE)

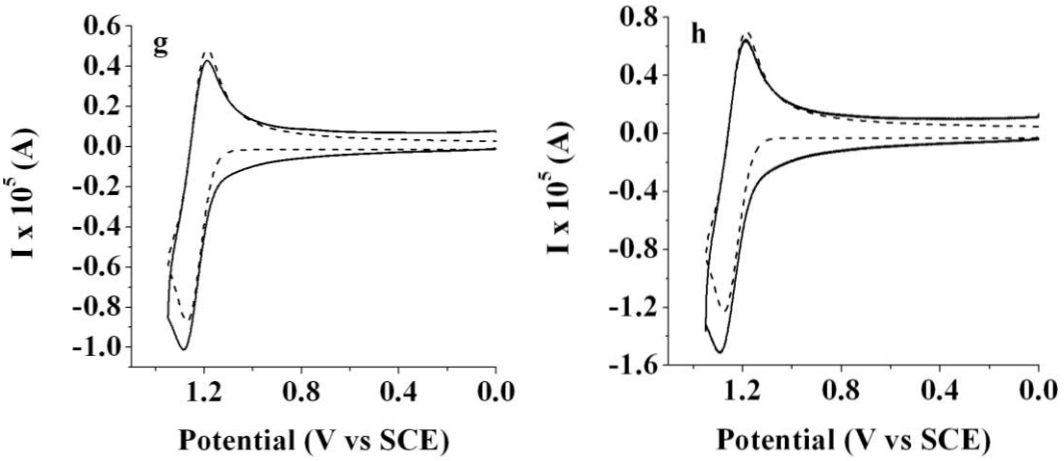


**Figure 35.** Experimental (solid) and simulated (dashed) line cyclic voltammograms of 0.6 mM of **aza-BODIPY monomer 19** during (a-d) scans into the positive and (e-h) negative direction. Scan rate: (a) and (e) 0.1 V/s; (b) and (f) 0.25 V/s; (c) and (g) 0.5 V/s; (d) and (h) 1 V/s. Experimental data: solvent: DCM; supporting electrolyte: 0.1 M $TBAPF_6$; electrode area: 0.0314 $cm^2$. Simulated data: diffusion coefficient of the monomer is 7.0 x $10^{-6}$ $cm^2/s$ and dimer 5.2 x $10^{-6}$ $cm^2/s$; uncompensated resistance 1000 Ω, capacitance 3 x $10^{-7}$ F and kinetics constant of 2 $s^{-1}$ were used in simulations for reduction and 400 $M^{-1}$ $s^{-1}$ dimerization constant and deprotonation constant of $10^{10}$ $s^{-1}$ for oxidation. As shown, the current scale encompasses $\pm 5$ μA.

The **aza-BODIPY dimer 20** shows four reduction waves in DCM (Figure 35). The first two transitions correspond to the addition of one electron to each monomer unit and the second one to the addition of an additional electron to each unit. An experiment with the analogous $C^8$ **dimer 14** and **15** in THF at room temperature also shows the presence of four peaks at more negative potentials, but the reversibility is much poorer under these conditions (Figure 35e). The separation between the first two sequential waves (and also the third and fourth wave) was ~0.12 V, very close to the results for the $C^8$-BODIPY dimers. The separation between the first two waves on oxidation is larger than that for the reduction. The separation between first and third reduction wave was ~1.0 V, which is

similar to the results for the monomer. The reason for that was determined to be steric in the aza-BODIPY core.

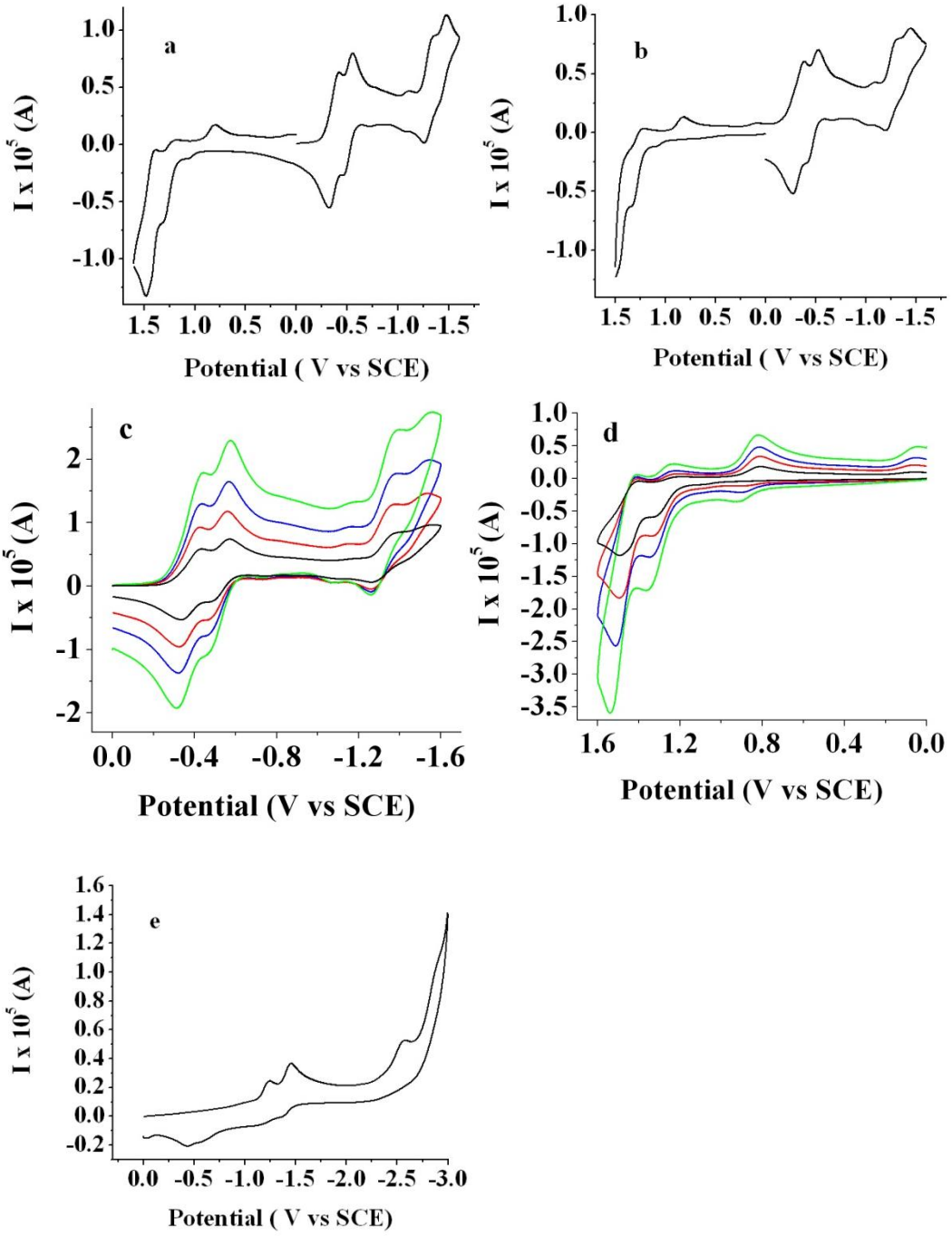

**Figure 36.** Cyclic voltammograms of 0.9 mM **aza-BODIPY dimer** at a scan rate of 0.1 V/s in DCM at platinum working electrode (area = 0.0314 $cm^2$); supporting electrolyte: 0.1 M $TBAPF_6$; (a) forward scan to the negative direction; (b) forward scan to the positive direction; scan rate dependence for (c) oxidation and (d) reduction; (e) reduction of 0.3 mM of **dimer 2** in THF.

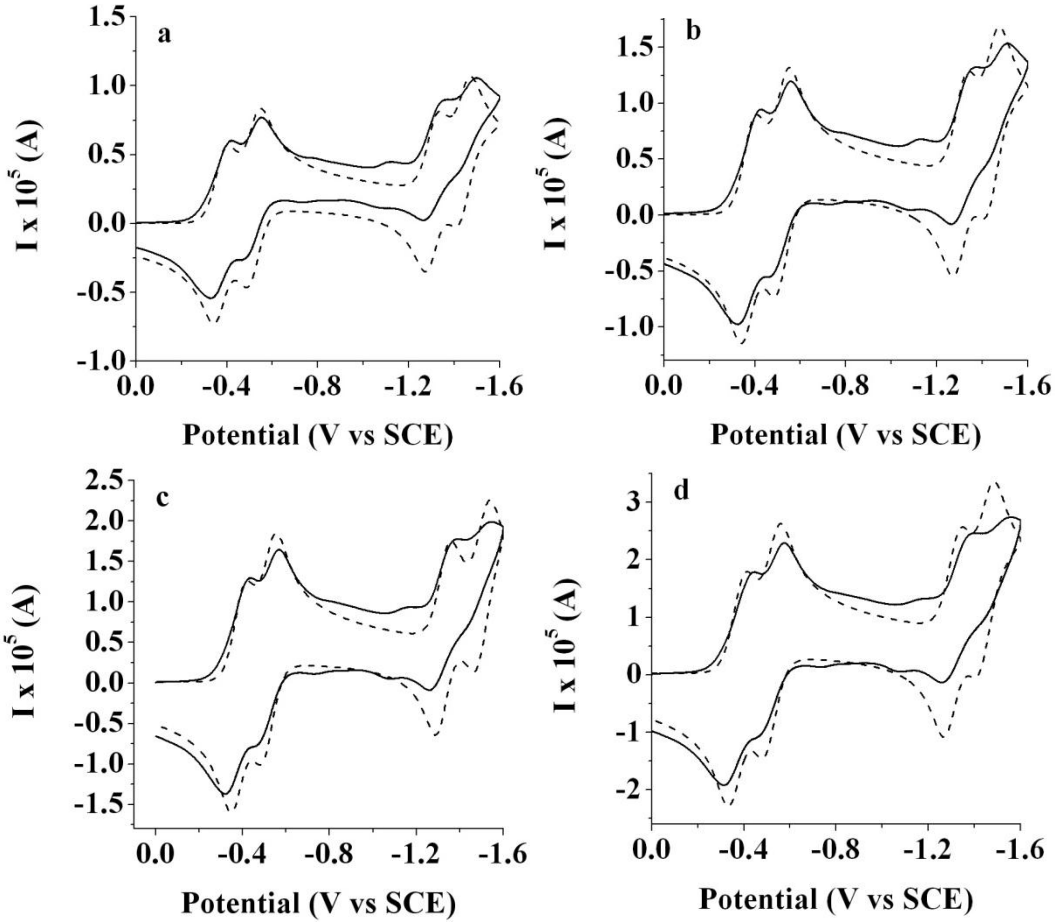

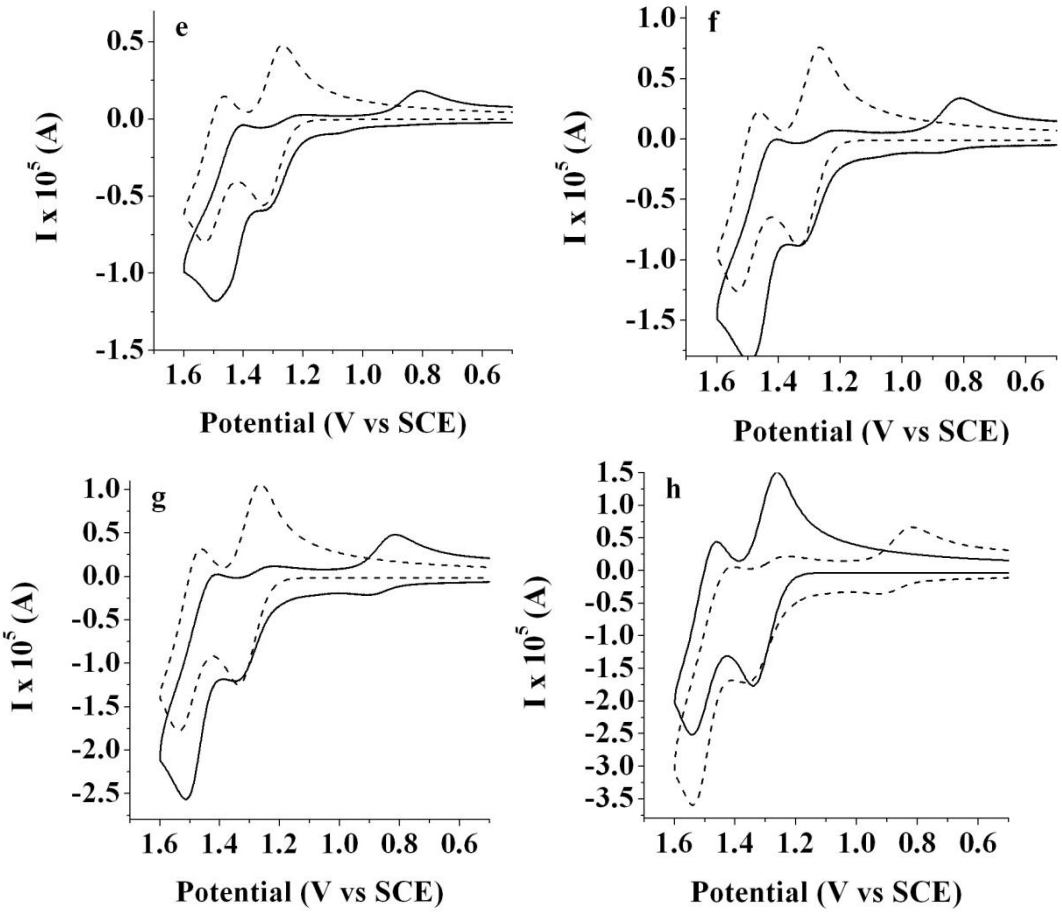


**Figure 37.** Experimental (solid) and simulated (dashed) cyclic voltammograms of 0.9 mM of **aza-BODIPY dimer**; Scan rate: (a) and (e) 0.1 V/s; (b) and (f) 0.25 V/s; (c) and (g) 0.5 V/s; (d) and (h) 1 V/s. Experimental data: solvent DCM; platinum electrode area 0.0314 $cm^2$. Simulated data: diffusion coefficient of the **aza-BODIPY dimer** 5.2 x $10^{-6}$ $cm^2/s$; uncompensated resistance: 500 Ω; capacitance 3 x $10^{-7}$ F.

### 3.4.3. Electrogenerated chemiluminescence

Electrogenerated chemiluminescence properties of the range of compounds are presented in Figures 38-41.

ECL of the both monomers showed relatively weak emission while stepping in both positive and negative direction (Figure 38a,b).

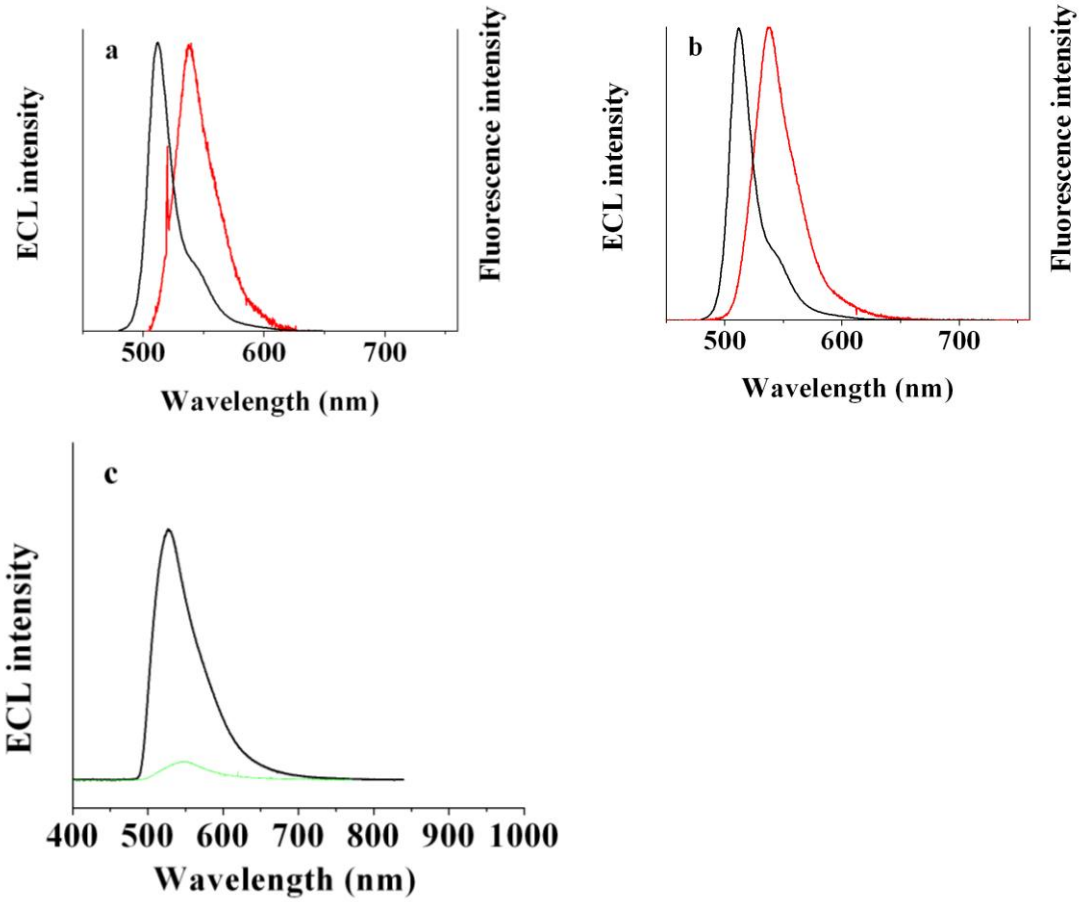


**Figure 38.** Electrogenerated (red line) and fluorescence (black line) of investigated monomers; (a) annihilation spectrum for (a)1.1 mM **13**; (b) spectra generated in the presence of 5 mM of benzoyl peroxide; (c) comparative spectra of the annihilation results (green line) and in the presence of coreactant (black line); solvent: DCM; supporting electrolyte: 0.1 M $TBAPF_6$; platinum electrode area: 0.0314 $cm^2$.

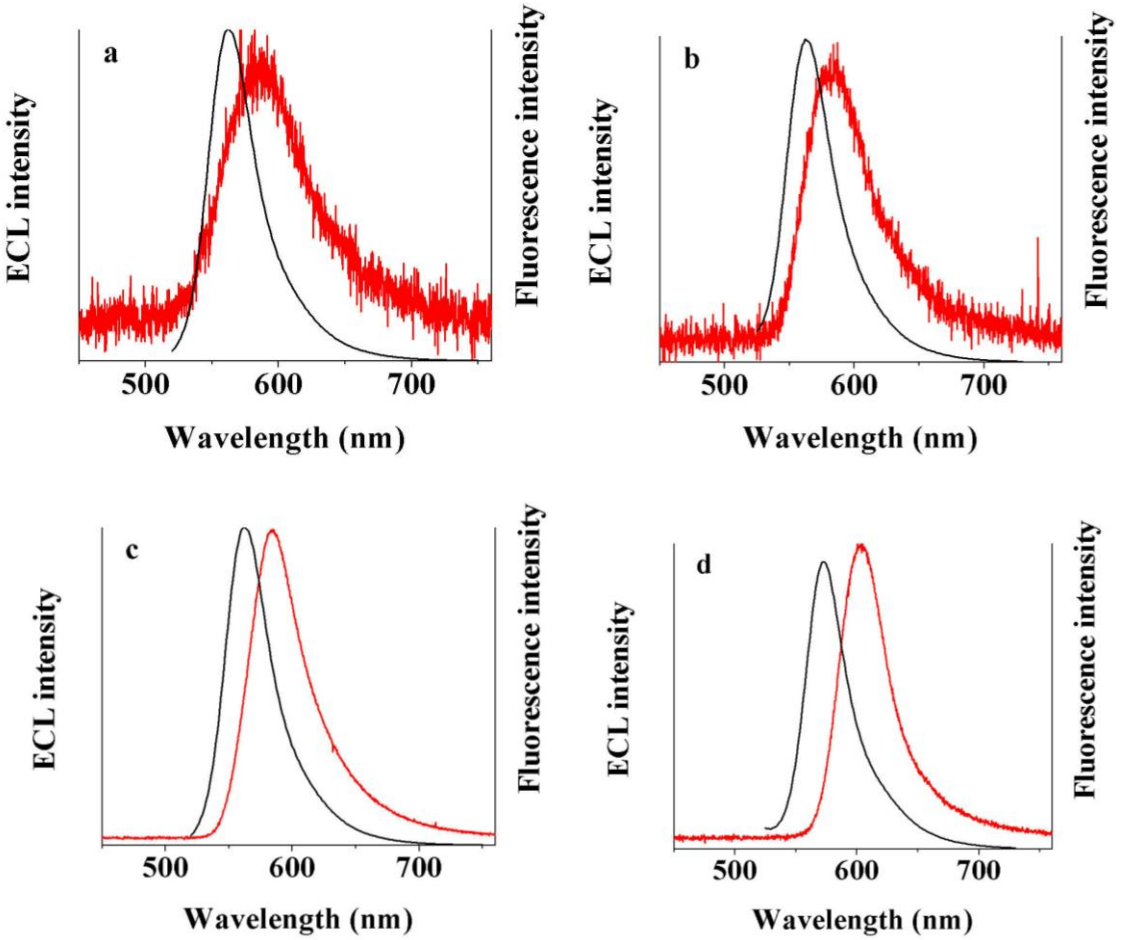


**Figure 39.** Electrogenerated (red line) and fluorescence spectra (black line) for the investigated dimers; (a) and (b) annihilation spectrum for 0.14 mM **dimer 14** (a) and 0.2 mM **dimer 15** (b); (c) and (d) spectra generated in the presence of 5 mM of benzoyl peroxide; solvent: DCM; supporting electrolyte: 0.1 M $TBAPF_6$; platinum electrode area: 0.0314 $cm^2$.

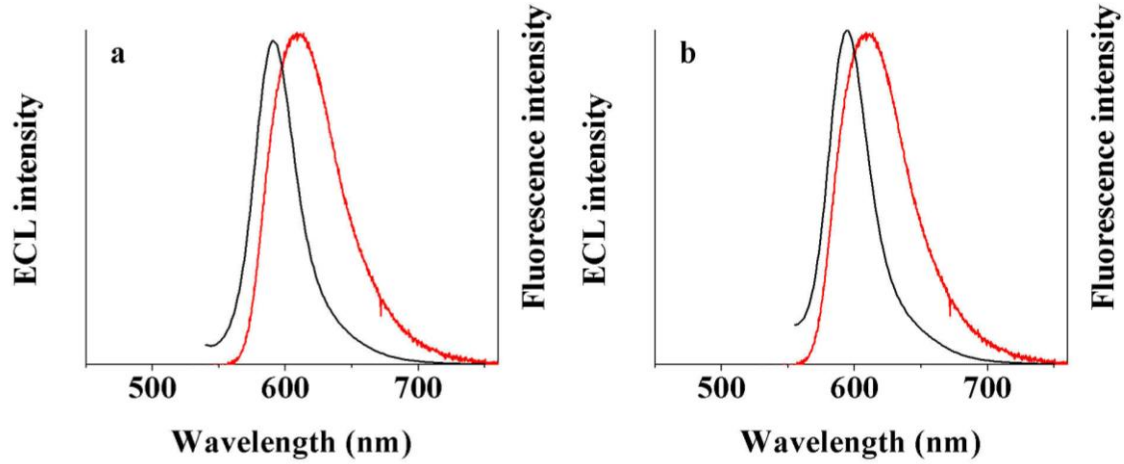

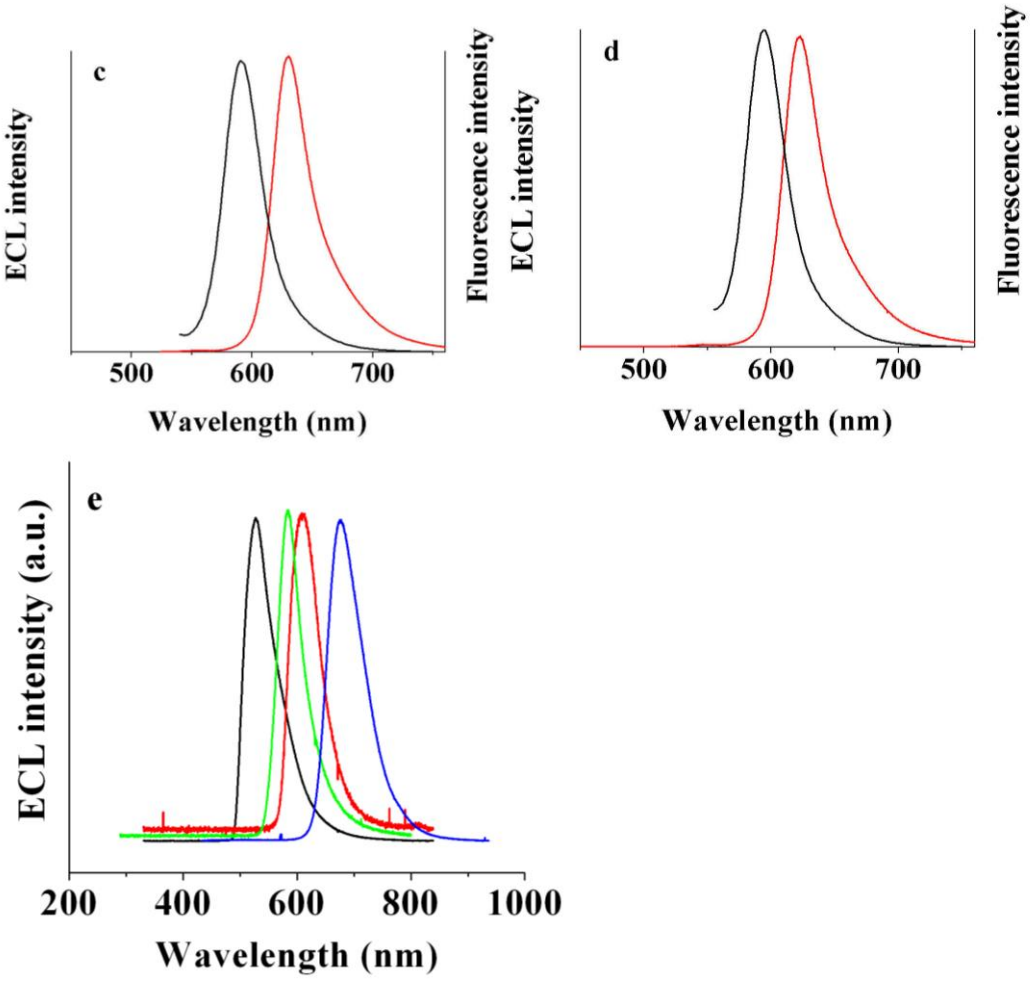


**Figure 40.** Electrogenerated spectra of the corresponded trimers; (a) and (b) annihilation spectrum for 0.1 mM **trimer 16** (a) and 0.24 mM **trimer 17** (b); (c) and (d) spectra generated in the presence of 5 mM of benzoyl peroxide; (e) comparison of the ECL spectra for 1.0 mM **3** (black line), 0.14 mM **dimer 14** (green line), 0.1 mM **trimer 16** (red line) and 0.5 mM **angular dimer 11** (blue line) in the presence of 5.0 mM benzoyl peroxide. All spectra were normalized to the same height. Solvent: DCM; supporting electrolyte: 0.1 M $TBAPF_6$; platinum electrode area: 0.0314 $cm^2$.

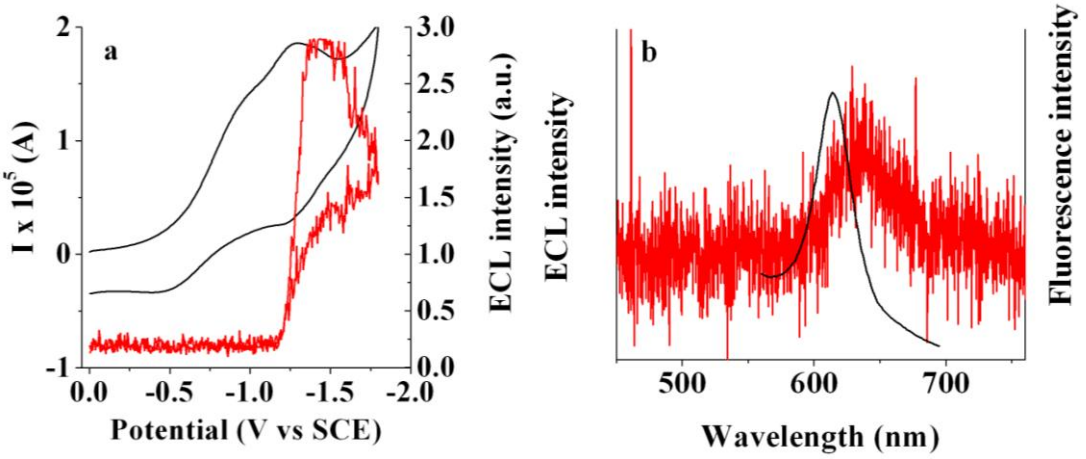


**Figure 41.** (a) Simultaneous ECL-CV measurement for 0.1 mM **polymer 18** in the presence of 1 mM benzoyl peroxide at a scan rate of 1 V/s; (b) ECL spectra generated in the presence of 5 mM benzoyl peroxide. Solvent: $CH_2Cl_2$, supporting electrolyte: 0.2 M $TBAPF_6$; electrode area: 0.12 $cm^2$.

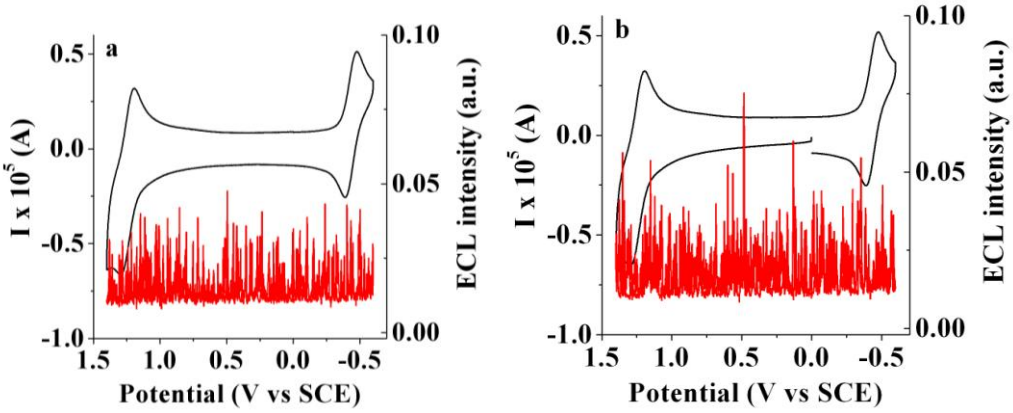

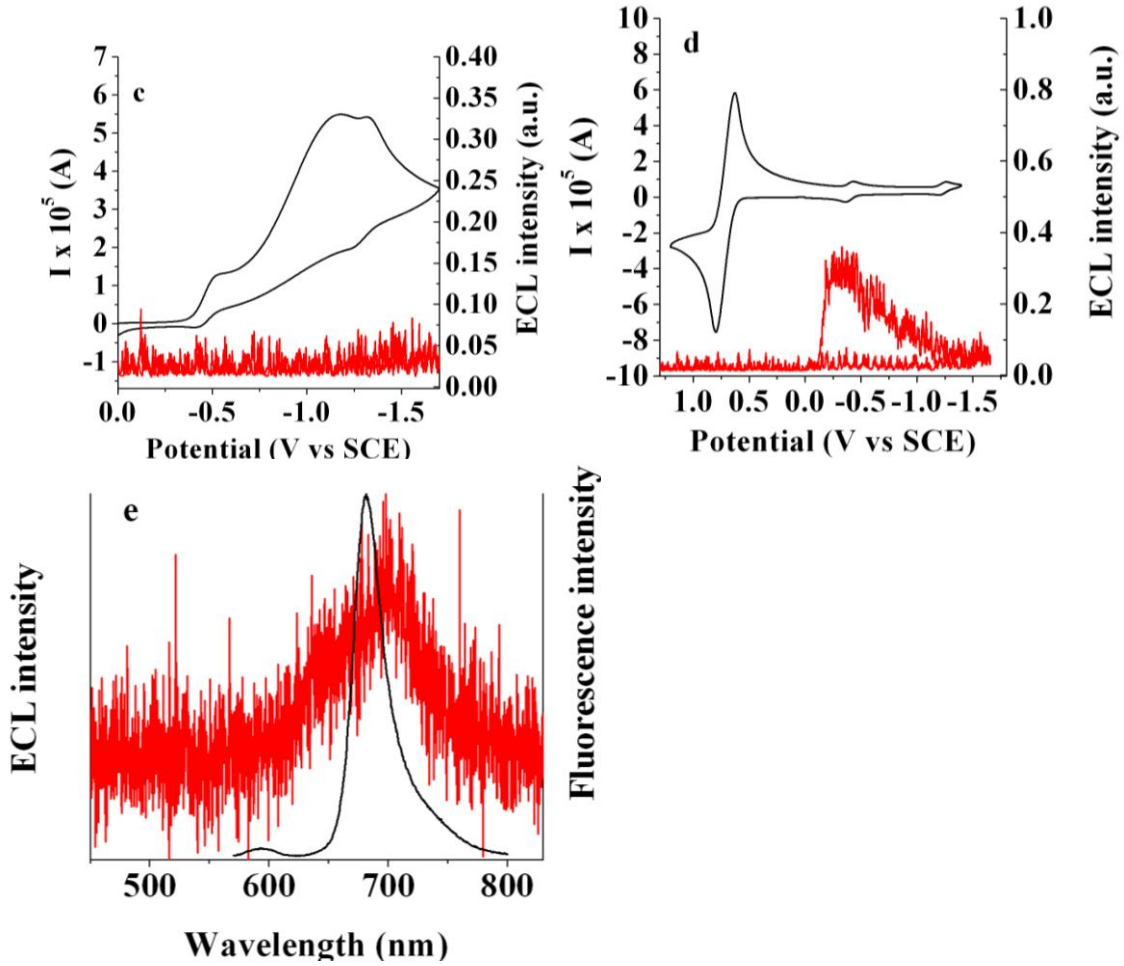


**Figure 42.** Simultaneous ECL-CV cyclic voltammograms of the 0.5 mM of the **aza-BODIPY monomer 19** during scans into the (a) negative and (b) positive direction at a scan rate of 1 V/s; (c) in the presence of 3.0 mM benzoyl peroxide; (d) in the presence of 3.0 mM 10-MP; (e) ECL spectra for 0.5 mM (red line) and fluorescence spectra (black line) for 2 mM **aza-BODIPY monomer 19** in the presence of 5.0 mM 10-MP. ECL spectrum was generated from 80 mV of the peaks of the reduction of aza-BODIPY monomer and oxidation of 10-MP. Solvent: $CH_2Cl_2$, supporting electrolyte: 0.1 M $TBAPF_6$; electrode area: 0.0314 $cm^2$.

The ECL emission was about 15 times larger with the coreactant and also showed a much higher stability with time compared with the annihilation ECL (Figure 38c). The ECL annihilation spectrum can be generated only for a few minutes while in the presence of the benzoyl peroxide it was stable for more than an hour. The ECL-spectral maximum

was similar to that of the fluorescence with the slight difference due to an inner filter effect. No features that can be assigned to formation of the dimer, trimer or some other species were seen. The same relatively weak annihilation intensity was found with the dimers and trimers, with dimers showing perhaps a bit higher ECL annihilation emission, and trimers slightly higher compared with the monomer (Figures 39,40). There is also an increase in ECL intensity with the addition of the benzoyl peroxide for both dimers and trimers. The ECL maxima wavelengths for the dimers and trimers is blue shifted compared with **11** in agreement with the fluorescence and electrochemical results (Figure 40). ECL studies of **aza-BODIPY** monomer and dimer 1**9** and **20** did not show substantial ECL signal by annihilation or by using benzoyl peroxide as a coreactant (Figures 41,42). This can attributed to two factors: one of them is a decrease in the photoluminescence quantum efficiency with a shift of the reduction potential to the positive direction compared with the $C^8$ dye and the other one is instability on oxidation. The first factor is probably more important, as there was substantial annihilation ECL signal for $C^8$-BODIPY. A small ECL signal can be produced for the dimer by a mixed system, with 10-methylphenothiazine (10-MP) as the radical cation precursor (Figure 42).

### 3.5. Chemical and Electrochemical Dimerization of BODIPY Compounds

#### 3.5.1. Photophysical studies

UV-Vis absorption behavior of the **21** monomer is shown in Figure 43 (Scheme 10).

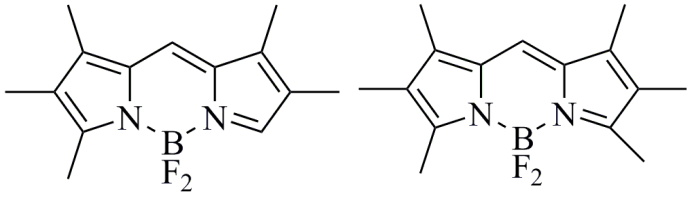

**21**, 1(x3,8) **22**, 2(x8)

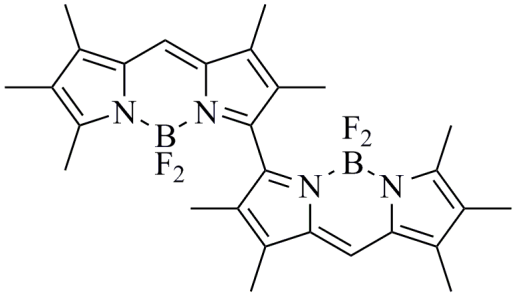

**23**, 3,3'-dimer

**Scheme 10.** Chemical structure of the dyes used in this chapter.

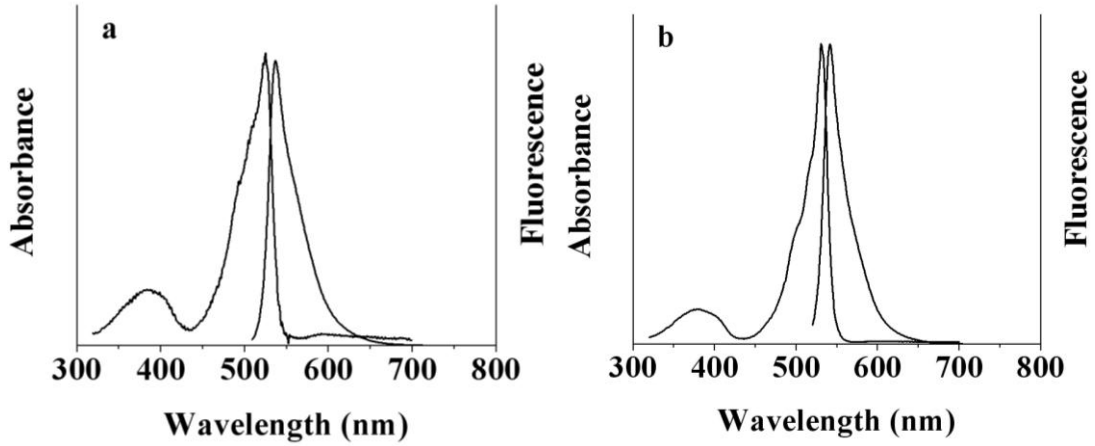

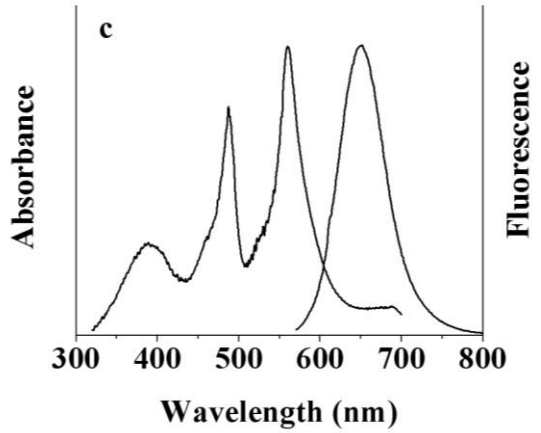


**Figure 43.** Absorption and fluorescence spectra of 2 μM BODIPY dyes in methylene chloride: (a) **21** (**1**(x3,8)); (b)**22** (**2**(x8)); (c) **23** (3,3'-dimer).

The behavior is characteristic of simple BODIPY monomer with two absorption maxima at 383 and 524 nm which correspond to the S2-S0 and S1-S0 transitions, with the fluorescence maximum at 537 nm. The Stokes shift for the monomer **21** is small, which is characteristic of BODIPY monomers (Figure 43a). The **22** shows similar behavior with slightly red shifted wavelength for absorption and fluorescence due to the presence of the additional methyl group at position 3 (Figure 43b). The 3,3'- dimer **23** shows characteristic excitonic splitting of the absorption spectra with one lower and one higher energetic process, producing three absorption features at 387, 489 and 562 nm (Figure 43c). The dimer also shows a larger Stokes shift with the fluorescence maximum at 650 nm. The quantum yield for the dimer is smaller than that of the monomer because of splitting of excited state leading to an increase in intersystem crossing and nonradiative decay. The results obtained here are close to the photophysical results for the dimers obtained for two-fold $BF_2$ coordination of the free-base ligands.

### 3.5.2. Electrochemical studies

Two general principles govern the electrochemical behavior of BODIPY compounds. First, the $\alpha$ and $\beta$ sites are subject to electrophilic and nucleophilic attack, so substitution of these positions serves to stabilize the radical ions. Second, second reduction and oxidation waves (i.e. from the radical ion to the di-ion) involve a much greater potential difference than in aromatic hydrocarbons and most heterocycles, so, in fact, multiple peaks are rarely seen within the solvent window for species with stable radical ions. The reason for this surprising difference is currently under investigation. Thus, the CV of **21** indicates some instability on reduction because of the absence of the substituent in the 3-position (Figure 44).

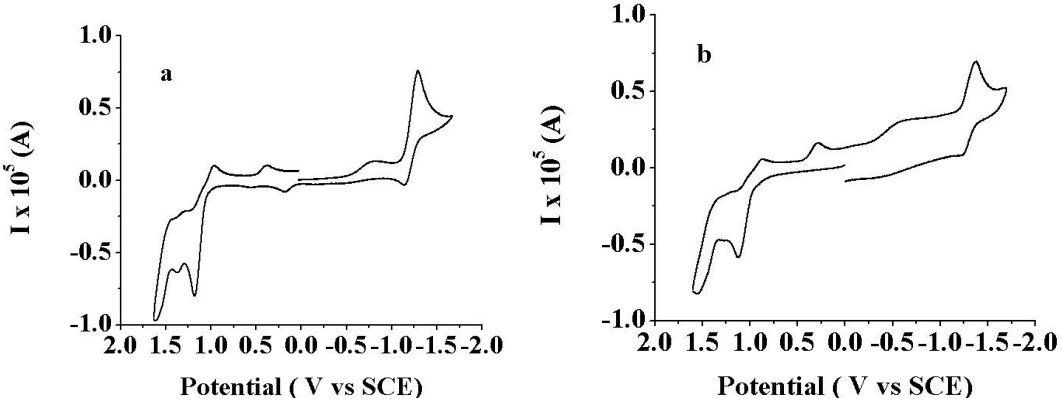

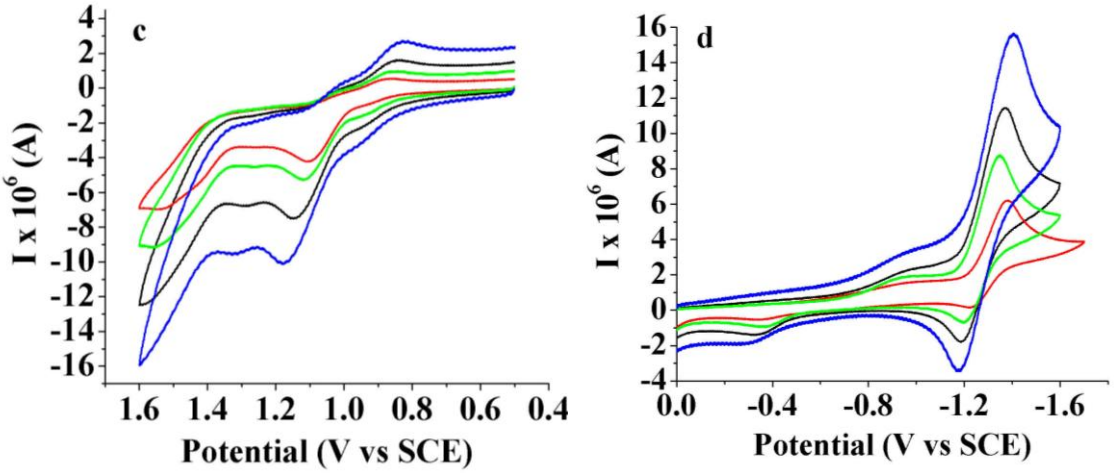


**Figure 44.** Cyclic voltammogram of 1.5 mM **21** (**1**(x3,8)) at a scan rate of 0.1 V/s in methylene chloride at platinum working electrode (area = 0.0314 $cm^2$); supporting electrolyte: 0.1 M $TBAPF_6$; (a) forward scan to the negative direction; (b) forward scan to the positive direction; scan rate dependence for oxidation (c) and reduction (d).

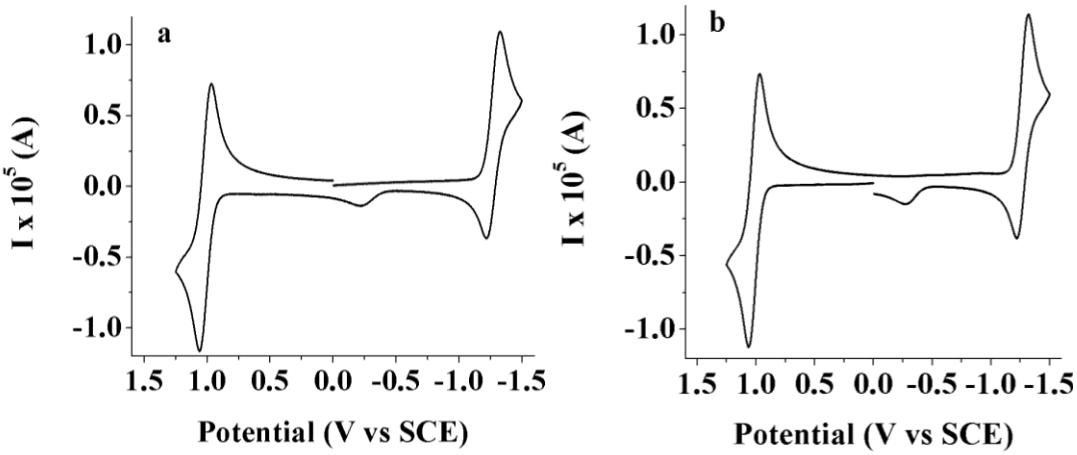


**Figure 45.** Cyclic voltammogram of 1.5 mM **22** (**2**(x8)) at a scan rate of 0.1 V/s in methylene chloride at platinum working electrode (area = 0.0314 $cm^2$); supporting electrolyte: 0.1 M $TBAPF_6$; (a) forward scan to the negative direction; (b) forward scan to the positive direction.

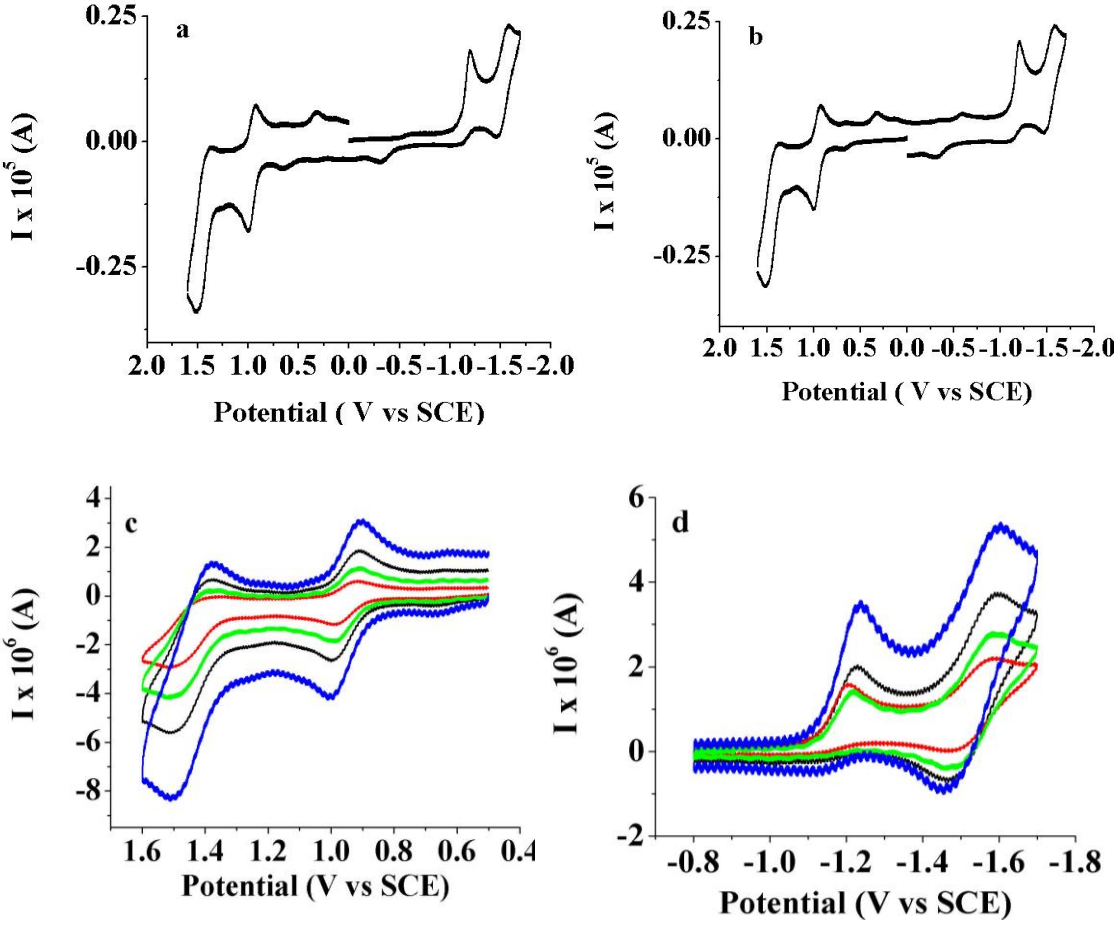


**Figure 46.** Cyclic voltammograms of 0.7 mM **23** (3,3'-dimer) at a scan rate of 0.1 V/s in methylene chloride at platinum working electrode (area = 0.0314 $cm^2$); supporting electrolyte: 0.1 M $TBAPF_6$; (a) forward scan to the negative direction; (b) forward scan to the positive direction; scan rate dependence for (c) oxidation and (d) reduction.

Further, the appearance of the two peaks on oxidation suggests a follow-up reaction of the radical cation to produce a species that is oxidized in separate waves. The reduction peak for this compound, at -1.32 V, is close to that of other BODIPY dyes that emit at similar wavelengths. The formation of the dimer on oxidation is seen for a variety of scan rates which can be seen as a proof for the fast dimerization process. There are seen two oxidation peaks at 1.12 V and 1.57 V which can be seen as a proof for the chemical

reaction and formation of new bonds. This results correlates fairly well with the results for the chemical dimerization (Scheme 11):

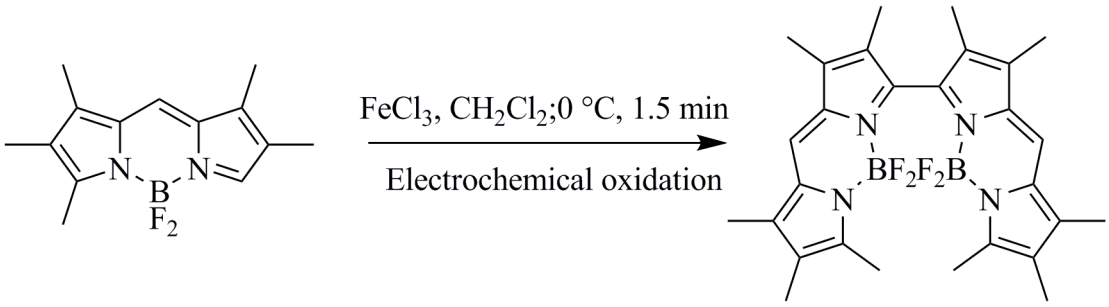


**Scheme 11.** Chemical and electrochemical dimerization mechanism.

In contrast to the CV results for the **21 22** shows the appearance of the nernstian reduction at -1.30 V and quasi-reversible oxidation at 1.11 V (Figure 45). The reduction potential is close to the **21** (**1**(x3,8)) with slightly higher chemical reversibility.

The CV of the chemically-synthesized **23**, shown in Figure 46, indicates oxidation at a chemically reversible peak at 1.0 V and less reversible one at 1.5 V. The reduction of the dimer shows two peaks at -1.23 V and -1.6 V that are less reversible. The irreversibility of the first peak confirms the importance of the presence of substitution in the *meso*-position on the stability of the radical ion. Scan rate dependence of the reduction are shown in Figure 46c,d and it corresponds pretty well with the Randles-Ševčik equation which exclude high influence of adsorption and any surface processes on the cyclic voltammograms for a short period of time. Dimerization constant can also be determined by using digital simulations and fitting them to the experimental curve (Figure 47).

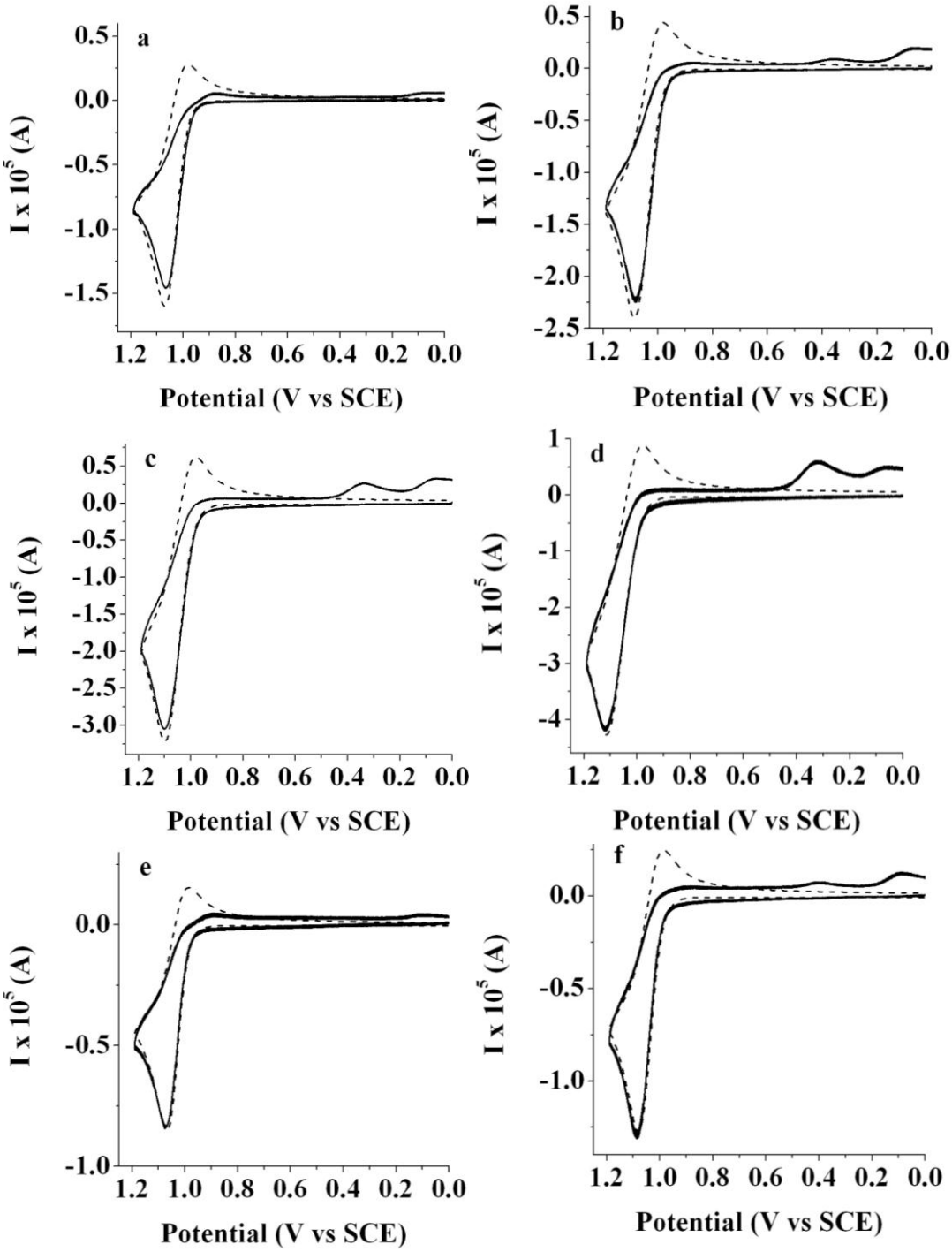
a
b
c
d
e
f
I x 10^5 (A)
Potential (V vs SCE)

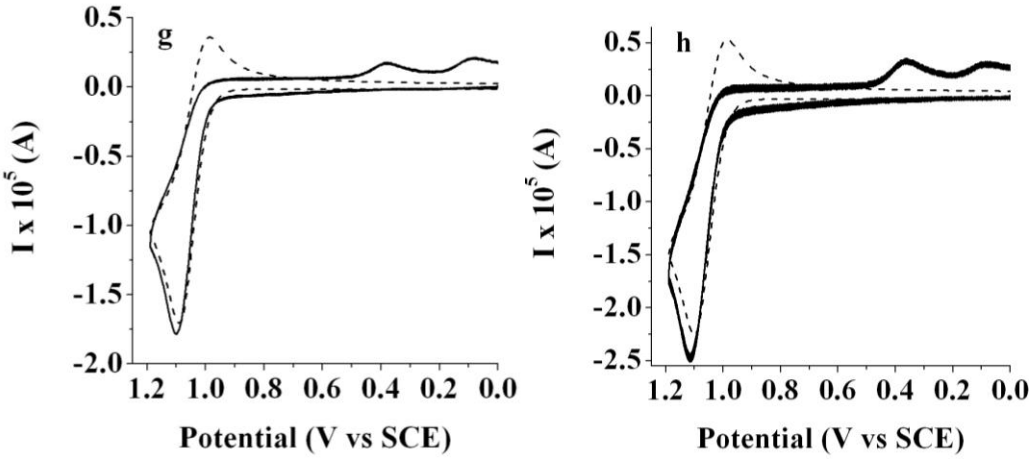


**Figure 47.** Experimental (solid) and simulated (dashed) line cyclic voltammograms of (a-d) 1.5 mM and (e-h) 0.8 mM **21** (**1**(x3,8)) during the positive direction scan. Scan rate: (a), (e) 0.1 V/s; (b), (f) 0.25 V/s; (c), (g) 0.5 V/s; (d), (h) 1 V/s. Experimental data: solvent: methylene chloride; supporting electrolyte: 0.1 M $TBAPF_6$; electrode area: 0.0314 $cm^2$. Simulated data: diffusion coefficient of the dye is 6.8 x $10^{-6}$ $cm^2/s$ for the monomer and 5.2 x $10^{-6}$ $cm^2/s$ for the dimer; deprotonation constant very fast and equal $10^{10}$ $s^{-1}$ and the dimerization constant equal 4 x $10^4$ $M^{-1}$ $s^{-1}$; uncompensated resistance 800 Ω; capacitance 3 x $10^{-7}$ F.

Electrochemical studies of the **21** species and **22** shown in the previous paragraphs allows to obtain electrochemical potentials which can be used in simulations as they correspond with the potentials of the monomer and the dimer. Experimental cyclic voltammograms and simulated results for the dimerization are shown in Figure 48. The radical-radical cation (rrc) mechanism was taken into the account for the simulation as the mechanism as the cation-substrate coupling and ion-substrate coupling show large deviation from experimental data.[107] The best fit was obtained for the dimerization second order constant equal 4 x $10^4$ $M^{-1}$ $s^{-1}$. Simulations were done for two concentrations what can be seen as a proof for the reliability of current calculations.

### 3.5.3. Electrogenerated chemiluminescence

The ECL spectra resulting from the annihilation reaction of **21** radical ions are shown in Figures 48a-d.

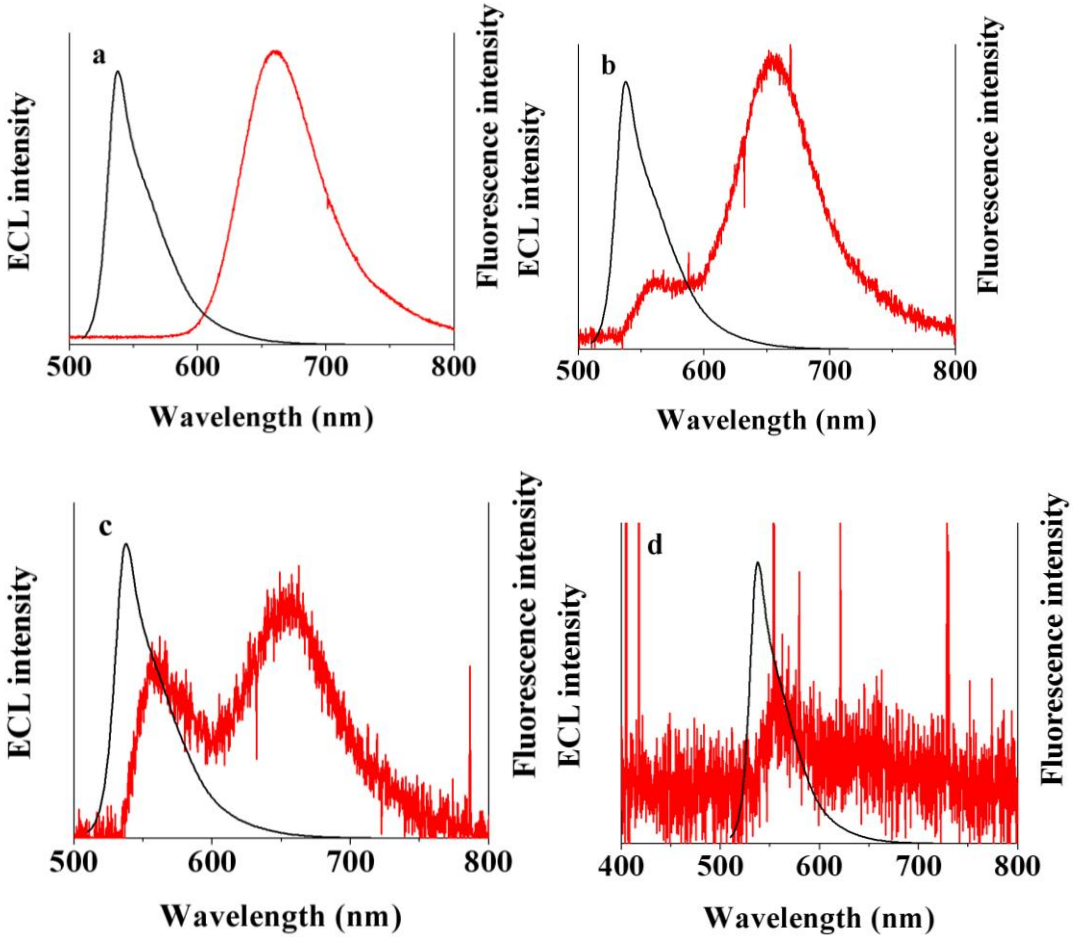

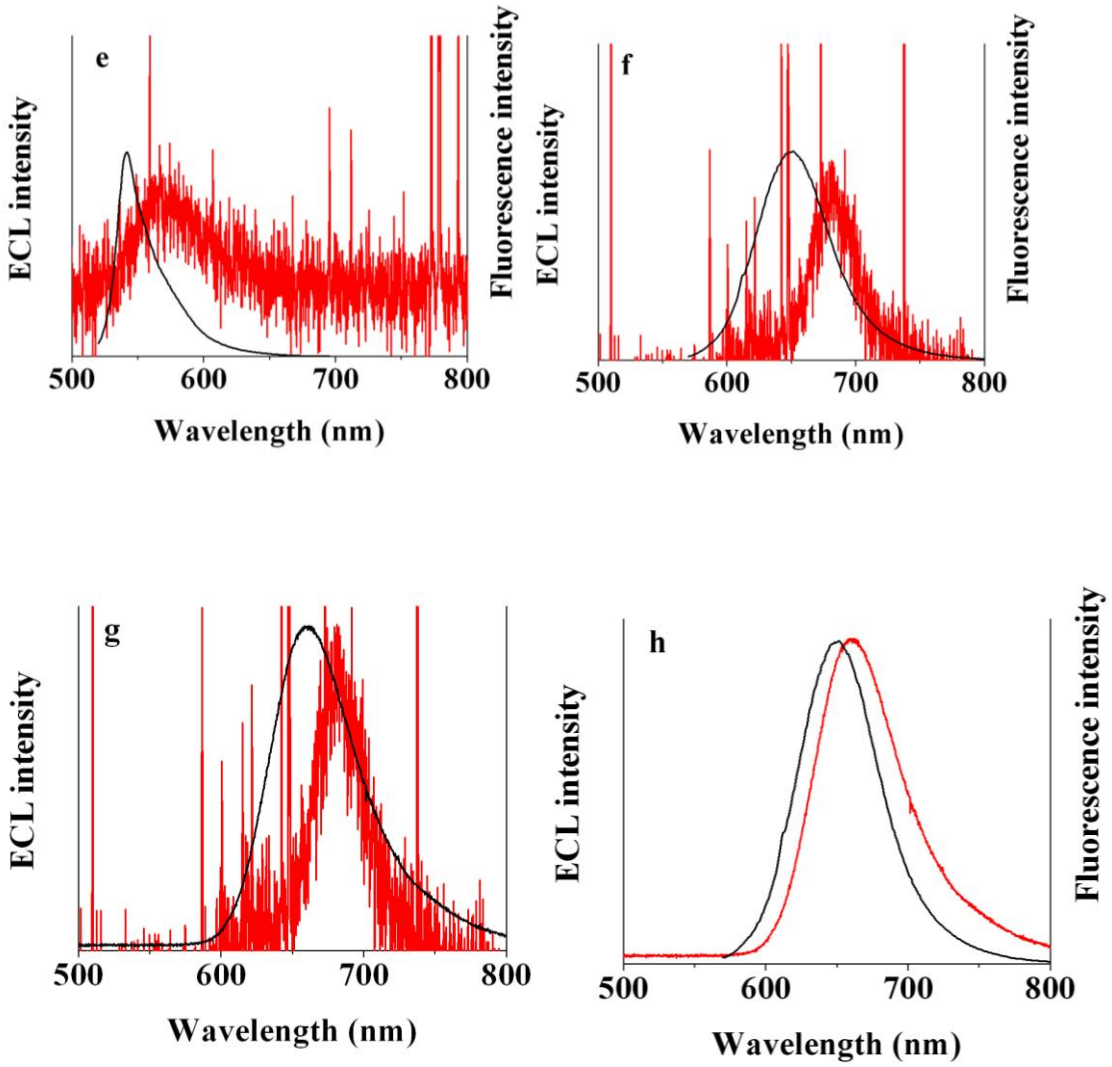


**Figure 48.** (a)- (d) ECL spectra for 1.5 mM (red line) and fluorescence spectra for 2 μM (black line) of the **21** (**1**(x3,8)) in methylene chloride. ECL spectra were generated by pulsing potential at a frequency from -1.4 V to 1.2 V for different times (min): a) 2; b) 4; c) 6 ; d) 8; (e) ECL (red line) and fluorescence spectra (black line) for 2 μM **22** (**2**(x8)) with stepping from -1.38 V to 1.19 V for 2 minutes; (f) ECL spectra for 0.7 mM (red line) and fluorescence spectra for 2 μM (black line) of **23** (3,3'-dimer). ECL spectra were generated by stepping potential from -1.68 V to 1.08 V; g) comparison of the ECL spectra of 0.7 mM **2**(x8) (red line) and **23** (3,3'-dimer) (black line); h) comparison of ECL (red line) spectra of 1.5 mM **21** (**1**(x3,8)) and fluorescence spectra of **23** (3,3'-dimer). Frequency of pulsing 10 Hz; platinum electrode area equal 0.0314 $cm^2$ and 0.1 M $TBAPF_6$ supporting electrolyte were used for all electrochemistry measurements.

These can be compared to the ECL from **22**, which show the formation of one ECL peak at 565 nm corresponding to the wavelength of monomer emission (Figure 48e). Most other BODIPY species show this kind of emission agreeing with the PL. With **1**(x3,8) we also find long wavelength emission at 656 nm, considerably red-shifted from the smaller monomer emission peak at 560 nm. The ECL intensity decreases somewhat during the consecutive stepping the growth of the short wavelength peak and decrease of the long wavelength emission, which we ascribe to film formation with time (Figures 48a-d). The low intensity of the ECL may also be connected to some degree to the irreversibility on both oxidation and reduction.

The 3,3'-dimer **23** shows the appearance of one ECL peak at 679 nm which agrees pretty well with the fluorescence results (Figure 48f). The long wavelength ECL signal at 656 nm found with **21** (**1**(x3,8)) correlates quite well with the ECL and fluorescence for the chemically synthesized dimer at 679 nm, thus providing strong evidence for the electrochemical formation of the dimer (Figure 45g,h). This also corresponds to the appearance of a second oxidation peak in the cyclic voltammograms. In work previously reported, we have found that second oxidation or reduction peaks in BODIPY compounds are generally spaced at much larger potential differences (~1 V) compared to aromatic hydrocarbons where potential differences ~0.5 to 0.6 V are found. The existence of two reduction and oxidation waves with the **23** suggests that the possibility of greater delocalization across the two units allows closer spacing of the second electron transfer waves.

The results here show the importance of the nature of substitution position on the electrochemical properties. Position 3 is shown to promote dimerization reaction as position 8 affects mostly protonation on reduction which influence the reversibility of the electrochemical process in time and stability of the radical anions. The mechanism of the formation of the dimer during ECL can be presented than as:

$$\mathbf{1}(x3,8) + e^- \rightarrow \mathbf{1}(x3,8)^{\bullet -} \quad (54)$$

$$\mathbf{1}(x3,8) - e^- \rightarrow \mathbf{1}(x3,8)^{\bullet +} \quad (55)$$

$$\mathbf{1}(x3,8)^{\bullet +} + \mathbf{1}(x3,8)^{\bullet +} \rightarrow 3,3'\text{-dimer-}H_2^{2+} \quad (56)$$

$$3,3'\text{-dimer-}H_2^{2+} \rightarrow 3,3\text{-dimer} + 2H^+ \quad (57)$$

$$3,3'\text{-dimer} - e^- \rightarrow 3,3'\text{- dimer}^{\bullet +} \quad (58)$$

$$\mathbf{1}(x3,8)^{\bullet -} + 3,3'\text{-dimer}^{\bullet +} \rightarrow \mathbf{1}(x3,8) + 3,3'\text{-dimer}^* \quad (59)$$

$$3,3'\text{-dimer}^* \rightarrow 3,3'\text{-dimer} + h\upsilon \quad (60)$$

There is also the possibility of ECL from doubly charged species by going to the second oxidation wave:

$$3,3'\text{-dimer}^{\bullet +} - e^- \rightarrow 3,3'\text{-dimer}^{2\bullet +} \quad (61)$$

$$\mathbf{1}(x3,8)^{\bullet -} + 3,3'\text{-dimer}^{2\bullet +} \rightarrow \mathbf{1}(x3,8) + 3,3'\text{-dimer}^* \quad (62)$$

It is seen that production of the single or double charged radical anion by oxidation cause the formation of the ECL signal for dimer by annihilation with the radical cation produced by reduction. The signal for the second oxidation peak was smaller due the instability of the radical ions in time.

## Chapter 5: Summary and Conclusions

BODIPY dyes are shown to be interesting compounds with distinct photophysical and electrochemical features. Linear and angular dimers show different behavior with separation of electrochemical waves depending on the position of the formed C-C bonds. All used monomers show presence of one electrochemical wave, dimers two, trimers three and polymers multiple waves. Electrogenerated chemiluminescence spectra with substantial intensity were formed for completely substituted monomers, dimers and trimers. Electrogenerated chemiluminescence was also shown to be useful technique in investigation formation of aggregates and dimers. Future development of the photophysical and electrochemical properties of these materials can make it possible to apply these materials for solar cell, biological sensing and batteries.

**The results shown in this dissertation was presented in a list of publications:**

1. Nepomnyashchii, A. B.; Bröring, M.; Ahrens, J.; Bard, A. J. Synthesis, Photophysical, Electrochemical and Electrogenerated Chemiluminescence Studies. Multiple Sequential Electron Transfers in BODIPY Monomers, Dimers, Trimers and Polymer. *Journal of American Chemical Society* **2011**, 133, 8633-8645.

2. Nepomnyashchii, A. B.; Bröring, M.; Ahrens, J.; Krüger, R.; Bard, A. J. Electrochemistry and Electrogenerated Chemiluminescence of n-Pentyl and Phenyl BODIPY Species: Formation of Aggregates from the Radical Ion Annihilation Reaction. *Journal of Physical Chemistry C* **2010**, *114*, 14453-14460.

3. Nepomnyashchii, A. B.; Cho, S.; Rossky, P. J. Bard, A. J. Dependence of Electrochemical and Electrogenerated Chemiluminescence Properties on the Structure of BODIPY Dyes. Unusually Large Separation Between Sequential Electron Transfers. *Journal of American Chemical Society* **2010**, *132,* 17550-17559.

4. Nepomnyashchii, A. B.; Bröring, M.; Ahrens, J.; Bard, A. J. Chemical and Electrochemical Dimerization of BODIPY Compounds. In Preparation.

**References**.


[1] Loudet, A.; Burgess, K. *Chem. Rev.* **2007**, *107*, 4891-4932.

[2] Sathyamoorthi, G.; Boyer, J. H.; Allik, T. H.; Chandra, S. *Heteroat. Chem.* **1994**, *5*, 403-407.

[3] Pavlopulos, T. G.; Shah, M.; Boyer, J. H. *Appl. Opt.* **1988**, *27*, 4998-4999.

[4] Pavlopulos, T. G.; Shah, M.; Boyer, J. H. *Opt. Commun.* **1989**, *70*, 425-427.

[5] Wang, D.; Miyamoto, R.; Shiraishi, Y.; Hirai, T. *Langmuir* **2009**, *25*, 13176-13182.

[6] Kennedy, D. P.; Kormos, C. M.; Burdette, S. *J. Am. Chem. Soc.* **2009**, *131*, 8578-8586.

[7] Rosenthal, J.; Lippard, S. J. *J. Am. Chem. Soc.* **2009**, *132*, 5536-5537.

[8] Lee, Y. C.; Hupp, J. T. *Langmuir* **2010**, *26*, 3760-3765.

[9] Godoy, J.; Vives, G.; Tour, J. M. *Org. Lett.* **2010**, *12*, 1464-1467.

[10] Nierth, A.; Kobitski, A. Y.; Nienhaus, G. U.; Jäschke, A. *J. Am. Chem. Soc.* **2010**, *132*, 2646-2654.

[11] Frein, S.; Camerel, F.; Ziessel, R.; Barbera, J.; Deschenaux, R. *Chem. Mater.* **2009**, *21*, 3950-3959.

[12] Lazarides, T.; McCormick, T. M.; Wilson, K. C.; Lee, S.; McCamant, D. W.; Eisenberg, R. *J. Am. Chem. Soc.* **2011**, *133*, 350-364.

[13] Collado, D.; Casado, J.; Rodriugez-Gonzales, S.; Lopez-Navarrete, J. T.; Suau, R.; Perez-Inestrosa, E.; Pappenfus, T. M.; Raposo, M. M. M. *Chem. Eur. J.* **2011**, *17*, 498-507.

[14] Ziessel, R.; Rihn, S.; Harriman, A. *Chem. Eur. J.* **2010**, *16*, 11942-11953.

[15] Ziessel, R.; Ulrich, G.; Harriman, A. *New. J. Chem.* 2007, 31, 496-501.

[16] Zrig, S.; Remy, P.; Andrioletti, B.; Rose, E.; Asselberghs, I.; Clays, K. *J. Org. Chem.* **2008**, *73*, 1563-1566.

[17] Ulrich, G.; Ziessel, R.; Harriman, A. *Angew. Chem. Int. Ed.* **2008**, *47*, 1184-1201.

[18] Li, Z.; Bittman, R. J. *J. Org. Chem.* **2007**, *72*, 8376-8382.

[19] Wakamiya, A.; Sugita, N.; Yamaguchi, S. *Chem. Lett.* **2008**, *37*, 1094-1095.

[20] Karolin, J.; Johansson, L.B-Å.; Strandberg, L.; Ny, T. *J. Am. Chem. Soc.* **1994**, *116*, 7801-7806.

[21] Wagner, R. W.; Lindsey, J. S. *Pure Appl. Chem.* **1996**, *68*, 1373-1380.

[22] Yee, M.-C.; Fas, S. C.; Stohlmeyer, M. M.; Wandless, T. J.; Climprich, K. A. *J. Biol. Chem.* **2005**, *280*, 29053-29059.

[23] Tan, K.; Jaquinod, L.; Paolesse, R.; Nardis, S.; Di Natale, C.; Di Carlo, A.; Prodi, L.; Montalti, M.; Zaccheroni, N.; Smith, K. M. *Tetrahedron* **2004**, *60*, 1099-1106.

[24] Liras, M.; Prieto, J. B.; Pintado-Sierra, M.; Arbeloa, F. L.; Garcia-Moreno, I.; Costela, A.; Infantes, L.; Sastre, R.; Amat-Guerri, F. *Org. Lett.* **2007**, *9*, 4183-4186.

[25] Bröring, M.; Krüger, R.; Link, S.; Kleeberg, C.; Kohler, S.; Xie, X.; Ventura, B.; Flamigni, L. *Chem.-Eur. J.* **2008**, *14*, 2976-2983.

[26] Treibs, A.; Kreuzer, F.-H. *Liebigs Ann. Chem.* **1968**, *718*, 208-223.

[27] Haugland, R. P., in Handbook of Molecular Probes and Research Products, Molecular Probes, Inc., Eugene, OR, 9th ed. 2002.

[28] Urano, Y.; Asunama, D.; Hama, Y.; Koyama, Y.; Barrett, T.; Kamiya, M.; Nagano, T.; Watanabe, T.; Hasegawa, A.; Choyke, P. L.; Kobayashi, H. *Nat. Med.* **2009**, *15*, 104-109.

[29] Gabe, Y.; Urano, Y.; Kikuchi, K.; Kojima, H.; Nagano, T. *J. Am. Chem. Soc.* **2004**, 126, 3357-3367.

[30] Ueno, T.; Urano, Y.; Kojima, H.; Nagano, T. *J. Am. Chem. Soc.* **2006**, *128*, 10640-10641.

[31] Gomez-Duran, C. F. A.; Garcia-Moreno, I.; Costela, A.; Martin, V.; Sastre, R.; Bañuelos, J.; Arbeloa, F. L.; Arbeloa, I. L. Peña-Cabrere, E. *Chem. Commun.* **2010**, *46*, 5103-5105.

[32] Zhu, S.; Zhang, J.; Vegesna, G.; Luo, F. T.; Green, S. A.; Liu, H. *Org. Lett.* **2011**, *13*, 438-441.

[33] Sabatini, R. P.; McCormick, T. M.; Lazarides, T.; Wilson, K. C.; Eisenberg, R.; McCamant, D. W. *J. Phys. Chem. Lett.* **2011**, *2*, 223-227.

[34] Kim, B.; Ma, B.; Donuru, V. R.; Liu, H.; Frechet, J. M. J. *Chem. Commun.* **2010**, *46*, 4148-4150.

[35] Lee, C. Y.; Hupp, J. T. *Langmuir* **2010**, *26*, 3760-3765.

[36] Lai, R. Y.; Bard, A. J. *J. Phys. Chem. B* **2003**, *107*, 5036-5042.

[37] Sartin, M. A.; Camerel, F.; Ziessel, R.; Bard, A. J. *J. Phys. Chem. C* **2008**, *112*, 10833-10841.

[38] Kollmansberger, M.; Garies, T.; Heinl, S.; Breu, J.; Daub, J. *Angew. Chem. Int. Ed.* 1997, 36, 1333-1335.

[39] Röhr, H.; Trieflinger, C.; Rurack, K.; Daub, J. *Chem. Eur. J.* **2006**, *12*, 689-700.

[40] Trieflenger, C.; Röhr, H.; Rurack, K.; Daub, J. *Angew. Chem. Int. Ed.* **2005**, *44*, 6943-6947.

[41] Richards, T. C.; Bard, A. J. *Anal. Chem.* **1995**, *67*, 3140-3147.

[42] Chen, F.-C.; Ho, J.-H.; Chen, C.-Y.; Su, O.; Ho, T.-I. *J. Electroanal. Chem.* **2001**, *499*, 17-23.

[43] Bard, A. J. *J. Am. Chem. Soc.* **2010,** *132*, 7559-7567.

[44] Demortier, A.; Bard, A. J. *J. Am. Chem. Soc.* **1973**, *95*, 3495-3500.

[45] Smith, W. H.; Bard, A. J. *J. Am. Chem. Soc.* **1975**, *97*, 6491-6495.

[46] Smith, W. H.; Bard, A. J. *J. Am. Chem. Soc.* **1975**, *97*, 5203-5210.

[47] Amatore, C.; Badoz-Lambling, J.; Bonnel-Huyghes, C.; Pinson, J.; Saveant, J. M.; Thiebault, A. *J. Am. Chem. Soc.* **1982**, *104*, 1979-1986.

[48] Meerholz, K.; Heinze, J. *J. Am. Chem. Soc.* **1989**, *111*, 2325-2326.

[49] Aten, A. C.; Burthker, C.; Hoytink, G. J. *Trans. Faraday Soc.* **1959**, *55*, 324-330.

[50] Bard, A. J.; Santhanam, K. S. V. *J. Am. Chem. Soc.* **1966**, *88*, 2669-2675.

[51] Bard, A. J. *Pure Appl. Chem.* **1971**, *25*, 379-394.

[52] Hoytink, G. J. In Advances in Electrochemistry and Electrochemical Engineering; Delahay, P., Ed.; Wiley Interscience: New York, 1970; Vol. 7 and references therein.

[53] Maloy, J. T.; Bard, A. J. *J. Am. Chem. Soc.* **1971**, *93*, 5968-5981.

[54] Dietz, R.; Larcombe, B. E. *J. Chem. Soc. B* **1970**, 1369-1373.

[55] Evans, D. H. *Chem. Rev.* **2008**, *108*, 2113-2144.

[56] Geiger, W. E.; LeSuer, R. L. *Angew. Chem. Int. Ed.* **2000**, *39*, 248-250.

[57] Barriere, F.; Geiger, W. E. *J. Am. Chem. Soc.* **2006**, *128*, 3980-3989.

[58] Camire, N.; Nafady, A.; Geiger, W. E. *J. Am. Chem. Soc.* **2002**, *124*, 7260-7261.

[59] Barriere, F.; Camire, N.; Geiger, W. E.; Westerhoff-Mueller, U. T.; Sanders, R. *J. Am. Chem. Soc.* **2002**, *124*, 7262-7263.

[60] Heinze, J.; Frontana-Uribe, B. A.; Ludwigs, S. *Chem. Rev.* **2010**, *110*, 4724-4771.

[61] Heinze, J.; Mortensen, J.; Müllen, K.; Schenk, R. J. *Chem. Soc., Chem. Commun.* **1987**, 701-703.

[62] Meerholz, K.; Gregorius, H.; Müllen, K.; Heinze, J. *Adv. Mater.* **1994**, *6*, 671-674.

[63] Itaya, K.; Bard, A. J.; Szwarc, M. *Z. Phys. Chem NF* **1978**, *112*, 1-9.

[64] Lai, R. Y.; Fabrizio, E. F.; Lu, L.; Jenekhe, S. A.; Bard, A. J. *J. Am. Chem. Soc.* **2001**, *123*, 9112-9118.

[65] Shen, M.; Rodriguez-Lopez, J. Huang, J.; Liu, Q; Zhu, X. H.; Bard, A. J. *J. Am. Chem. Soc.* **2010**, *132*, 13453-13461.

[66] Ikeda, T.; Aprahamian, I.; Stoddart, J. F. *Org. Lett.* **2007**, *9*, 1481-1484.

[67] Janowska, I.; Miomandre, F.; Clavier, G.; Audebert, D.; Zakrzewski, J.; Thi, K. H.; Ledoux-Rak, I. *J. Phys. Chem. A* **2006**, *110*, 12971-12975.

[68] (a) Electrogenerated Chemiluminescence; Bard, A. J., Ed.; Marcel Dekker; New York, 2004. (b) Richter, M. *Chem. Rev.* **2008**, *108*, 2506-2553. (c) Miao, W. Chem. Rev. 2008, 108, 2506-2553.

[69] Chang, M. M.; Saji, T.; Bard, A. J. *J. Am. Chem. Soc.* **1977**, *99*, 5399-5403.

[70] Rubinstein, I.; Bard, A. J. *J. Am. Chem. Soc.* **1981**, *103*, 512-516.

[71] Leland, J. K.; Powell, M. J. *J. Electrochem. Soc.* **1990**, *137*, 3127-3131.

[72] Miao, W.; Choi, J. P.; Bard, A. J. *J. Am. Chem. Soc.* **2002**, *124*, 14478-14485.

[73] White, H. S.; Bard, A. J. *J. Am. Chem. Soc.* **1982**, *104*, 6891-6895.

[74] Faulkner, L. R.; Bard, A. J. *J. Am. Chem. Soc.* **1969**, *91*, 209-210.

[75] Faulkner, L. R.; Tachikawa, H.; Bard, A. J. *J. Am. Chem. Soc.* **1972**, *94*, 691-699.

[76] Santhanam, K. S. V.; Bard, A. J. *J. Am. Chem. Soc.* **1965**, *87*, 139-140.

[77] Tokel, N. E.; Keszthelyi, C. P.; Bard, A. J. *J. Am. Chem. Soc.* **1972**, *94*, 4872-4877.

[78] Chandross, E.A.; Sonntag, F.I. *J. Am. Chem. Soc.* **1966**, *88*, 1089-1096.

[79] Santa-Cruz, T. D.; Akins, D. L.; Birke, R. L. *J. Am. Chem. Soc.* **1976**, *98*, 1677-1682.

[80] Akins, D. L.; Birke, R. L. *Chem. Phys. Lett.* **1974**, *29*, 428-435.

[81] Yang, H.; Leland, J. K.; Yost, D.; Massey, R. J. *Bio/Technology*, **1994**, *12*, 193-194.

[82] Elecsys is a registered trademark of a Member of the Roche group.

[83] Kibbey, M. C.; MacAllan, D.; Karaszkiewicz, J. W. *J. Assoc. Lab. Automation* **2000**, *5*, 45-48.

[84] Choi, J.-P.; Wong, K.-T.; Chen, Y.-M.; Yu, J.-K. Chou, P.-T.; Bard, A. J. *J. Phys. Chem. B* **2003**, *107*, 14407-14413.

[85] Zhang, D.; Wen, Y.; Xiao, Y.; Yu, G.; Liu, Y.; Qian, X. *Chem. Commun.* **2008**, 39, 4777-4779.

[86] Prieto, I.; Teetsov, J.; Fox, M. A.; Vanden Bout, D.; Bard, A. J. *J. Phys. Chem. A* **2001**, *105*, 520-523.

[87] Lai, R. Y.; Flemming, J. J.; Merner, B. L.; Vermeij, R. J.; Bodwell, G. J.; Bard, A. J. J. Phys. Chem. A **2004**, *108*, 376-383.

[88] Rashidnadimi, S.; Hung, T. H.; Wong, K. T.; Bard, A. J. *J. Am. Chem. Soc.* **2008**, *130*, 634-639.

[89] Park, S. M.; Bard, A. J. *J. Am. Chem. Soc.* **1975**, *97*, 2978-2985.

[90] Ketter, J. B.; Wightman, R. M. *J. Am. Chem. Soc.* **2004**, *126*, 10183-10189.

[91] Libert, M.; Bard, A. J. *J. Electrochem. Soc.* **1976**, *123*, 814-818.

[92] Fabrizio, E. F.; Prieto, I.; Bard, A. J. *J. Am. Chem. Soc.* **2000**, *122*, 4996-4997.

[93] Maloy, J. T.; Prater, K. B.; Bard, A. J. *J. Phys. Chem.* **1968**, *72*, 4348-4350.

[94] Freed, D. J.; Faulkner, L. R. *J. Am. Chem. Soc.* **1971**, *93*, 3565-3568.

[95] Keszthelyi, C. P.; Tachikawa, H.; Bard, A. J. *J. Am. Chem. Soc.* **1972**, *94*, 1522-1527.

[96] Slaterbeck, A. F.; Meehan, T. D.; Gross, E. M.; Wightman, R. M. *J. Phys. Chem. B* **2002**, *106*, 6088-6095.

[97] Walker, E. K.; Vanden Bout, D.; Stevenson, K. J. *J. Phys. Chem. C* **2011**, *115*, 2470-2475.

[98] Eisele, D. M.; Knoester, J.; Kirstein, S.; Rabe, J. P. Vanden Bout, D. A. *Nat. Nanotechnol.* **2009**, *4*, 658-663.

[99] Slavnova, T. D.; Görner, H.; Chibisov, A. K. *J. Phys. Chem. B* **2011**, *115*, 3379-3384.

[100] Sahami, S.; Weaver, M. *J. Electroanal. Chem.* **1981**, *122*, 155-170.

[101] User Manual for Princeton Instruments Spec-10 System: version 2B, 2004, Princeton Instruments, Trenton, NJ.

[102] Rudolph, M. *J. Electroanal. Chem.* **1991**, *314*, 13-22.

[103] Rudolph, M. *J. Electroanal. Chem.* **1992**, *338*, 85-98.

[104] Mocak, J.; Feldberg, S. W. *J. Electroanal. Chem.* **1997**, *378*, 31-37.

[105] Feldberg, S. W.; Goldstein, C. I.; Rudolph, M. *J. Electroanal. Chem.* **1996**, *413*, 25-36.

[106] Eberson, L.; Nyberg, K. Carboxylic Acids, Esters and Anhydrides. In Encyclopedia of the Electrochemistry of the Elements: Organic Section; Bard, A. J., Lund, H., Eds.; Marcel Dekker: New York, 1978; Vol. 12, p. 291.

[107] Nadjo, L.; Saveant, J. M. *J. Electroanal. Chem.* **1973**, *44*, 327-366.

[108] Debad, J. D.; Morris, J. C.; Magnus, P.; Bard, A. J. *J. Org. Chem.* **1997**, *62*, 530-537.

[109] Zhou, F.; Unwin, P. R.; Bard, A. J. *J. Phys. Chem.* **1992**, *96*, 4917-4924.

[110] Cho, S. Ph. D. Thesis, The University of Texas at Austin: Austin, TX, 2009;

Chapter 4.

[111] Schmidt am Busch, M.; Knapp, E. W. *J. Am. Chem. Soc.* **2005**, *127*, 15730-15737.

[112] Kasha, M.; Rawls, R.; El-Bayoumi, M. A. *Pure Appl. Chem.* **1965**, *11*, 371-392.

[113] Ventura, B.; Marconi, G.; Bröring, M. Krüger, R.; Flamigni, L. *New J. Chem.* **2009**, *33*, 428-438.

[114] Bergström, F.; Mikhaylov, I.; Hagglöf, P.; Wortmann, R.; Ny, T.; Johansson, L. B. Å.

*J. Am. Chem. Soc.* **2002**, *124*, 196-204.

[115] Pagano, R. E.; Chen, C.-S. *Ann. N. Y. Acad. Sci.* **1998**, *845*, 152-160.

[116] Omer, K. M.; Kanibolotsky, A. L.; Skabara, P. L.; Perepichka, I. F.; Bard, A. J.

*J. Phys. Chem. B* **2007**, *111*, 6612-6619.

[117] Flanagan, J. B.; Margel, S.; Bard, A. J.; Anson, F. C. *J. Am. Chem. Soc.* **1978**, *100*, 4248-4253.

## Vita

Alexander Borisovich Nepomnyashchii was born in Saint Petersburg (Leningrad) Russia on September 24 1979. He studied at the school 330 with the emphasis on physics in math from 1986 to 1996. He entered Herzen State Pedagogical University of Russia to pursue degree in Chemistry and English in 1996 and graduated in 2001. He started his Candidate of Science program in 2001 and finished it in 2005 under the supervision of Dr. Vyacheslav N. Pak. He spent two years in the University of Northern Iowa from 2003 to 2004 where he obtained his MS degree under the supervision of Dr. Shoshanna R. Coon. He started his doctoral program in September 2005 under the guidance of Dr. Allen J. Bard. The planned time of graduation is summer of 2011.

This dissertation was typed by Alexander Borisovich Nepomnyashchii